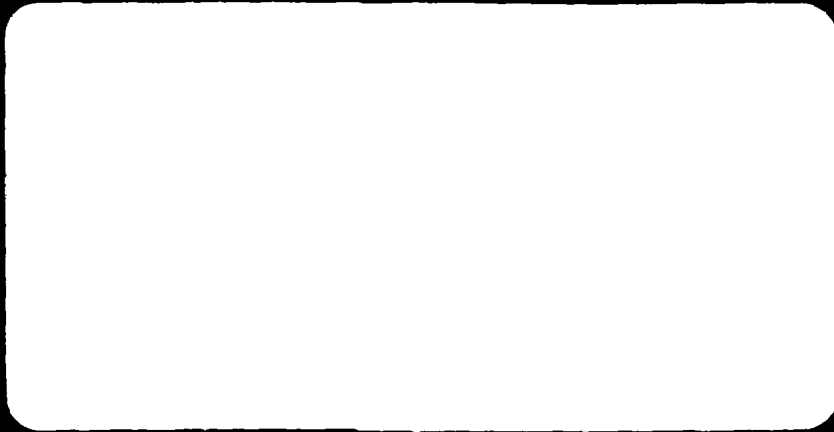


AD A I I 3347

①



S
DTC
ELECTE
APR 13 1982
E

TASC

ONE JACOB WAY/READING, MASSACHUSETTS 01867/(617) 944-6850

This document has been approved
for public release and sale; its
distribution is unlimited.

THE ANALYTIC SCIENCES CORPORATION

TR-1480-1

**APPLICATIONS OF KALMAN FILTERING AND
MAXIMUM LIKELIHOOD PARAMETER
IDENTIFICATION TO HYDROLOGIC FORECASTING**

1 April 1980

Prepared under:

Contract No. NA79SAC00668

for

U.S. DEPARTMENT OF COMMERCE
Washington, D.C.

Contract Monitor:

Mr. George Smith
National Weather Service
National Oceanic and Atmospheric Administration

Prepared by:

Jacob D. Goldstein
Wallace E. Larimore

Approved by:

Robert F. Brammer

THE ANALYTIC SCIENCES CORPORATION
Six Jacob Way
Reading, Massachusetts 01867

This document has been approved
for public release and sale; its
distribution is unlimited.

FOREWORD

This document presents the models, analysis and results obtained for the National Weather Service under Contract No. NA79SAC00668, "Applications of Kalman Filtering and Maximum Likelihood Parameter Identification to Hydrologic Forecasting".

A computer program, "SUBROUTINE REDO-UHG", and a report entitled "Reduced Order Unit Hydrograph Program Documentation" providing information on the design and use of the program have been previously delivered to the National Weather Service as part of the same contract.

This study has benefited from several conversations with E.A. Anderson, E.R. Johnson and G. Smith of the Hydrologic Research Laboratory of the National Weather Service and with Professor R.L. Bras of MIT and his assistants. Their cooperation is gratefully acknowledged.

Accession For	
NTIS GRA&I	<input checked="" type="checkbox"/>
DTIC TAB	<input type="checkbox"/>
Unannounced	<input type="checkbox"/>
Justification	<i>file on file</i>
By	
Distribution/	
Availability Codes	
Avail and/or	
Dist Special	
A	



ABSTRACT

↓
The applications of the canonical variate, Kalman filtering and maximum likelihood parameter identification techniques to the requirements of the National Weather Service in river flow forecasting are investigated.

State space reduced-order models for unit hydrographs are obtained with the use of canonical variate methods. A complete state-space model for a catchment consisting of the Sacramento model as the soil moisture system and the basin's unit hydrograph as the channel routing system is constructed. This model is used in the design of extended Kalman filters for the prediction of the channel discharge and the state of the system, and also in the design of an algorithm for the identification of catchment model parameters through the use of maximum likelihood techniques. The performance of the algorithms is demonstrated with synthetic data generated with the models for the Bird Creek and White River basins.

TABLE OF CONTENTS

	<u>Page No.</u>
Foreword	ii
Abstract	iii
List of Figures	vi
List of Tables	xiii
1. INTRODUCTION	1-1
1.1 Background	1-1
1.2 Study Objectives	1-1
1.3 Report Organization	1-4
2. ISSUES IN FILTER DESIGN	2-1
2.1 Model Structure	2-2
2.2 Model Equations - Continuous Time Components	2-10
2.2.1 SSM Model Equations	2-11
2.2.2 Rainfall Model	2-25
2.2.3 Equations for the Channel-Inflow and Rainfall Accumulator States	2-29
2.3 Model Equations - Discrete Time Components	2-30
2.4 Operation of the Model in the Simulation Mode	2-32
2.5 Operation of the Model in the Filtering Mode	2-36
2.6 Results	2-40
3. STATE-SPACE MODEL DEVELOPMENT FOR UNIT HYDROGRAPHS	3-1
3.1 Formulation of the Problem	3-2
3.2 Canonical Variate Decomposition of Past and Future	3-3
3.3 Optimality of Canonical Variate Analysis	3-6
3.3.1 Canonical Correlation Criterion	3-7
3.3.2 Canonical Prediction Criterion	3-9
3.4 Optimal Reduced-Order Modeling	3-11
3.4.1 State Vector Determination	3-11
3.4.2 State-Space Realization	3-12
3.4.3 Multirate Unit Hydrographs	3-15
3.4.4 Continuous Accumulation of Channel Inflow	3-18
3.5 Results	3-20
3.5.1 Reduced-Order State-Space Models	3-20
3.5.2 Multirate Unit Hydrographs	3-21

TABLE OF CONTENTS (Continued)

	<u>Page No.</u>
4. PARAMETER IDENTIFICATION FOR CATCHMENT MODELING	4-1
4.1 Likelihood Function for Dynamical Models	4-3
4.1.1 Dynamical Parametric Models	4-3
4.1.2 Likelihood Function Calculations	4-4
4.1.3 Propagation of State and Covariance Sensitivities	4-8
4.2 Optimization	4-11
4.2.1 Identifiability Theory	4-12
4.2.2 Maximization of Likelihood Functions	4-14
4.2.3 Quadratic Algorithm for Identifiable Parameters	4-16
4.2.4 Acceleration of Convergence by Reparameterization	4-19
4.2.5 Statistical Convergence Criterion	4-20
4.3 Results	4-22
4.3.1 Parameter Identifiability	4-22
4.3.2 Demonstration of Algorithm	4-26
5. SUMMARY AND CONCLUSIONS	5-1
5.1 Issues in Filter Design	5-1
5.2 State-Space Model Development for Unit Hydrographs	5-2
5.3 Parameter Identification for Catchment Modeling	5-3
5.4 Recommendations	5-4
APPENDIX A	A-1
REFERENCES	R-1

LIST OF FIGURES

<u>Figure No.</u>		<u>Page No.</u>
1.2.1	Hierarchical Structure of Task Outputs	1-3
2.1-1	Convention on Measurements and Unit Hydrograph Operation Rate	2-5
2.1-2	Basin Model Components	2-5
2.2-1	Graph of the Function $f(\eta, \hat{\eta})$	2-22
2.2-2	Graph of the Function $g(\eta, \eta^0)$	2-23
2.2-3	Graph of the Function $h(\eta)$	2-23
2.2-4	Example of Accumulated Precipitation Produced with the Rainfall Simulation Model	2-26
2.6-1	Six-Hour Unit Hydrographs for Bird Creek: Original Hydrograph (Solid Line) and Fifth-Order State-Space Approximation (Dashed Line)	2-43
2.6-2	Six-Hour Unit Hydrograph for White River Basin	2-43
2.6-3	Precipitation Record BC1	2-44
2.6-4	Upper-Zone Tension-Water Content for Precipitation Record BC1: True Values (Solid Line) and Predicted Values With Measurement Covariance R_1 (Dashed Line)	2-45
2.6-5	Upper-Zone Tension-Water Content for Precipitation Record BC1: True Values (Solid Line) and Predicted Values With Measurement Covariance R_2 (Dashed Line)	2-45
2.6-6	Upper-Zone Free-Water Content for Precipitation Record BC1: True Values (Solid Line) and Predicted Values With Measurement Covariance R_1 (Dashed Line)	2-46
2.6-7	Upper-Zone Free-Water Content for Precipitation Record BC1: True Values (Solid Line) and Predicted Values With Measurement Covariance R_2 (Dashed Line)	2-46
2.6-8	Lower-Zone Tension-Water Content for Precipitation Record BC1: True Values (Solid Line) and Predicted Values With Measurement Covariance R_1 (Dashed Line)	2-47

LIST OF FIGURES (Continued)

<u>Figure No.</u>		<u>Page No.</u>
2.6-9	Lower-Zone Tension-Water Content for Precipitation Record BCl: True Values (Solid Line) and Predicted Values With Measurement Covariance R_2 (Dashed Line)	2-47
2.6-10	Lower-Zone Primary Aquifer Content for Precipitation Record BCl: True Values (Solid Line) and Predicted Values With Measurement Covariance R_1 (Dashed Line)	2-48
2.6-11	Lower-Zone Primary Aquifer Content for Precipitation Record BCl: True Values (Solid Line) and Predicted Values With Measurement Covariance R_2 (Dashed Line)	2-48
2.6-12	Lower-Zone Supplementary Aquifer Content for Precipitation Record BCl: True Values (Solid Line) and Predicted Values With Measurement Covariance R_1 (Dashed Line)	2-49
2.6-13	Lower-Zone Supplementary Aquifer Content for Precipitation Record BCl: True Values (Solid Line) and Predicted Values With Measurement Covariance R_2 (Dashed Line)	2-49
2.6-14	Excess of the Additional Impervious Area Content Over the Upper-Zone Tension-Water Content for Precipitation Record BCl: True Values (Solid Line) and Predicted Values With Measurement Covariance R_1 (Dashed Line)	2-50
2.6-15	Excess of the Additional Impervious Area Content Over the Upper-Zone Tension-Water Content for Precipitation Record BCl: True Values (Solid Line) and Predicted Values With Measurement Covariance R_2 (Dashed Line)	2-50
2.6-16	Six-Hour Accumulated Channel-Inflow for Precipitation Record BCl: True Values (Solid Line) and Predicted Values With Measurement Covariance R_1 (Dashed Line)	2-51
2.6-17	Six-Hour Accumulated Channel-Inflow for Precipitation Record BCl: True Values (Solid Line) and Predicted Values With Measurement Covariance R_2 (Dashed Line)	2-51
2.6-18	Instantaneous Discharge for Precipitation Record BCl: True Values (Solid Line) and Predicted Values With Measurement Covariance R_1 (Dashed Line)	2-52

LIST OF FIGURES (Continued)

<u>Figure No.</u>		<u>Page No.</u>
2.6-19	Instantaneous Discharge for Precipitation Record BC1: True Values (Solid Line) and Predicted Values With Measurement Covariance R_2 (Dashed Line)	2-52
2.6-20	Precipitation Record BC2	2-55
2.6-21	Upper-Zone Tension-Water Content for Precipitation Record BC2: True Values (Solid Line) and Predicted Values With $P(0) = P'$ (Dashed Line)	2-56
2.6-22	Upper-Zone Tension-Water Content for Precipitation Record BC2: True Values (Solid Line) and Predicted Values With $P(0) = P''$ (Dashed Line)	2-56
2.6-23	Upper-Zone Free-Water Content for Precipitation Record BC2: True Values (Solid Line) and Predicted Values With $P(0) = P'$ (Dashed Line)	2-57
2.6-24	Upper-Zone Free-Water Content for Precipitation Record BC2: True Values (Solid Line) and Predicted Values With $P(0) = P''$ (Dashed Line)	2-57
2.6-25	Lower-Zone Tension-Water Content for Precipitation Record BC2: True Values (Solid Line) and Predicted Values With $P(0) = P'$ (Dashed Line)	2-58
2.6-26	Lower-Zone Tension-Water Content for Precipitation Record BC2: True Values (Solid Line) and Predicted Values With $P(0) = P''$ (Dashed Line)	2-58
2.6-27	Lower-Zone Primary Free-Water Content for Precipitation Record BC2: True Values (Solid Line) and Predicted Values With $P(0) = P'$ (Dashed Line)	2-59
2.6-28	Lower-Zone Primary Free-Water Content for Precipitation Record BC2: True Values (Solid Line) and Predicted Values With $P(0) = P''$ (Dashed Line)	2-59
2.6-29	Lower-Zone Supplementary Free-Water Content for Precipitation Record BC2: True Values (Solid Line) and Predicted Values With $P(0) = P'$ (Dashed Line)	2-60
2.6-30	Lower-Zone Supplementary Free-Water Content for Precipitation Record BC2: True Values (Solid Line) and Predicted Values With $P(0) = P''$ (Dashed Line)	2-60

LIST OF FIGURES (Continued)

<u>Figure No.</u>		<u>Page No.</u>
2.6-31	Excess of the Additional Impervious Area Content Over the Upper-Zone Tension-Water Content for Precipitation Record BC2: True Values (Solid Line) and Predicted Values With $P(0) = P'$ (Dashed Line)	2-61
2.6-32	Excess of the Additional Impervious Area Content Over the Upper-Zone Tension-Water Content for Precipitation Record BC2: True Values (Solid Line) and Predicted Values With $P(0) = P''$ (Dashed Line)	2-61
2.6-33	Six-Hour Accumulated Channel-Inflow for Precipitation Record BC2: True Values (Solid Line) and Predicted Values With $P(0) = P'$ (Dashed Line)	2-62
2.6-34	Six-Hour Accumulated Channel-Inflow for Precipitation Record BC2: True Values (Solid Line) and Predicted Values With $P(0) = P''$ (Dashed Line)	2-62
2.6-35	Instantaneous Discharge for Precipitation Record BC2: True Values (Solid Line) and Predicted Values with $P(0) = P'$ (Dashed Line)	2-63
2.6-36	Instantaneous Discharge for Precipitation Record BC2: True Values (Solid Line) and Predicted Values With $P(0) = P''$ (Dashed Line)	2-63
2.6-37	Precipitation Record for White River Basin	2-65
2.6-38	White River Basin. Upper-Zone Tension-Water Content: True Values (Solid Line) and Predicted Values (Dashed Line)	2-67
2.6-39	White River Basin. Upper-Zone Free-Water Content: True Values (Solid Line) and Predicted Values (Dashed Line)	2-67
2.6-40	White River Basin. Lower-Zone Tension-Water Content: True Values (Solid Line) and Predicted Values (Dashed Line)	2-68
2.6-41	White River Basin. Lower-Zone Primary Free-Water Content: True Values (Solid Line) and Predicted Values (Dashed Line)	2-68

LIST OF FIGURES (Continued)

<u>Figure No.</u>		<u>Page No.</u>
2.6-42	White River Basin. Lower-Zone Supplementary Free-Water Content: True Values (Solid Line) and Predicted Values (Dashed Line)	2-69
2.6-43	White River Basin. Excess of the Additional Impervious Area Content Over the Upper-Zone Tension-Water Content: True Values (Solid Line) and Predicted Values (Dashed Line)	2-69
2.6-44	White River Basin. Six-Hour Accumulated Channel-Inflow: True Values (Solid Line) and Predicted Values (Dashed Line)	2-70
2.6-45	White River Basin. Mean Daily Discharge: True Values (Solid Line) and Predicted Values (Dashed Line)	2-70
2.6-46	White River Basin. Instantaneous Discharge: True Values (Solid Line) and Predicted Values (Dashed Line)	2-71
3.1-1	Approximation of Unit Hydrograph by a Reduced Order Filter	3-3
3.4-1	Partial Innovations Representation of Optimal Reduced Order Filter	3-13
3.4-2	Multirate Unit Hydrograph	3-16
3.4-3	Relationship Between Continuous and Discrete Time Unit Pulse Response	3-19
3.5-1	6-Hour Unit Hydrographs for Bird Creek, Original Hydrograph (Solid Line) and Fourth-Order State-Space Approximation Using the Canonical Correlation Procedure (Dashed Line)	3-22
3.5-2	6-Hour Unit Hydrographs for Bird Creek, Original Hydrograph (Solid Line) and Eight-Order State-Space Approximation Using the Canonical Correlation Procedure (Dashed Line)	3-22

LIST OF FIGURES (Continued)

<u>Figure No.</u>		<u>Page No.</u>
3.5-3	Squared Magnitude Transfer Function of 6-Hour Unit Hydrographs for Bird Creek, Original Hydrograph (Solid Line) and Fourth-Order State-Space Approximation Using the Canonical Correlation Procedure (Dashed Line)	3-23
3.5-4	Squared Magnitude Transfer Function of 6-Hour Unit Hydrograph for Bird Creek, Original Hydrograph (Solid Line) and Eight-Order State-Space Approximation Using the Canonical Correlation Procedure (Dashed Line)	3-23
3.5-5	6-Hour Unit Hydrographs for Bird Creek, Original Hydrograph (Solid Line) and Fourth-Order State-Space Approximation Using the Canonical Prediction Procedure (Dashed Line)	3-24
3.5-6	6-Hour Unit Hydrographs for Bird Creek, Original Hydrograph (Solid Line) and Eight-Order State-Space Approximation Using the Canonical Prediction Procedure (Dashed Line)	3-24
3.5-7	Squared Magnitude Transfer Function of 6-Hour Unit Hydrographs for Bird Creek, Original Hydrograph (Solid Line) and Fourth-Order State-Space Approximation Using the Canonical Prediction Procedure (Dashed Line)	3-25
3.5-8	Squared Magnitude Transfer Function of 6-Hour Unit Hydrographs for Bird Creek, Original Hydrograph (Solid Line) and Eight-Order State-Space Approximation Using the Canonical Prediction Procedure (Dashed Line)	3-25
3.5-9	Multirate Unit Hydrograph With 6-hour Inputs and 3-Hour Outputs	3-26
3.5-10	Squared Magnitude Transfer Function of Multirate Unit Hydrograph Showing Output Components in Response to a 1.5 cyc/day Input	3-27
3.5-11	Input Sine Wave and Sample Values	3-27
3.5-12	Output Function with 1.5 cyc/day and 2.5 cyc/day Components	3-28

LIST OF FIGURES (Continued)

<u>Figure No.</u>		<u>Page No.</u>
4.3-1	Precipitation Innovations	4-30
4.3-2	Deterministic Component of Channel Discharge Innovations for True (Solid Line) and Estimated (Dashed Line) Parameter Values	4-30
4.3-3	Discharge Innovations for True (Solid Line) and Estimated (Dashed Line) Parameter Values	4-31
4.3-4	Normalized Innovations for True (Solid Line) and Estimated (Dashed Line) Parameter Values	4-31

LIST OF TABLES

<u>Table No.</u>		<u>Page No.</u>
2.1-1	Basin Model State Description	2-7
2.1-2	Critical Time Variation of State Variables	2-9
2.2-1	SSM Model Parameters	2-12
2.6-1	SSM Model Parameters for Bird Creek and White River Basins	2-41
4.3-1	Comparison of Moderate and Heavy Rainfall Cases	4-23
4.3-2	Identifiability of Catchment Parameters for Heavy Rainfall Case	4-24
4.3-3	Identifiability of Catchment Parameters for Moderate Rainfall Case	4-26
4.3-4	Iterations of Parameter Estimation Algorithm	4-28
A-1	Comparison of Evapotranspiration and Drainage Rates	A-5

1. INTRODUCTION

1.1 BACKGROUND

The National Weather Service (NWS) has the responsibility for hydrologic forecasting in the United States. This responsibility includes the production of both flood warnings and stream-flow forecasts. Accurate and timely flood warnings are required for a wide variety of flood classes including flash floods as well as floods of longer duration. Stream-flow forecasts are required for diverse applications including the planning of irrigation, the prediction of available hydroelectric power, the maintenance of water quality standards, and the planning of river navigation.

There is a continuing need for new techniques useful for creating more accurate and cost-effective flood warning and stream-flow predictions. It is highly desirable to increase the amount of automation used in the creation of hydrologic forecasts and to be able to take advantage of newly-developing advances in computer and communications capabilities and in computational and algorithmic techniques.

1.2 STUDY OBJECTIVES

The objective of this study was to investigate the application of Kalman filtering, canonical variate and maximum likelihood parameter identification techniques to the requirements of the National Weather Service in improving hydrologic forecasting. The work was organized into three principal tasks:

Task 1 ISSUES IN FILTER DESIGN

Under this task, the differential equations corresponding to the Sacramento Soil Moisture model were derived and several theoretical modifications were developed. The equations of the soil moisture model were combined with a reduced-order state-space model for a unit hydrograph and an extended Kalman filter that produces six-hour lead forecasts of a basin's discharge was designed and implemented. The details of the analysis and a set of results obtained with the SSM model parameters of the Bird Creek and White River drainage basins are included in this report.

Task 2 STATE-SPACE MODEL DEVELOPMENT FOR UNIT HYDROGRAPHS

Under this task, a computer program has been developed for applying the canonical variate technique to the development of discrete-time reduced-order state-space models for the approximation of unit hydrographs. The computer program (Subroutine REDO-UHG) accompanied with supporting documentation (Ref. 1) has been delivered to NOAA/NWS for use as an operation in the Version 5.0 NWSRFS Forecast Component. The principles on which the design of the computer program was based are described in this report together with some examples of their application.

Task 3 PARAMETER IDENTIFICATION FOR CATCHMENT MODELING

Under this task, an initial investigation of the applications of the technique of maximum likelihood parameter identification to the problem of catchment calibration has been performed. Parameter estimation algorithms appropriate to the catchment model of the National Weather Service have been developed and tested with simulated data to determine parameter estimation error, parameter identifiability and numerical behavior of the algorithms.

Figure 1.2-1 presents the hierarchical structure of the outputs of the three tasks described above. The state-space models of unit-hydrographs obtained with the canonical variate technique under Task 2 have direct application to the

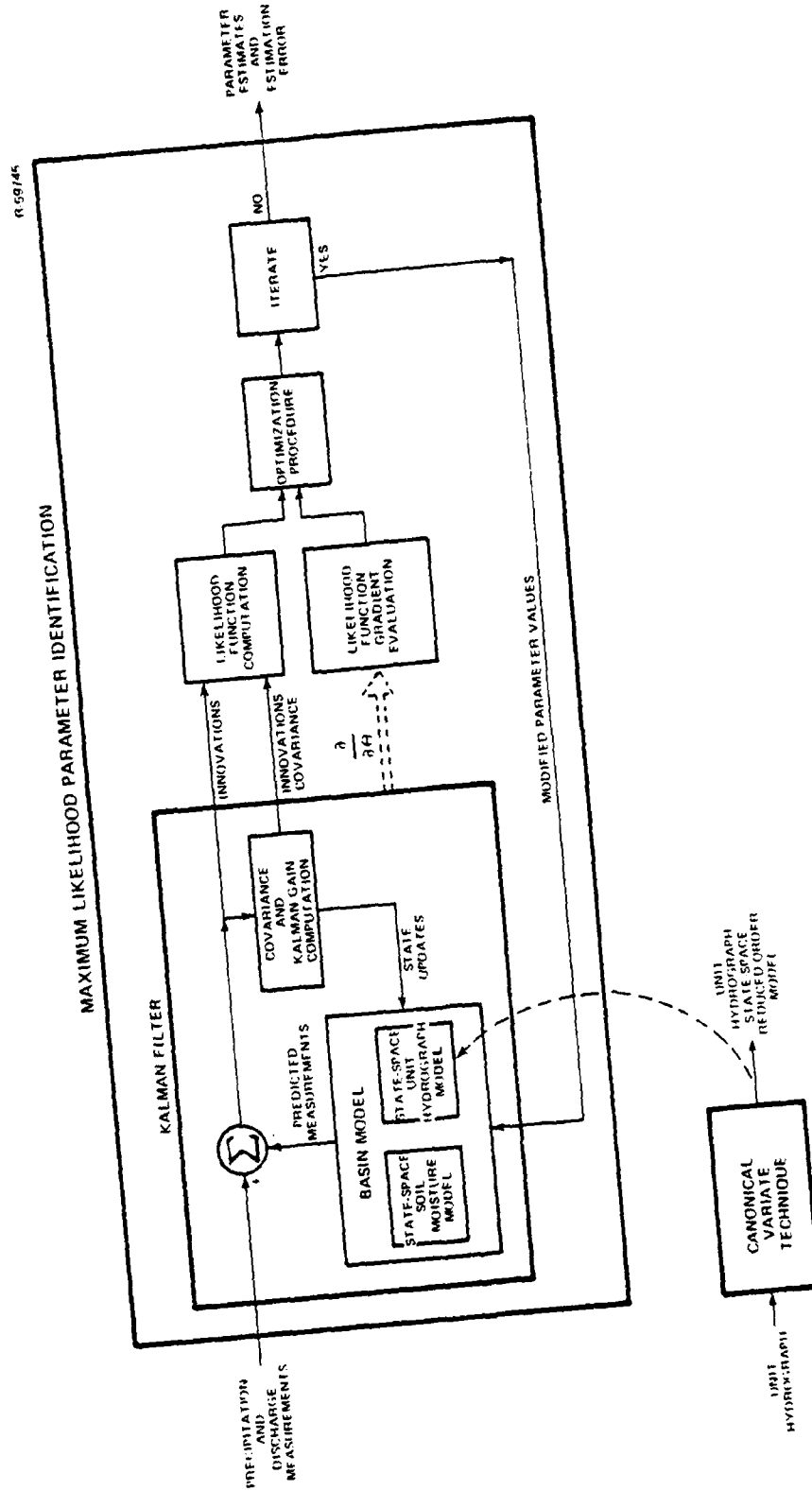


Figure 1.2-1 Hierarchical Structure of Task Outputs

simplification of the processing of channel-inflow time series. These models for unit hydrographs are used in Task 1 to create complete state-space models for catchments which, in turn, form the basis for the design and operation of Kalman filters for the prediction of a basin's channel discharge and for the estimation of the state of the system.

The maximum likelihood parameter identification procedure of Task 3 is an iterative algorithm which uses a Kalman filter as one of its main constituents. The filter innovations (differences between actual and predicted measurements) are used in the evaluation of the likelihood function. An optimization procedure utilizes the values of the likelihood function and its functional gradient computed by symbolically differentiating the operations of the filter to evaluate a vector parameter increment in the direction that maximizes the likelihood function. The catchment model parameters are modified and the process repeated until a convergence criterion is satisfied.

1.3 REPORT ORGANIZATION

The organization of this report is as follows: Section 2 deals with the catchment model and the design of extended Kalman filters for the prediction of a basin's channel discharge. Section 3 presents the canonical variate technique and its application to the synthesis of reduced-order state-space models for unit hydrographs. Section 4 describes the algorithms for maximum likelihood identification of the parameters of the catchment model and presents some examples of their application. Section 5 contains a review of the information contained in this report. An appendix containing some technical considerations on the constraint on the ratio of free to tension water for the upper zone of the soil moisture model is also included.

THE ANALYTIC SCIENCES CORPORATION

For the sake of completeness, some of the material contained in previous progress reports (Refs. 2 through 5) is also included in this report.

2.

ISSUES IN FILTER DESIGN

This section presents the details of the analysis and synthesis of an Extended Kalman Filter (EKF) for improving the estimation of the state and channel discharge of a basin. The basin's model considered in this study consists of the Sacramento model as the soil moisture system and a unit hydrograph as the channel routing system.

Pioneering work on the applications of Kalman filtering to the National Weather Service's river flow forecasting system is described in Ref. 6. The present work differs conceptually from that of Ref. 6 in that the soil moisture process is viewed as occurring in continuous-time rather than in discrete-time as in Ref. 6.* In addition, channel routing is modeled by the basin's unit hydrograph while in Ref. 6 a linear reservoir with variable outflow rate is used.

The Kalman filtering formulation requires that the system be modeled in state-space form. The state-space differential equations of the Sacramento Soil Moisture (SSM) model were derived in Refs. 2, 3, and 4. To complement these equations, channel routing was modeled by a suitable order state-space model approximation to the basin's unit hydrograph obtained with the methods described in Chapter 3 of this report.

The basic idea behind the EKF formalism is to approximate the system behavior, for a short time interval, by the

*A comparison of the state-equations of Ref. 6 and those used in the present study is given in Ref. 2. Other differences between the two studies are also noted in Ref. 2.

linearized form of the state-equations about the operating point at the beginning of the interval. The optimal filter for the resulting linear system is used to propagate the state estimates and their covariance matrix during the time interval under consideration. A detailed treatment of extended Kalman filtering is given in Ref. 7.

In order to test the performance of the filter and the consistency of the formulation, synthetic data was generated using the model in the simulation mode. These data were then used as input to the filter, and the state and discharge estimates so obtained were compared to the truth values previously generated. The SSM model parameters and unit hydrographs used in these tests were those of the National Weather Service River Forecasting System (NWSRFS) calibration of the Bird Creek and White River drainage basins.

This chapter is organized as follows: Section 2.1 discusses the overall model structure and the interface between the soil moisture model and the system associated with the unit hydrograph. Section 2.2 presents the state-equations of the continuous-time part of the model including the SSM model and a simple precipitation model. Section 2.3 discusses the discrete-time equations associated with the unit hydrograph system. Sections 2.4 and 2.5 describe in detail the operation of the model in the simulation and filtering modes, respectively. Section 2.6 presents a collection of representative results obtained with the techniques described in previous subsections.

2.1 MODEL STRUCTURE

Traditionally, NWS has used deterministic models in forecasting river flows based on meteorological data. Thus,

necessarily, the intrinsic rate at which the soil moisture model operates has been the same as the rate at which precipitation data are collected. When a stochastic conceptual model is used, however, the input rate to the soil moisture model need not be the same as the rate at which accumulated channel inflow estimates are produced. In fact, with a continuous-time stochastic soil moisture model, the best estimate of the channel-inflow rate given all previous measurements of precipitation and channel discharge can be computed at any time.

Thus, even though the SSM model is a discrete-time model, it was necessary to derive a continuous-time model whose discretized version was in congruence with the SSM model. In addition to the advantage of being able to compute state-estimates at any time, there were two other reasons for modeling the soil moisture process in continuous-time. First, the physical processes, in themselves, take place continuously in time. For example, the effects of a severe storm of short duration cannot be properly modeled using a predetermined equally spaced sequence of times. Evidence for the need of considering the dynamic behavior of the system in continuous-time is found in the LAND subroutine. There, depending on the availability of free water in the upper zone, the basic time interval is partitioned into a number of subintervals for the computation of the percolation function. This computation determines the distribution of water to the lower zone, the amount of surface runoff, etc. Secondly, the threshold values associated with many of the variables can be attained at times which, in general, do not coincide with the endpoints of arbitrarily chosen time intervals. These thresholds determine when the system switches from one mode of operation to another and are of fundamental importance in the analysis.

Channel routing, on the other hand, is modeled as a discrete-time system. A k -hour unit hydrograph yields instantaneous discharge rates when given an input sequence consisting of k -hourly accumulated channel inflow values. For most of the unit hydrographs used by NWS the input sample rate is equal to the output sample rate; i.e., estimates of the discharge rate are produced at intervals of k hours.* All hydrographs considered in this chapter belong to this category.

In the present analysis measurements of accumulated precipitation are assumed to occur at an ℓk -hourly rate and observations of mean discharge occur every $m\ell k$ hours. For example, the situation in which $k=6$, $\ell=1$, $m=1$ represents the case where continuous estimation of the state of the system is performed given 6-hour measurements of accumulated precipitation and instantaneous discharge; $k=6$, $\ell=1$, $m=4$ corresponds to 6-hour measurements of precipitation and daily observations of mean discharge. Figure 2.1-1 summarizes the above convention.

In order to combine the state-space model of the soil moisture accounting procedure, which yields continuous-time estimates of the channel inflow rate, with the unit hydrograph system, which requires k -hourly accumulated channel inflow at its input, it is necessary to introduce an additional state. The role of this state is to integrate the channel inflow rate for periods of k hours. A schematic diagram depicting the interrelation between the different components of the model is given in Fig. 2.1-2. The additional state mentioned above can be visualized as a reservoir, labeled Channel Inflow Accumulator in Fig. 2.1-2, whose contents are dumped into the unit hydrograph system every k hours.

*In some instances, NWS uses unit hydrographs for which the output rate is higher than the input rate (see Section 3.4.3).

0.51645

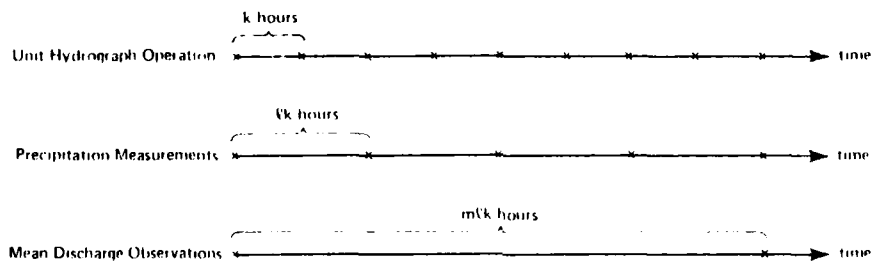


Figure 2.1-1 Convention on Measurements and Unit Hydrograph Operation Rate

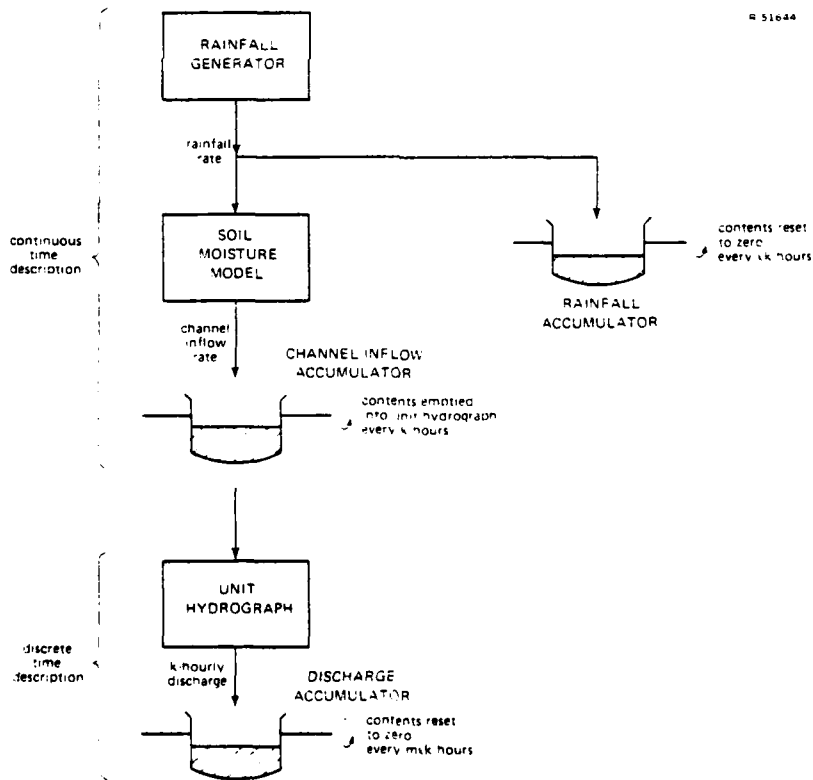


Figure 2.1-2 Basin Model Components

Two more accumulator states are needed to account for the memory-type measurements. The rainfall accumulator in the upper right corner of Fig. 2.1-2 integrates the rainfall rate for periods of ℓk hours and the discharge accumulator in the lower left corner of Fig. 2.1-2 adds up the $m\ell$ discharge rates whose average yields the $m\ell k$ -hour mean discharge.

The basin's state-space model contains $10+M$ states where M is the order of the state-space model approximation to the unit hydrograph system. A description of the states is given in Table 2.1-1. It was shown in Ref. 2 that six states suffice to represent the SSM model. The first six states in Table 2.1-1 correspond to the SSM model. Their equivalents in the LAND subroutine are indicated in parentheses in the table. States 7, 9, and $10+M$ are associated with the accumulators previously described. State 8 provides the basis for the rainfall model which is presented in detail in Section 2.2.2. The remaining states (10 through $9+M$) correspond to the unit hydrograph system.

It is convenient to partition the state-vector, \underline{x} , as

$$\underline{x} = \begin{pmatrix} \underline{x}_c \\ \underline{x}_d \end{pmatrix} \quad (2.1-1)$$

where \underline{x}_c and \underline{x}_d stand for the first 9 and last $M+1$ components of \underline{x} , respectively. The subvector \underline{x}_c evolves continuously in time while \underline{x}_d changes only at times which are multiples of the hydrograph rate, k . These times ($vk; v=0,1,\dots$) are referred to as critical times in the sequel.

The operation of the filter can be described in general terms as follows. Between critical times there are no measure-

TABLE 2.1-1
BASIN MODEL STATE DESCRIPTION

STATE	DESCRIPTION
1	Upper-zone tension-water content (UZTWC)
2	Upper-zone free-water content (UZFWC)
3	Lower-zone tension-water content (LZTWC)
4	Lower-zone primary free-water content (LZFPC)
5	Lower-zone supplementary free-water content (LZFSC)
6	Excess of the additional impervious storage over the upper-zone tension-water content (ADIMC-UZTWC)
7	Channel-inflow accumulator content
8	Rainfall generator model
9	Rainfall accumulator content
10	} Unit hydrograph model
:	
:	
9+M	
10+M	Chanrel discharge accumulator

ments. The continuous part of the state estimate, $\hat{\underline{x}}_c^*$, is propagated in accordance with the associated differential equations, but the discrete part, $\hat{\underline{x}}_d$, remains unchanged. When a critical time is reached, the channel routing portion of the model is updated taking into account the accumulated channel-inflow during the past k hours. At this point, if there are any measurements, the Kalman gains are computed and used to modify all the state values by incorporating optimally all of

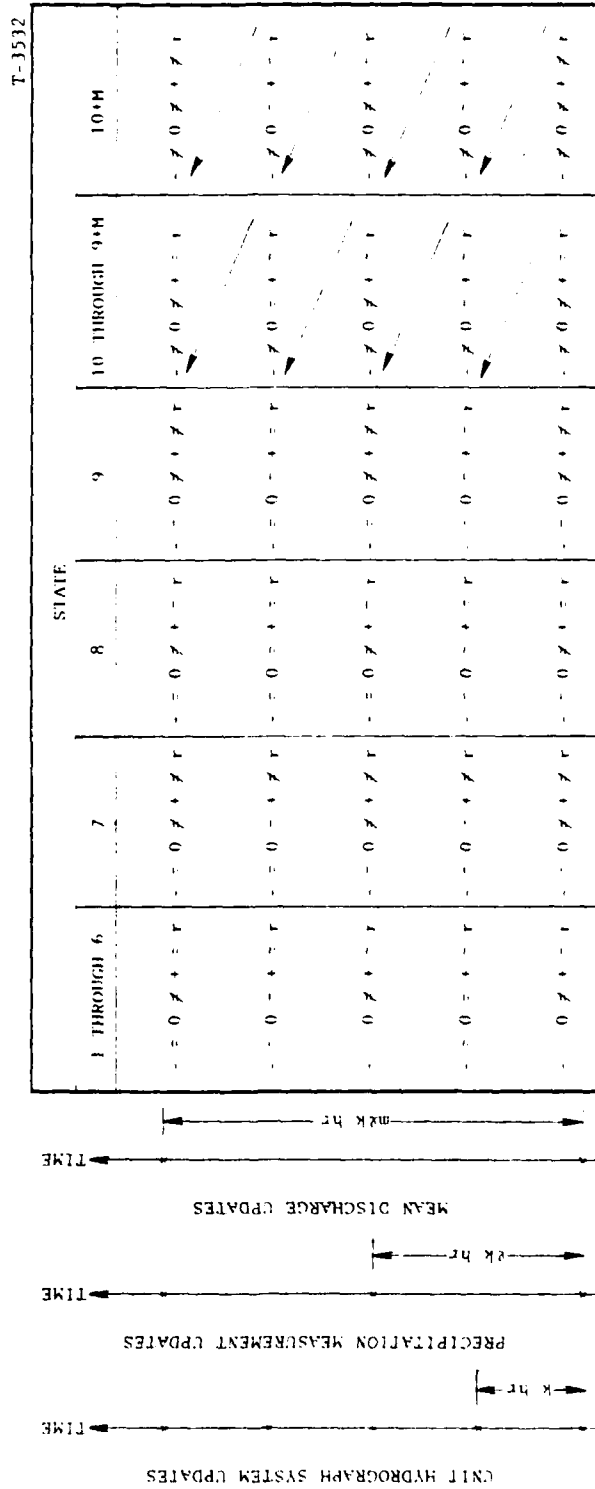
* $\hat{\underline{x}}$ is the estimate of \underline{x} .

the information contained in the measurements. Finally, the contents of the appropriate accumulators are reset to zero and propagation of the continuous part of the state for the next k hours begins.

It is convenient to introduce a notation of superscripts to be affixed to the critical times in order to distinguish the various state values computed at these times. If t is a critical time, $\underline{x}(t^-)$ stands for the state vector immediately after propagation of the continuous part for the last k hours has been completed, $\underline{x}(t^0)$ represents the state after the discrete transition for the unit hydrograph part of the model has taken place, $\underline{x}(t^+)$ denotes the value of the state following a Kalman update and $\underline{x}(t^r)$ is the state after resetting any accumulator to zero. Table 2.1-2 summarizes the behavior of the state values for a full cycle of operation of the model ($m\ell k$ hours) using symbolically the notation introduced above. For example, the notation $- = 0 \neq + \neq r$ means $\underline{x}(t^-) = \underline{x}(t^0) \neq \underline{x}(t^+) \neq \underline{x}(t^r)$.

Thus, the transition from t^- to t^0 only affects the discrete states of the model (last two columns in Table 2.1-2). The transition from t^0 to t^+ corresponds to a Kalman update. Since all state estimates can be expected to improve following a Kalman update, Table 2.1-2 indicates $0 \neq +$ for all states at the times at which there is at least one measurement. The transition from t^+ to t^r only affects the accumulator states. State seven, the channel-inflow accumulator, is reset to zero at all critical times. State nine, the rainfall accumulator, and state $10+M$, the discharge accumulator, are set to zero following a rainfall or discharge measurement, respectively. The arrows in the last two columns of Table 2.1-2 indicate that the discrete part of the model does not vary between critical times, i.e., if t_i and t_{i+1} are two successive critical times, then

TABLE 2.1.1-2
CRITICAL TIME VARIATION OF STATE VARIABLES



$$\hat{\underline{x}}_d(t_i^r) = \hat{\underline{x}}_d(t_{i+1}^-) \quad (2.1-2)$$

2.2 MODEL EQUATIONS - CONTINUOUS TIME COMPONENTS

The state-equations for the complete basin model are of the form ($v=0,1,\dots$)

$$\dot{\underline{x}}_c(t) = \underline{F}_c(\underline{x}_c, t) + G_c \zeta(t) \quad (2.2-1)$$

$$\underline{x}_d[(vk)^0] = A \underline{x}_d[(vk)^-] + B \underline{x}_c[(vk)^-] \quad (2.2-2)$$

where $\underline{F}_c(\underline{x}_c, t)$ is a nonlinear time-varying vector function of the continuous part of the state, the time dependency being through the potential evapotranspiration demand, $u_2(t)$. G_c is a 9×1 matrix and ζ is a scalar gaussian white noise input that drives the rainfall model (see Section 2.2.2). Thus, the only nonzero entry in G_c appears in row eight. The factors A and B are $(M+1) \times (M+1)$ and $(M+1) \times 9$ constant matrices, respectively.

In addition to Eqs. 2.2-1 and 2.2-2, the accumulators' contents are reset to zero at the appropriate times

$$x_7[(n)^r] = 0 \quad ; \quad n=0, k, 2k, \dots \quad (2.2-3)$$

$$x_9[(n)^r] = 0 \quad ; \quad n=0, \ell k, 2\ell k, \dots \quad (2.2-4)$$

$$x_{10+M}[(n)^r] = 0 \quad ; \quad n=0, m\ell k, 2m\ell k, \dots \quad (2.2-5)$$

Changes in the discrete part of the state vector, \underline{x}_d , occur only at the critical times. If $vk < t < (v+1)k$ the state-equations for \underline{x}_d can be thought of to be

$$\dot{\underline{x}}_d(t) = 0 \quad (2.2-6)$$

Let y_1 and y_2 be the measured values of precipitation and mean discharge, respectively. The measurement equations are

$$y_1(v\ell k) = x_9[(v\ell k)^0] + \xi_1(v\ell) \quad (2.2-7)$$

$$y_2(v\ell k) = \frac{1}{m\ell} x_{10+M}[(v\ell k)^0] + \xi_2(v\ell) \quad (2.2-8)$$

where ξ_1 and ξ_2 represent the errors in the measurements modeled as white noise sequences.

This section presents the individual differential equations associated with Eq. 2.2-1. It is organized as follows: Subsection 2.2.1 treats the SSM model equations, Subsection 2.2.2 introduces the rainfall model equations, and Subsection 2.2.3 gives the equations for the channel-inflow and rainfall accumulator states. Section 2.3 presents the discrete equations corresponding to Eq. 2.2-2.

2.2.1 SSM Model Equations

The state equations corresponding to the Sacramento Soil Moisture model were derived from the NWSRFS LAND subroutine documentation (Ref. 8). Six states (labeled one through six in Table 2.1-1) are necessary to represent the model: two states for the upper zone, three for the lower zone and one for the additional impervious area content. The parameters of the model are listed in Table 2.2-1. The relationship given in Table 2.2-1 between the instantaneous drainage coefficients, d_u , d_l' and d_l'' and their counterparts in the LAND subroutine, UZK, LZPK and LZSK was derived in Ref. 2.

The SSM model contains several threshold-type nonlinearities associated with the bounds on the contents of the elements of the upper and lower zones and with constraints on

TABLE 2.2-1
SSM MODEL PARAMETERS

T-3536

NOTATION	LAND EQUIVALENT	DESCRIPTION
x_1^0	UZTWM	Upper-zone tension-water capacity (mm)
x_2^0	UZFWM	Upper-zone free-water capacity (mm)
x_3^0	LZTWM	Lower-zone tension-water capacity (mm)
x_4^0	LZFBM	Lower-zone primary free-water capacity (mm)
x_5^0	LZFSM	Lower-zone secondary free-water capacity (mm)
d_u	$-\rho n(1-UZK)/24$	Upper-zone instantaneous drainage coefficient (1/hr)
d_p^0	$-\rho n(1-LZPK)/24$	Lower-zone primary instantaneous drainage coefficient (1/hr)
d_s^0	$-\rho n(1-LZSK)/24$	Lower-zone secondary instantaneous drainage coefficient (1/hr)
γ	ZPERC	Parameter in percolation function
α	REXP	Exponent in percolation function
p_1	PFREE	Fraction of percolated water assigned to the lower zone free water aquifers
μ	SIDE	Fraction of baseflow not appearing in river flow
a_1	ADIMP	Fraction of basin that becomes impervious when tension water requirements are met
a_2	PCTIN	Fraction of basin permanently impervious
r	RSERV	Fraction of the lower zone free-water capacity unavailable to supply lower zone tension requirements
s	RIVA	Fraction of residual evapotranspiration demand actually contributed by stream surfaces and riparian vegetation

ratios of free to tension-water content for the two zones. A derivation of the implications of these constraints in a continuous-time SSM model was included in Ref. 2. For the upper-zone, the constraint can be written as

$$x_2/x_2^0 \leq x_1/x_1^0 \quad (2.2-9)$$

and for the lower-zone,

$$1 - \frac{x_4 + x_5}{x_4^0 + x_5^0} \geq (1 - r) \left(1 - \frac{x_3}{x_3^0} \right) \quad (2.2-10)$$

Furthermore, at any time, t , when equality holds in Eq. 2.2-9 or in Eq. 2.2-10, the right derivatives of the states must satisfy

$$\dot{x}_2(t^+)/x_2^0 \leq \dot{x}_1(t^+)/x_1^0 \quad (2.2-11)$$

or

$$(1 - r) \frac{\dot{x}_3(t^+)}{x_3^0} > \frac{\dot{x}_4(t^+) + \dot{x}_5(t^+)}{x_4^0 + x_5^0} \quad (2.2-12)$$

respectively.

In addition to the threshold-type nonlinearities there are other nonlinearities in the SSM model. The most important nonlinearity is associated with the percolation function. At any given time, the percolation rate from the upper to the lower zone is given by

$$p = p^0 \frac{x_2}{x_2^0} \left[1 + \gamma \left(1 - \frac{x_3 + x_4 + x_5}{x_3^0 + x_4^0 + x_5^0} \right)^\alpha \right] \quad (2.2-13)$$

with

$$p^0 = d'_\ell x_4^0 + d''_\ell x_5^0 \quad (2.2-14)$$

Let z_3 , z_4 and z_5 be the percolation rate inflow into the lower zone's tension-water, primary free-water and supplementary free-water elements respectively. In the SSM model, under normal operation (i.e., no threshold active), the total percolation is divided into the lower zone's elements as

$$z_3 = (1 - p_f)p \quad (2.2-15)$$

$$z_4 = \frac{x_4^0}{x_4^0 + x_5^0} \cdot \frac{2(1 - x_4/x_4^0)}{2 - \frac{x_4}{x_4^0} - \frac{x_5}{x_5^0}} p_f p \quad (2.2-16)$$

$$z_5 = 1 - \frac{x_4^0}{x_4^0 + x_5^0} \cdot \frac{2(1 - x_4/x_4^0)}{2 - \frac{x_4}{x_4^0} - \frac{x_5}{x_5^0}} p_f p \quad (2.2-17)$$

Thus, a fraction, $(1 - p_f)$, of the total percolation is assigned to the tension-water element and the remainder of the percolation is divided between the free-water aquifers according to Eqs. 2.2-16 and 2.2-17.

In Refs. 2 and 3 the exact differential equations of the SSM model were derived. The equations given there correspond to the distribution of the percolation rate indicated by Eqs. 2.2-15, 2.2-16 and 2.2-17. There is a difficulty associated with the use of this distribution of the percolation rate: if $x_4^0 > x_5^0$, the fraction of $p_f p$ assigned to the primary free-water aquifer, Eq. 2.2-16, is larger than 1 and the fraction assigned to the secondary free-water aquifer, Eq. 2.2-17, is negative for a certain range of values of x_4 and x_5 . Accordingly the distribution of the percolation rate to the lower zone was slightly modified. The modification (Ref. 4) is described below.

The percolation function, Eq. 2.2-13 can also be written as

$$p = d'_l x_4^0 \frac{x_2}{x_2^0} + d''_l x_5^0 \frac{x_2}{x_2^0} + \tilde{p} \quad (2.2-18)$$

with

$$\tilde{p} = p^0 \gamma \frac{x_2}{x_2^0} \left(1 - \frac{x_3 + x_4 + x_5}{x_3^0 + x_4^0 + x_5^0} \right)^\alpha \quad (2.2-19)$$

With the aid of Eq. 2.2-18 the total percolation rate can be interpreted as consisting of two parts. One part, corresponding to the first two terms in Eq. 2.2-18, depends on the maximum baseflow rate from the free water aquifers and on the availability of water in the upper-zone free-water element. The other part, corresponding to the term \tilde{p} in Eq. 2.2-18, depends on the lower zone's deficiency ratio as well as on the upper-zone free-water normalized content.

The modified distribution of the total percolation is

$$z_3 = (1 - p_f) \tilde{p} \quad (2.2-20)$$

$$z_4 = d'_l x_4 \frac{x_2^0}{x_2^0} + \frac{x_4^0 - x_4}{x_4^0 - x_4 + x_5^0 - x_5} p_f \tilde{p} \quad (2.2-21)$$

$$z_5 = d''_l x_5 \frac{x_2^0}{x_2^0} + \frac{x_5^0 - x_5}{x_4^0 - x_4 + x_5^0 - x_5} p_f \tilde{p} \quad (2.2-22)$$

instead of Eqs. 2.2-15, 2.2-16 and 2.2-17. Thus, each of the free water aquifers receives a part of the percolation which is proportional to its maximum outflow rate and to the availability of water in the upper-zone free-water element, and a second part which depends on the element's deficiency as a fraction of the total deficiency in the free water elements and, also, on the lower zone's deficiency ratio.

With the aid of the functions

$$h_f(\eta) = \begin{cases} 1 & \text{if } \eta \geq 0 \\ 0 & \text{if } \eta < 0 \end{cases} \quad (2.2-23)$$

and

$$h_e(\eta) = 1 - h_f(\eta) \quad (2.2-24)$$

The state equations of the SSM model with the modified distribution of the percolation rate to the lower zone can be written as:

$$\begin{aligned} \dot{x}_1 = & \left(u_1 - u_2 \frac{x_1}{x_1^0} \right) [h_e(x_1 - x_1^0) + h_f(x_1 - x_1^0) h_f(u_2 - u_1)] \\ & \times \left[h_e\left(\frac{x_2}{x_2^0} - \frac{x_1}{x_1^0}\right) + h_f\left(\frac{x_2}{x_2^0} - \frac{x_1}{x_1^0}\right) h_f(g') \right] \\ & + \frac{x_1^0}{x_1^0 + x_2^0} \left[u_1 - u_2 \frac{x_1}{x_1^0} - d_u x_2 - p \right] h_f\left(\frac{x_2}{x_2^0} - \frac{x_1}{x_1^0}\right) h_e(g') \end{aligned} \quad (2.2-25)$$

$$\begin{aligned} \dot{x}_2 = & [(u_1 - u_2) h_f(x_1 - x_1^0) h_e(u_2 - u_1) - d_u x_2 - p] \\ & \times \{h_e(x_2 - x_2^0) + h_f(x_2 - x_2^0) \\ & \times h_f[d_u x_2^0 + p - (u_1 - u_2) h_f(x_1 - x_1^0) h_e(u_2 - u_1)]\} \\ & \times \left[h_e\left(\frac{x_2}{x_2^0} - \frac{x_1}{x_1^0}\right) + h_f\left(\frac{x_2}{x_2^0} - \frac{x_1}{x_1^0}\right) h_f(g') \right] \\ & + \frac{x_2^0}{x_1^0 + x_2^0} \left[u_1 - u_2 \frac{x_1}{x_1^0} - d_u x_2 - p \right] h_f\left(\frac{x_2}{x_2^0} - \frac{x_1}{x_1^0}\right) h_e(g') \end{aligned} \quad (2.2-26)$$

$$\begin{aligned} \dot{x}_3 = & \left[-u_2(1 - x_1/x_1^0) \frac{x_3}{x_1^0 + x_3^0} + (1 - p_f)\tilde{p} \right] \\ & \times [h_e(x_3 - x_3^0) + h_f(x_3 - x_3^0) h_f(m)] [h_e(w) + h_f(w) h_e(g'')] \\ & + \left[-u_2(1 - x_1/x_1^0) \frac{x_3}{x_1^0 + x_3^0} + z \right] \end{aligned}$$

$$\times [h_e(x_3 - x_3^0) + h_f(x_3 - x_3^0) h_f(m)] h_f(w) h_f(g'') \quad (2.2-27)$$

$$\begin{aligned} \dot{x}_4 = & \left[-d'_l x_4 + d'_l x_4^0 \frac{x_2}{x_2^0} + \frac{x_4^0 - x_4}{x_4^0 - x_4 + x_5^0 - x_5} p_f \tilde{p} \right] \\ & \times [h_e(x_3 - x_3^0) + h_f(x_3 - x_3^0) h_f(m)] [h_e(w) + h_f(w) h_e(g'')] \\ & + \left[-d'_l x_4 + d'_l x_4^0 \frac{x_2}{x_2^0} + \frac{x_4^0 - x_4}{x_4^0 - x_4 + x_5^0 - x_5} (\tilde{p} - z) \right] \\ & \times [h_e(x_3 - x_3^0) + h_f(x_3 - x_3^0) h_f(m)] h_f(w) h_f(g'') \\ & + \left\{ -d'_l x_4 + d'_l x_4^0 \frac{x_2}{x_2^0} + \frac{x_4^0 - x_4}{x_4^0 - x_4 + x_5^0 - x_5} \left[\tilde{p} - u_2 (1 - x_1/x_1^0) \frac{x_3}{x_1^0 + x_3^0} \right] \right\} \\ & \times h_f(x_3) h_e(m) \quad (2.2-28) \end{aligned}$$

$$\begin{aligned} \dot{x}_5 = & \left[-d''_l x_5 + d''_l x_5^0 \frac{x_2}{x_2^0} + \frac{x_5^0 - x_5}{x_4^0 - x_4 + x_5^0 - x_5} p_f \tilde{p} \right] \\ & \times [h_e(x_3 - x_3^0) + h_f(x_3 - x_3^0) h_f(m)] [h_e(w) + h_f(w) h_e(g'')] \\ & + \left[-d''_l x_5 + d''_l x_5^0 \frac{x_2}{x_2^0} + \frac{x_5^0 - x_5}{x_4^0 - x_4 + x_5^0 - x_5} (\tilde{p} - z) \right] \\ & \times [h_e(x_3 - x_3^0) + h_f(x_3 - x_3^0) h_f(m)] h_f(w) h_f(g'') \\ & + \left\{ -d''_l x_5 + d''_l x_5^0 \frac{x_2}{x_2^0} + \frac{x_5^0 - x_5}{x_4^0 - x_4 + x_5^0 - x_5} \left[\tilde{p} - u_2 (1 - x_1/x_1^0) \frac{x_3}{x_1^0 + x_3^0} \right] \right\} \\ & \times h_f(x_3) h_e(m) \quad (2.2-29) \end{aligned}$$

$$\begin{aligned}
 \dot{x}_6 &= (u_1 - u_2) h_f(x_1 - x_1^0) - u_2(1 - x_1/x_1^0) \frac{x_6}{x_1^0 + x_3^0} \\
 &\quad - (u_1 - u_2) \left(\frac{x_6}{x_3^0}\right)^2 h_f(x_1 - x_1^0) \\
 &\quad - (u_1 - u_2 - d_u x_2^0 - p) \left[1 - \left(\frac{x_6}{x_3^0}\right)^2\right] h_f(x_1 - x_1^0) h_f(x_2 - x_2^0)
 \end{aligned}
 \tag{2.2-30}$$

In the above equations u_1 and u_2 stand for the instantaneous precipitation and potential evapotranspiration demand rates, respectively. In addition

$$\begin{aligned}
 g' &= \frac{1}{x_1^0} \left(u_1 - u_2 \frac{x_1}{x_1^0}\right) [h_e(x_1 - x_1^0) + h_f(x_1 - x_1^0) h_f(u_2 - u_1)] \\
 &\quad - \frac{1}{x_2^0} [(u_1 - u_2) h_f(x_1 - x_1^0) h_e(u_2 - u_1) - d_u x_2 - p] \\
 &\quad \times \{h_e(x_2 - x_2^0) + h_f(x_2 - x_2^0)\} \\
 &\quad \times h_f[d_u x_2^0 + p - (u_1 - u_2) h_f(x_1 - x_1^0) h_e(u_2 - u_1)]
 \end{aligned}
 \tag{2.2-31}$$

$$w = (1 - r)(1 - x_3/x_3^0) - \left[1 - \frac{x_4 + x_5}{x_4^0 + x_5^0}\right]
 \tag{2.2-32}$$

$$\begin{aligned}
 z &= \frac{1}{x_3^0 + (1 - r)(x_4^0 + x_5^0)} \left\{ (1 - r) (x_4^0 + x_5^0) u_2 (1 - x_1/x_1^0) \frac{x_3}{x_1^0 + x_3^0} \right. \\
 &\quad \left. + x_3^0 (p - d'_l x_4 - d''_l x_5) \right\}
 \end{aligned}
 \tag{2.2-33}$$

$$g'' = z - (1 - p_f)\tilde{p} \quad (2.2-34)$$

and

$$m = u_2(1 - x_1/x_1^0) \frac{x_3}{x_1^0 + x_3^0} - (1 - p_f)\tilde{p} \quad (2.2-35)$$

The propagation of state values in the simulation model and the EKF technique are both based in successive linear approximations to the state-equations. For a short time interval the nonlinear vector function \underline{F}_c in Eq. 2.2-1 is replaced by its tangent hyperplane at the point corresponding to the state value at the beginning of the time interval. The choice of the length of the time interval is discussed in Section 2.4. The inference is that the present approach to simulation and filtering imposes restrictions on the form of the state-equations: the nonlinear function \underline{F}_c must possess continuous partial derivatives with respect to all states.

The function \underline{F}_c that results from using the differential equations 2.2-25 through 2.2-30 directly in Eq. 2.2-1 does not have continuous derivatives. In fact, it is not even continuous. The discontinuities arise from the threshold values associated with the elements of the upper and lower zones as well as from the constraints on ratios of free to tension-water present in the SSM model.

Use of the EKF technique on the reduced SSM model requires modification of the state-equations 2.2-25 through 2.2-30 to eliminate the threshold discontinuities. This is a step of cardinal importance in the analysis. Some of the most essential features of the SSM model such as the supply of water to the upper-zone free-water element, the distribution of water to the lower zone and the appearance of surface runoff are critically affected by the approximation. Arbitrary smoothing

of the discontinuities in the state-equations may yield to physical inconsistency (the principle of mass conservation may be violated) and mathematical inconsistency (a solution may fail to exist).

An analogy with electric circuits was used in Ref. 5 to obtain a set of smoothed equations corresponding to the SSM model with the constraints on ratios of free to tension water removed from the model. It is shown in the Appendix that for all basins examined the constraint for the upper zone is superfluous. Even though situations in which the lower-zone constraint is activated cannot be ruled out a priori, they have not been observed in the results obtained to date. When the lower-zone constraint is introduced, the smoothed equations of the SSM model become

$$\dot{x}_1 = \underbrace{u_1}_{\text{moisture input}} - \underbrace{u_2 x_1 / x_1^0}_{\text{evapotranspiration from the upper zone}} - \underbrace{g(x_1, x_1^0)}_{\text{excess upper-zone tension-water supply}} \quad (2.2-36)$$

$$\dot{x}_2 = \underbrace{g(x_1, x_1^0)}_{\text{excess from tension-water}} - \underbrace{d_u x_2}_{\text{interflow}} - \underbrace{d'_l x_4 \frac{x_2}{x_2^0} - d''_l x_5 \frac{x_2}{x_2^0}}_{\text{percolation to lower zone}} - \tilde{p} - \underbrace{g(x_2, x_2^0)}_{\text{surface runoff}} \quad (2.2-37)$$

$$\dot{x}_3 = \underbrace{(1-p_f)\tilde{p}}_{\text{percolation supply}} - \underbrace{\frac{u_2}{x_1^0+x_3^0} (1-x_1/x_1^0)x_3}_{\text{evapotranspiration from the lower zone}} - \underbrace{g(x_3, x_3^0)}_{\text{excess lower-zone tension-water supply}}$$

$$+ \underbrace{f(z, (1-p_f)\tilde{p}) h(w)}_{\text{effect of lower-zone constraint}} \quad (2.2-38)$$

$$\dot{x}_4 = \underbrace{\frac{x_4^0-x_4}{x_4^0-x_4+x_5^0-x_5} [p_f\tilde{p} + g(x_3, x_3^0)] + d'_l x_4 \frac{x_2}{x_2^0}}_{\text{moisture supply (percolation + excess tension-water)}}$$

$$- \underbrace{d'_l x_4}_{\text{baseflow from primary}} - \underbrace{\frac{x_4^0-x_4}{x_4^0-x_4+x_5^0-x_5} f(z, (1-p_f)\tilde{p}) h(w)}_{\text{effect of lower-zone constraint}}$$

(2.2-39)

$$\dot{x}_5 = \underbrace{\frac{x_5^0-x_5}{x_4^0-x_4+x_5^0-x_5} [p_f\tilde{p} + g(x_3, x_3^0)] + d''_l x_5 \frac{x_2}{x_2^0}}_{\text{moisture supply (percolation + excess tension-water)}}$$

$$- \underbrace{d''_l x_5}_{\text{baseflow from supplementary}} - \underbrace{\frac{x_5^0-x_5}{x_4^0-x_4+x_5^0-x_5} f(z, (1-p_f)\tilde{p}) h(w)}_{\text{effect of lower-zone constraint}}$$

(2.2-40)

where w and z are given by Eqs. 2.2-32 and 2.2-33 respectively and where the functions f , g and h are given by

$$f(\eta, \tilde{\eta}) = \begin{cases} 0 & \text{if } \eta \leq \tilde{\eta} - \delta \\ \frac{(\eta + \delta - \tilde{\eta})^2}{4\delta} & \text{if } \tilde{\eta} - \delta \leq \eta \leq \tilde{\eta} + \delta \\ \eta - \tilde{\eta} & \text{if } \eta \geq \tilde{\eta} + \delta \end{cases} \quad (2.2-41)$$

$$g(\eta, \eta^0) = \begin{cases} 0 & \text{if } \eta \leq \eta^0 \\ \frac{e}{\eta^0} (\eta - \eta^0)^2 & \text{if } \eta \geq \eta^0 \end{cases} \quad (2.2-42)$$

$$h(\eta) = \begin{cases} 0 & \text{if } \eta \leq -\delta \\ \frac{(\eta + \delta/2)^2}{\delta} & \text{if } -\delta \leq \eta \leq -\delta/2 \\ 1 - \frac{(\eta - \delta/2)^2}{\delta} & \text{if } -\delta/2 \leq \eta \leq 0 \\ 1 & \text{if } \eta \geq 0 \end{cases} \quad (2.2-43)$$

where δ and e are constants, typical values of which are $\delta = 0.01$, $e = 100$. Graphs of the functions f , g and h are given in Figs. 2.2-1, 2.2-2 and 2.2-3, respectively.

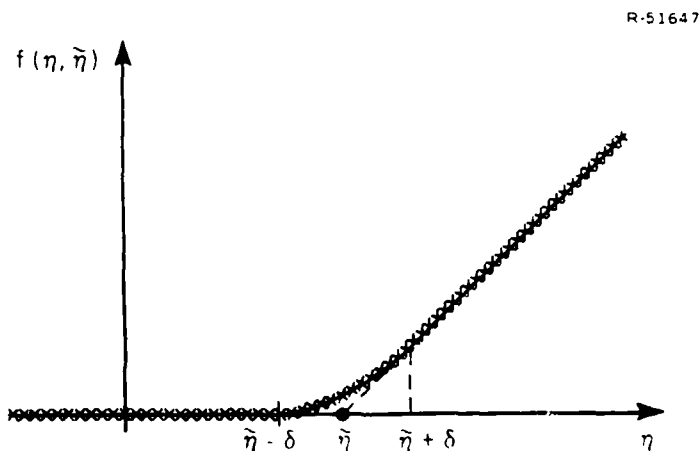


Figure 2.2-1 Graph of the Function $f(\eta, \tilde{\eta})$

R-51646

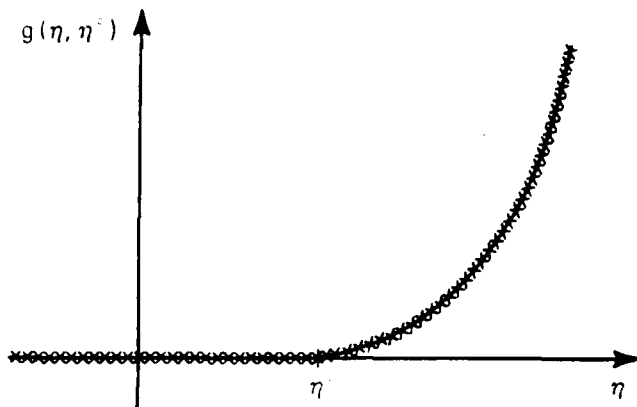


Figure 2.2-2 Graph of the Function $g(\eta, \eta^0)$

R-59516

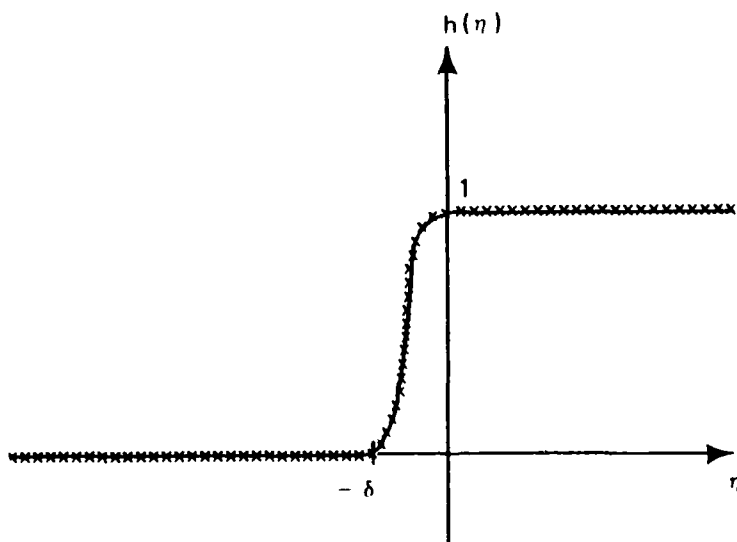


Figure 2.2-3 Graph of the Function $h(\eta)$

As a consequence of the approximation the upper bounds on the state values may, on occasion, be slightly exceeded. Examples of this behavior are given in Section 2.6.

By increasing the value of the constant e in Eq. 2.2-42, the possible excess of state values over their bounds may be reduced. Even though in the results obtained to date the lower-zone deficiency ratio, ρ , defined by

$$\rho = 1 - \frac{x_3 + x_4 + x_5}{x_3^0 + x_4^0 + x_5^0} \quad (2.2-44)$$

has always been greater than zero, there is the possibility that it may become negative during extreme flood periods. This ratio appears in the percolation function and if its value is negative, \tilde{p} given by Eq. 2.2-19 is undefined. The definition of \tilde{p} is completed by setting

$$\tilde{p} = \begin{cases} p^0 \gamma \frac{x_2}{x_2^0} \rho^\alpha & \rho \geq 0 \\ -p^0 \gamma \frac{x_2}{x_2^0} (-\rho)^\alpha & \rho \leq 0 \end{cases} \quad (2.2-45)$$

with ρ as in Eq. 2.2-44. Thus, when the lower zone deficiency ratio is negative, water is drawn out of the lower zone into the upper-zone free-water element. If the latter is full, the amount of water drawn out of the lower zone contributes to the surface runoff.

The equation for x_6 , the excess of the additional impervious storage over the upper-zone tension-water content, is

$$\dot{x}_6 = [g(x_1, x_1^0) - g(x_2, x_2^0)] [1 - (x_6/x_3^0)^2] - u_2(1 - x_1/x_1^0) \frac{x_6}{x_1^0 + x_3^0} \quad (2.2-46)$$

The equations for the moisture input u_1 in Eq. 2.2-36 are discussed in the following section.

2.2.2 Rainfall Model

The Kalman filtering formulation assumes that random inputs driving a system are solutions of stochastic differential equations. The simplest such input is the so-called first-order Markov process (Ref. 7) which is generated by the equation

$$\dot{x}_g(t) = -\beta x_g(t) + \zeta(t) \quad (2.2-47)$$

where β is a real number and ζ is a Gaussian white noise process with constant spectral density q . If x_g is interpreted as a rainfall rate with units of mm/hr, the units of ζ are mm/hr^2 , those of q are $(\text{mm/hr}^2)^2/(1/\text{hr})$, and the units of β are $1/\text{hr}$. If $\beta > 0$ a stationary solution, $x_g(t)$, to Eq. 2.2-47 exists, and its covariance function is*

$$E[x_g(t+\tau) x_g(t)] = \frac{q}{2\beta} e^{-\beta|\tau|} \quad (2.2-48)$$

The quantity $1/\beta$ is called the correlation time of the process.

The process $x_g(t)$ has a mean value of zero. Its sample functions oscillate about the time axis, and even though values much larger than the standard deviation, $(q/2\beta)^{1/2}$, have a low probability of occurrence, there is no actual upper or lower bound on the values the process may take. A precipitation model should reflect the existence of periods in which there is no rain and the fact that rainfall rates are never negative. Thus, Eq. 2.2-47, per se, does not constitute an appropriate precipitation model in a simulation. However, a

* E denotes the mathematical expectation operator.

simple nonlinear transformation of the process $x_g(t)$ yields a useful precipitation model for simulation purposes. Consider the precipitation rate defined as

$$u_1(t) = \tilde{f}(x_g(t), \tilde{x}_g) \quad (2.2-49)$$

where the function \tilde{f} is given by

$$\tilde{f}(\eta, \tilde{\eta}) = \begin{cases} 0 & \text{if } \eta \leq \tilde{\eta} \\ \eta - \tilde{\eta} & \text{if } \eta \geq \tilde{\eta} \end{cases} \quad (2.2-50)$$

Whenever the values of the process x_g are less than the threshold value \tilde{x}_g , the precipitation rate is zero. If x_g is larger than \tilde{x}_g , their difference is taken as the precipitation rate. An example of a typical realization of six-hour accumulated rainfall obtained with this model is given in Fig. 2.2-4. Other examples are given in Section 2.6.

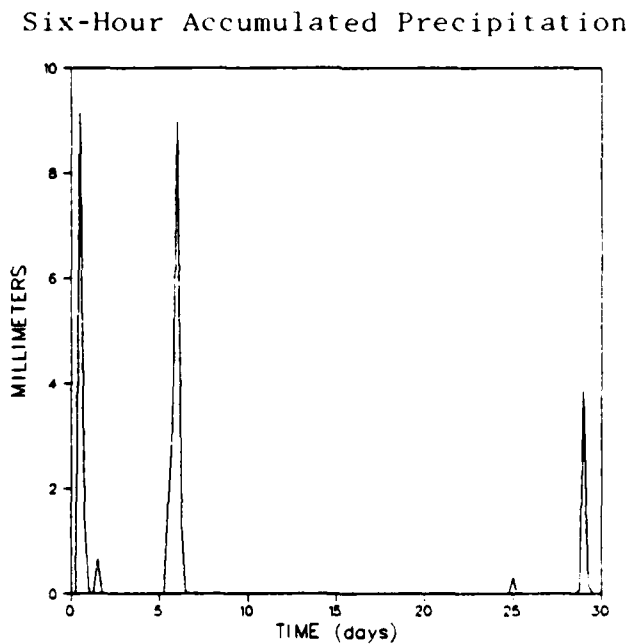


Figure 2.2-4 Example of Accumulated Precipitation Produced with the Rainfall Simulation Model

The fraction of time during which rain occurs is equal to the probability that $x_g(t)$ is greater than \tilde{x}_g and is given by

$$P[u_1(t) > 0] = 1 - \Phi(\tilde{x}_g/\sigma) \quad (2.2-51)$$

where

$$\Phi(a) = \frac{1}{\sqrt{2\pi}} \int_{-\infty}^a e^{-s^2/2} ds \quad (2.2-52)$$

is the standardized normal distribution function, and

$$\sigma = (q/2\beta)^{1/2} \quad (2.2-53)$$

is the standard deviation of $x_g(t)$. The expectation and variance of the precipitation rate given that it is actually raining can be computed to be

$$E[u_1(t) | u_1(t) > 0] = \lambda\sigma - \tilde{x}_g \quad (2.2-54)$$

$$\sigma_{u_1(t) | u_1(t) > 0}^2 = \sigma^2[1 - \lambda^2] + \lambda\sigma\tilde{x}_g \quad (2.2-55)$$

where

$$\lambda = \frac{e^{-\tilde{x}_g^2/2\sigma^2}}{1 - \Phi(\tilde{x}_g/\sigma)} \quad (2.2-56)$$

Equations 2.2-51, 2.2-54, and 2.2-55 may be used in fitting the model parameters, β , q , and \tilde{x}_g , to data records. The seasonal variation of rainfall can be modeled by letting the model parameters vary with time. For the results included in Section 2.6 corresponding to the Bird Creek basin and for the precipitation record of Fig. 2.2-4 the correlation time, $1/\beta$, was taken to be one day, $q = 0.285 \text{ (mm/hr}^2\text{)}^2 / (1/\text{hr})$ and $\tilde{x}_g = 2 \text{ mm/hr}$. And for the results corresponding to the White

River basin in Section 2.6, the parameters are $1/\beta = 12$ hr, $q = 0.015$ (mm/hr²)²/(1/hr) and $\tilde{x}_g = 0.153$ mm/hr. These parameters were chosen on the basis of NWS values of mean areal precipitation (MAP) for the Bird Creek and White River basins corresponding to the periods between April 19, 1959 and May 19, 1959 and between May 1, 1968 and June 1, 1968, respectively. These periods were chosen because the relatively high quantities of precipitation that were recorded served to illustrate the nonlinear behavior of the model in the results presented in Section 2.6.

The function \tilde{f} in Eq. 2.2-49 does not have a derivative when $x_g = \tilde{x}_g$. Since the operation of the simulation model requires the existence of derivatives for the linearization of the equations, the function \tilde{f} was replaced by f as defined by Eq. 2.2-41.

The above model is useful only for simulation purposes. It is referred as rainfall simulation model in the sequel. For reasons that were discussed in Ref. 5, this model is inappropriate for the filtering formulation.

Instead of the above simulation model, the model used in the filtering formulation is a linear rainfall rate model that has the same first and second-order moments as the rainfall simulation model. The rainfall rate is

$$u_1'(t) = \bar{u}_1 + x_g'(t) \quad (2.2-57)$$

where \bar{u}_1 is the average rainfall rate given by

$$\bar{u}_1 = P\{u_1(t) > 0\} E\{u_1(t) | u_1(t) > 0\} \quad (2.2-58)$$

or, in terms of the quantities previously introduced, by

$$\bar{u}_1 = [1 - \phi(\tilde{x}_8/\sigma)] [\lambda\sigma - \tilde{x}_8] \quad (2.2-59)$$

The process $x'_8(t)$ is a first-order Markov process satisfying the stochastic differential equation

$$\dot{x}'_8(t) = -\beta x'_8(t) + \zeta'(t) \quad (2.2-60)$$

where $\zeta'(t)$ is a Gaussian white noise process with spectral density

$$q' = \left\{ [1 - \phi(\tilde{x}_8/\sigma)] [1 + (\tilde{x}_8/\sigma)^2 - \lambda\tilde{x}_8/\sigma] - [1 - \phi(\tilde{x}_8/\sigma)]^2 [\lambda - \tilde{x}_8/\sigma]^2 \right\} q \quad (2.2-61)$$

The values of \bar{u}_1 and q' associated with the rainfall simulation models previously introduced are $\bar{u}_1 = 0.132$ mm/hr $q' = 0.0165$ (mm/hr²)²/(1/hr) for the Bird Creek basin and $\bar{u}_1 = 0.0583$ mm/hr, $q' = 0.00254$ (mm/hr²)²/(1/hr) for the White River basin. The rainfall model corresponding to Eqs. 2.2-57 and 2.2-60 is called rainfall filtering model in the sequel.

2.2.3 Equations for the Channel-Inflow and Rainfall Accumulator States

The contributors to the channel inflow accumulator are: rainfall over permanently impervious areas, direct runoff from the additional impervious area, surface runoff from the upper zone and from the additional impervious area, interflow and baseflow. To all these contributions the evapotranspiration from stream surfaces and riparian vegetation is subtracted. The equation for x_7 is easily found to be

$$\dot{x}_7 = f(y, 0) \quad (2.2-62)$$

where f is given by Eq. 2.2-41 and

$$\begin{aligned}
 y = & a_2 u_1 + a_1 [g(x_1, x_1^0) - g(x_2, x_2^0)] \left(\frac{x_6}{x_3^0} \right)^2 + (1-a_2)g(x_2, x_2^0) \\
 & + (1-a_1-a_2) \left[d_u x_2 + \frac{d'_l}{1+\mu} x_4 + \frac{d''_l}{1+\mu} x_5 \right] \\
 & - s u_2 (1 - x_1/x_1^0) \left(1 - \frac{x_3}{x_1^0 + x_3^0} \right) \quad (2.2-63)
 \end{aligned}$$

The equation for the rainfall accumulator is, simply,

$$\dot{x}_9 = u_1 \quad (2.2-64)$$

2.3 MODEL EQUATIONS - DISCRETE TIME COMPONENTS

In contrast with the equations for the continuous part of the model, those of the discrete part are linear. Let the state-space model of the unit hydrograph be (see Section 3.4.4)

$$\underline{x}_h(j) = \phi_h \underline{x}_h(j-1) + G_h u_h(j) \quad (2.3-1)$$

$$v_h(j) = H_h \underline{x}_h(j) \quad (2.3-2)$$

where \underline{x}_h is the state vector, u_h the input, v_h the discharge rate, ϕ_h the $M \times M$ one-step transition matrix, G_h the $M \times 1$ input matrix and H_h the $1 \times M$ output matrix of the unit hydrograph and where time ($j=0,1,\dots$) is measured in multiples of the unit hydrograph rate.

It is convenient to express the discharge at time j in terms of the state vector at time $j-1$. Replacing $\underline{x}_h(j)$ in Eq. 2.3-2 by the expression on the right of Eq. 2.3-1 yields

2.4 OPERATION OF THE MODEL IN THE SIMULATION MODE

Between two consecutive critical times $(v-1)k$ and vk . The equations for the continuous part of the system,

$$\dot{\underline{x}}_c(t) = \underline{F}_c(\underline{x}_c(t), t) + G_c \zeta(t) \quad (2.4-1)$$

are linearized at the operating point corresponding to time $t_0 = vk$. The resulting linear equations

$$\dot{\underline{x}}_c(t) = \tilde{\underline{F}}_c [\underline{x}_c(t) - \underline{x}_c(t_0)] + \underline{h} + G_c \zeta(t) \quad (2.4-2)$$

with

$$\tilde{\underline{F}}_c = \frac{\partial \underline{F}_c}{\partial \underline{x}_c} (\underline{x}_c(t_0), t_0) \quad (2.4-3)$$

and

$$\underline{h} = \underline{F}_c(\underline{x}_c(t_0), t_0) \quad (2.4-4)$$

are used to obtain a first approximation to the state values at time $t_0 + \Delta$ with $\Delta = vk - (v-1)k = k$.

The state vector at the end of the time interval of length Δ is the value of the solution to Eq. 2.4-2 at time $t_0 + \Delta$. This value, denoted by $\underline{x}'_c(t_0 + \Delta)$, is found to be

$$\underline{x}'_c(t_0 + \Delta) = \underline{x}_c(t_0) + (\Phi_c(\Delta) - I) \tilde{\underline{F}}_c^{-1} \underline{h} + \xi' \quad (2.4-5)$$

where I is the identity matrix, $\Phi_c(s)$ the transition matrix for an interval of length s given by

$$\Phi_c(s) = e^{\tilde{\underline{F}}_c s} \quad (2.4-6)$$

and ξ' a vector randomly chosen from the multivariate normal distribution with mean zero and covariance matrix

$$Q = q \int_0^{\Delta} \phi_c(\Delta-s) G_c G_c^T \phi_c^T(\Delta-s) ds \quad (2.4-7)$$

The vector ξ' accounts for the contribution of the random input, ζ , of the rainfall simulation model to the change in the state values during the time interval of length Δ .

Because of the strong nonlinearities present in the model, it is possible that the behavior of the linearized system, Eq. 2.4-2, departs considerably from that of the nonlinear system, Eq. 2.4-1, during the time of propagation; i.e., the length of the time interval, Δ , may be inappropriately large for a valid approximation. In order to avoid this difficulty, the length of the time interval for propagation of the linear system is chosen adaptively. The simulation utilizes a nominal step length of $\Delta = k$ hr, but if any of a collection of inequalities, $\underline{W}(\underline{x}_c, \underline{x}'_c) \leq \underline{0}$, is violated, the length of the time interval is halved and propagation is attempted anew. When propagation for a subinterval is successfully completed, Eq. 2.4-1 is linearized at the new operating point, Δ is set equal to the time step necessary to reach the next critical time and the procedure is repeated.

Four inequalities were used in the simulation. The first two place limits on the changes in the contents of the upper-zone tension-water and free-water elements; these differences are not allowed to exceed 1 mm^{*}; i.e.,

$$|x_1(t_0) - x_1(t_0 + \Delta)| \leq 1 \quad (2.4-8)$$

*This amount is a conservative choice. Good results were obtained with its use.

$$|x_2(t_0) - x_2'(t_0 + \Delta)| \leq 1 \quad (2.4-9)$$

The third inequality concerns the percolation. It is required that

$$\frac{\tilde{p}(\underline{x}(t_0)) + \tilde{p}(\underline{x}'(t_0 + \Delta))}{2} \Delta \leq 1 \quad (2.4-10)$$

The expression on the left in Inequality 2.4-10 is Simpson's integration formula applied to the instantaneous percolation rate, \tilde{p} . Thus, 2.4-10 can be interpreted as a limit on the total percolation during the time interval of length Δ . The last inequality sets a limit on the amount of surface runoff:

$$\frac{[g(x_2(t_0), x_2^0) + g(x_2'(t_0 + \Delta), x_2^0)]}{2} \Delta \leq 1 \quad (2.4-11)$$

When the critical time vk is reached, the last value of the continuous state vector, \underline{x}_c , obtained by the propagation of Eq. 2.4-1 is interpreted as $\underline{x}_c[(vk)^-]$. The corresponding value of the discrete state is $\underline{x}_d[(vk)^-] = \underline{x}_d[((v-1)k)^+]$. The discrete part of the model is updated next according to

$$\underline{x}_d[(vk)^0] = A \underline{x}_d[(vk)^-] + B \underline{x}_c[(vk)^-] \quad (2.4-12)$$

where the matrices A and B are given by Eqs. 2.3-5 and 2.3-6.

At this point in the simulation the output measurements, Eqs. 2.2-7 and 2.2-8, are evaluated. It is convenient to introduce a matrix notation for this computation. Equations 2.2-7 and 2.2-8 can be represented as

$$y(vk) = H(vk) \underline{x}[(vk)^0] + \xi(vk) \quad (2.4-13)$$

where the quantities \underline{y} , H and $\underline{\xi}$ are given by

$$\underline{y} = \begin{pmatrix} y_1 \\ y_2 \end{pmatrix} \quad (2.4-14)$$

$$H = \begin{pmatrix} \overbrace{0 \dots 0}^8 & 1 & \overbrace{0 \dots 0}^M & 0 \\ \overbrace{0 \dots 0}^8 & 0 & \overbrace{0 \dots 0}^M & 1/m\ell \end{pmatrix} \quad (2.4-15)$$

$$\underline{\xi} = \begin{pmatrix} \xi_1 \\ \xi_2 \end{pmatrix} \quad (2.4-16)$$

when v is a multiple of $m\ell$; i.e., when there are rainfall and discharge measurements, and given by

$$\underline{y} = y_1 \quad (2.4-17)$$

$$H = \begin{pmatrix} \overbrace{0 \dots 0}^8 & 1 & \overbrace{0 \dots 0}^M & 0 \end{pmatrix} \quad (2.4-18)$$

$$\underline{\xi} = \xi_1 \quad (2.4-19)$$

when v is not a multiple of $m\ell$ but is a multiple of ℓ , i.e., when there is only a rainfall measurement. If v is not a multiple of ℓ there are no measurements computed. In the above equations ξ_1 and ξ_2 represent measurement noise. Their values are independent samples from the normal distribution with zero mean and variances σ_1^2 and σ_2^2 , respectively.

Since the filter is not in operation, the definition of time $(vk)^+$ is superfluous in the simulation mode. Equivalently,

$$\underline{x}[(vk)^+] = \underline{x}[(vk)^0] \quad (2.4-20)$$

As a final step of the state propagation corresponding to a critical time, the contents of the appropriate accumulators are reset to zero, i.e.,

$$x_7[(vk)^r] = 0 \quad ; \quad v = 0, 1, 2, \dots \quad (2.4-21)$$

$$x_9[(vk)^r] = 0 \quad ; \quad v = 0, \ell, 2\ell, \dots \quad (2.4-22)$$

$$x_{10+M}[(vk)^r] = 0 \quad ; \quad v = 0, m\ell, 2m\ell, \dots \quad (2.4-23)$$

and propagation of the continuous part of the state vector to the next critical time begins.

2.5 OPERATION OF THE MODEL IN THE FILTERING MODE

The operation of the filter follows in the same lines as the simulation procedure described in Section 2.4. The system equations are identical to the equations used in the simulation mode except that the rainfall filtering model is used instead of the rainfall simulation model. The state estimates, $\hat{\underline{x}}$, are propagated according to the equations

$$\dot{\hat{\underline{x}}}_c(t) = \underline{F}_c(\hat{\underline{x}}_c(t), t) \quad ; \quad t \in ((v-1)k, vk) \quad (2.5-1)$$

$$\dot{\hat{\underline{x}}}_d(t) = 0 \quad ; \quad t \in ((v-1)k, vk) \quad (2.5-2)$$

$$\hat{\underline{x}}_d[(vk)^0] = A \hat{\underline{x}}_d[(vk)^-] + B \hat{\underline{x}}_c[(vk)^-] \quad (2.5-3)$$

However, in order to compute the Kalman gains, it is necessary to propagate the state error covariance matrix, $P(t)$, defined by

$$P(t) = E\{[\hat{\underline{x}}(t) - \underline{x}(t)][\hat{\underline{x}}(t) - \underline{x}(t)]^T\} \quad (2.5-4)$$

Following the subdivision of the state-vector into its continuous and discrete parts, \underline{x}_c and \underline{x}_d , define

$$P_c(t) = E\{[\hat{\underline{x}}_c(t) - \underline{x}_c(t)][\hat{\underline{x}}_c(t) - \underline{x}_c(t)]^T\} \quad (2.5-5)$$

$$P_{cd}(t) = E\{[\hat{\underline{x}}_c(t) - \underline{x}_c(t)][\hat{\underline{x}}_d(t) - \underline{x}_d(t)]^T\} \quad (2.5-6)$$

$$P_{dc}(t) = P_{cd}^T(t) \quad (2.5-7)$$

$$P_d(t) = E\{[\hat{\underline{x}}_d(t) - \underline{x}_d(t)][\hat{\underline{x}}_d(t) - \underline{x}_d(t)]^T\} \quad (2.5-8)$$

Thus $P(t)$ is partitioned as

$$P(t) = \begin{pmatrix} P_c(t) & | & P_{cd}(t) \\ \hline P_{dc}(t) & | & P_d(t) \end{pmatrix} \quad (2.5-9)$$

The operation of the filter is best described in the form of an algorithm.

Filtering Algorithm

1. [Initialize elapsed time, state-estimates and error covariance matrix]

$$\text{Set } t \leftarrow 0, \hat{\underline{x}} \leftarrow \hat{\underline{x}}(0), P_c \leftarrow P_c(0), P_{cd} \leftarrow P_{cd}(0), P_d \leftarrow P_d(0)$$

2. [Initialize step size, Δ , and time to reach next critical time, $\bar{\Delta}$.]

$$\text{Set } \Delta \leftarrow k, \bar{\Delta} \leftarrow k$$

3. [Linearize Eq. 2.5-1 about current operating point]

$$\text{Compute } \tilde{F}_c = \frac{\partial \underline{F}_c}{\partial \underline{x}_c}(\hat{\underline{x}}_c, t), \underline{h} = \underline{F}_c(\hat{\underline{x}}_c, t)$$

4. [Evaluate transition matrix]

$$\text{Compute } \phi_c = e^{\tilde{F}_c \Delta}$$

5. [Compute tentative state-estimate]
 Set $\hat{\underline{x}}'_c \leftarrow \hat{\underline{x}}_c + (\phi_c - I) \tilde{F}_c^{-1} \underline{h}$
6. [Verify suitability of step size]
 If none of the inequalities $\underline{W}(\hat{\underline{x}}_c, \hat{\underline{x}}'_c) \leq \underline{0}$ is violated go to step 8 (\underline{W} is defined by Eqs. 2.4-8 through 2.4-11)
7. [Redefine step size]
 Set $\Delta \leftarrow \Delta/2$ and go to step 4
8. [Update state-estimate, elapsed time and time to next critical time]
 Set $\hat{\underline{x}}_c \leftarrow \hat{\underline{x}}'_c$, $t \leftarrow t + \Delta$, $\tilde{\Delta} \leftarrow \tilde{\Delta} - \Delta$
9. [Propagate covariance matrix to account for continuous transition]
 Set $P_c \leftarrow \phi_c P_c \phi_c^T + Q$, $P_{cd} \leftarrow \phi_c P_{cd}$
 where Q is the matrix defined by the expression on the right of Eq. 2.4-7.
10. [Verify if critical time has been reached]
 If $\tilde{\Delta} \neq 0$ set $\Delta \leftarrow \tilde{\Delta}$ and go to step 3
11. [Propagate discrete part of state vector]
 Compute state vector at time t^0 by setting

$$\hat{\underline{x}}_d \leftarrow A \hat{\underline{x}}_d + B \hat{\underline{x}}_c$$
12. [Propagate covariance matrix to account for discrete transition]
 Set $P_d \leftarrow A P_d A^T + B P_{cd} A^T + (B P_{cd} A^T)^T + B P_c B^T$
 and $P_{cd} \leftarrow P_{cd} A^T + P_c B^T$
 in the above order
13. [Determine if there is a precipitation measurement]
 If t is not a multiple of ℓk then
 13.1 [Reset channel inflow accumulator]
 State at time t^r obtained by setting $\hat{x}_7 = 0$

13.2 [Modify covariance matrix to reflect reset]

Set the seventh row and column of P equal to zero

13.3 Go to step 2

14. [Determine if there is a discharge measurement]

If t is a multiple of mΔk set FLAG ← TRUE

If t is not a multiple of mΔk set FLAG ← FALSE

(FLAG = TRUE indicates the presence of a discharge measurement)

15. [Define measurement equations]

If FLAG = TRUE define H as in Eq. 2.4-15 and set

$$\underline{y} \leftarrow \begin{pmatrix} y_1 \\ y_2 \end{pmatrix}, \quad R \leftarrow \begin{pmatrix} \sigma_1^2 & 0 \\ 0 & \sigma_2^2 \end{pmatrix}$$

If FLAG = FALSE define H as in Eq. 2.4-18 and set

$$\underline{y} \leftarrow y_1 \quad R \leftarrow \sigma_1^2$$

(y_1 and y_2 are the values of the rainfall and mean discharge measurements, R is the covariance matrix of the errors in the measurements)

16. [Compute Kalman gains]

Evaluate $K = P H^T (HPH^T + R)^{-1}$

17. [Perform Kalman update on state-estimate]

State at time t^+ is obtained by setting

$$\underline{\hat{x}} \leftarrow \underline{\hat{x}} + K[\underline{y} - H\underline{\hat{x}}]$$

18. [Modify covariance matrix to account for Kalman update]

Set $P \leftarrow P - KHP$

19. [Reset accumulators]

19.1 Set $\hat{x}_7 \leftarrow 0$ and $\hat{x}_9 \leftarrow 0$

19.2 If FLAG = TRUE set $\hat{x}_{10+M} \leftarrow 0$

20. [Modify covariance matrix to account for reset]
 - 20.1 Set the seventh and ninth rows and columns of P equal to zero
 - 20.2 If FLAG = TRUE set the last row and column of P equal to zero
21. [Continue operation]
Go to step 2

2.6 RESULTS

The parameters of the SSM model for the Bird Creek and White River basins were used in testing the behavior of the simulation and filtering algorithms described in Sections 2.4 and 2.5.

In all instances data were generated using the model in the simulation mode. These data were then used by the filter to obtain six-hour lead forecasts under several assumptions on the filter parameters. The results so obtained were then compared to the true values obtained in the simulation. Excellent agreement between true and predicted discharge was obtained in all test cases.

The Bird Creek basin model was used to investigate the sensitivity of the filter behavior to changes in the measurement error covariance matrix, R, and to changes in the initial state error covariance matrix, P(0). The White River basin model was used to illustrate the filter response for a different set of SSM parameters.

The parameters of the SSM model for the Bird Creek and White River basin are listed in Table 2.6-1. In addition

TABLE 2.6-1
SSM MODEL PARAMETERS FOR BIRD CREEK
AND WHITE RIVER BASINS

PARAMETER	BIRD CREEK	WHITE RIVER
x_1^0 (mm)	120	50
x_2^0 (mm)	15	30
x_3^0 (mm)	160	250
x_4^0 (mm)	140	80
x_5^0 (mm)	14	170
d_u (1/hr)	1.486E-2	1.486E-2
d'_l (1/hr)	5.452E-4	5.875E-4
d''_l (1/hr)	5.612E-3	2.578E-3
γ	48	25
α	2.1	4.0
P_f	0.02	0.4
μ	3.55	0.0
a_1	0.17	0.0
a_2	0.001	0.0
r	0.3	0.3
s	0.0	0.2

to the parameters given in the table, constant rates of $u_2 = 1.375E-2$ mm/hr and $u_2 = 4.583E-2$ mm/hr were used for the instantaneous potential evapotranspiration demand for the Bird Creek and White River basins, respectively.

Fifth-order state-space models for the six-hour unit hydrographs for the Bird Creek and White River basins were used. These models were obtained with the subroutine REDO-UHG (Ref. 1) delivered to NOAA/NWS for use as a constituent of the Version 5.0 NWSRFS Forecast Component. The theoretical basis underlying the operation of this subroutine is described in Chapter 3 of this report. Figure 2.6-1 compares the original Bird Creek hydrograph (solid line) with the approximation used in the simulation and filtering algorithms (dashed line). The White River basin hydrograph (Fig. 2.6-2) contains five lags and, thus, agrees exactly with the fifth-order state-space model used in the simulation and filtering algorithms.

For the Bird Creek basin the initial state values were chosen arbitrarily as $x_1(0) = 100$ mm, $x_2(0) = 12$ mm, $x_3(0) = 130$ mm, $x_4(0) = 110$ mm, $x_5(0) = 11$ mm, and $x_i(0) = 0$ for $i > 5$. These values were the same in the simulation and filtering operations.

For the Bird Creek model, different random number sequences were used in testing the sensitivity of the filter response to changes in the measurement and initial state error covariance matrices. The particular precipitation records included in this section are not typical of the results produced by the rainfall simulation model. They were chosen because the substantial amounts of rainfall obtained with the particular random number sequences excite extreme dynamical responses in the system and serve to illustrate the behavior of the filter in the nonlinear operating region for the upper-zone elements.

The precipitation record of Fig. 2.6-3 for the Bird Creek basin was used in determining differences in filter response to changes in the measurement error covariance matrix, R . This precipitation record is referred as BCl in the sequel.

Bird Creek Unit Hydrographs

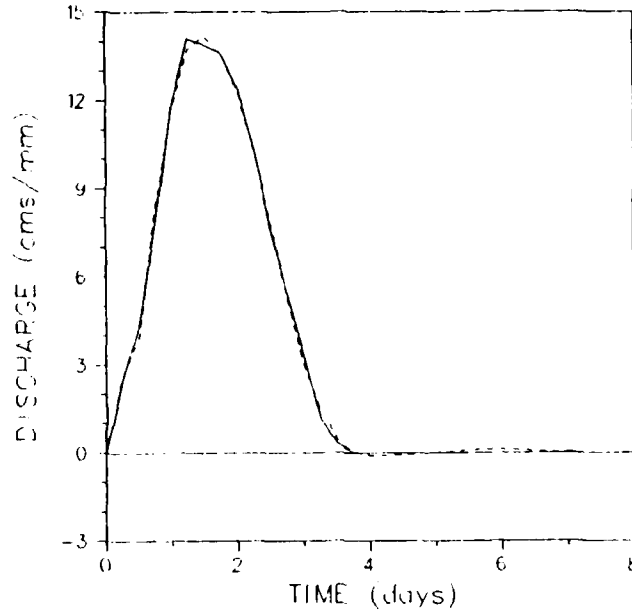


Figure 2.6-1 Six-Hour Unit Hydrographs for Bird Creek: Original Hydrograph (Solid Line) and Fifth-Order State-Space Approximation (Dashed Line)

White River Unit Hydrograph

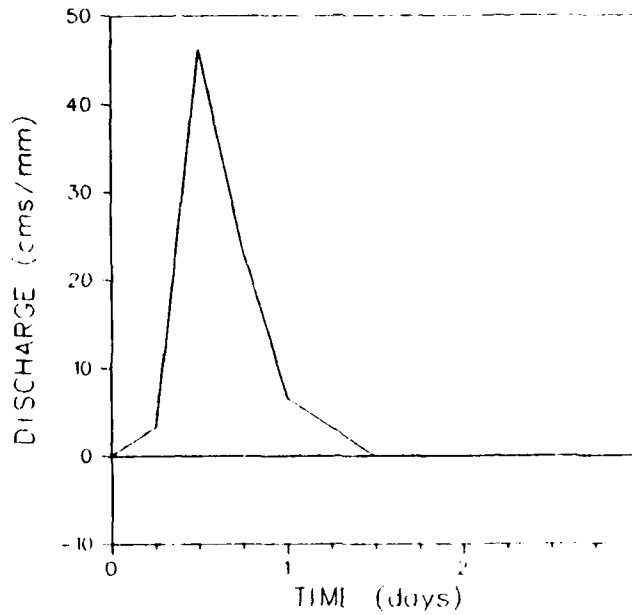


Figure 2.6-2 Six-Hour Unit Hydrograph for White River Basin

Six-Hour Accumulated Precipitation

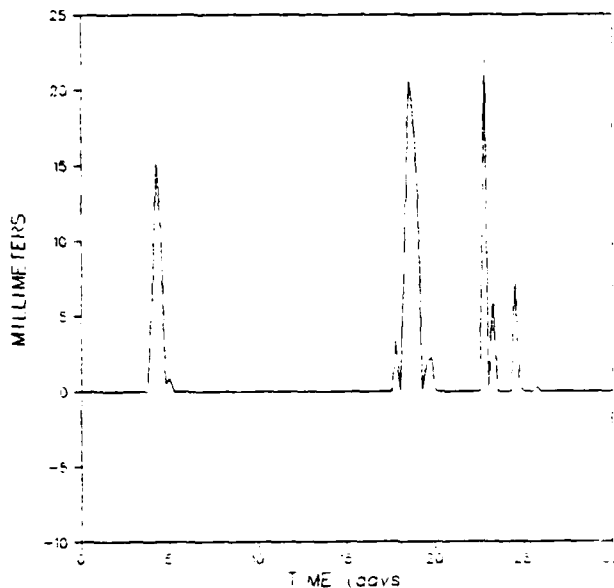


Figure 2.6-3 Precipitation Record BCl

For the comparisons of filter performance under different assumptions on the measurement noise level, simulated values of accumulated precipitation and instantaneous discharge were produced at six-hour intervals. Thus, in the notation of previous sections, the values of k , ℓ , and m were $k=6$, $\ell=1$ and $m=1$.

Results for two different measurement error covariance matrices are illustrated in Figs. 2.6-4 through 2.6-19. Solid lines represent the values obtained in the simulation while dashed lines correspond to the one-step ahead (six hour) filter prediction. Even numbered figures correspond to the measurement covariance matrix

$$R_1 = \begin{pmatrix} 0.0054 & 0 \\ 0 & 0.083 \end{pmatrix} \quad (2.6-1)$$

Upper-Zone Tension-Water Element

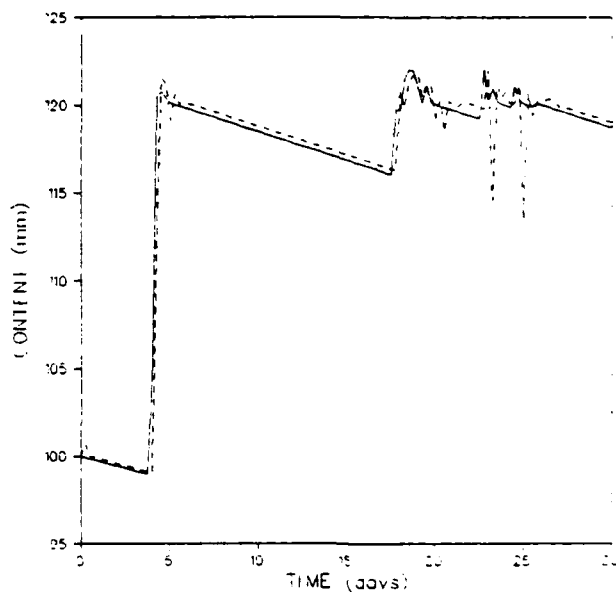


Figure 2.6-4 Upper-Zone Tension-Water Content for Precipitation Record BCl: True Values (Solid Line) and Predicted Values With Measurement Covariance R_1 (Dashed Line)

Upper-Zone Tension-Water Element

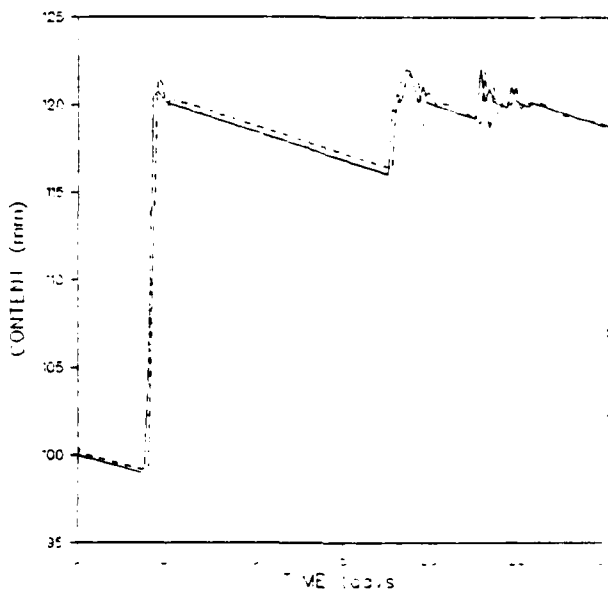


Figure 2.6-5 Upper-Zone Tension-Water Content for Precipitation Record BCl: True Values (Solid Line) and Predicted Values With Measurement Covariance R_2 (Dashed Line)

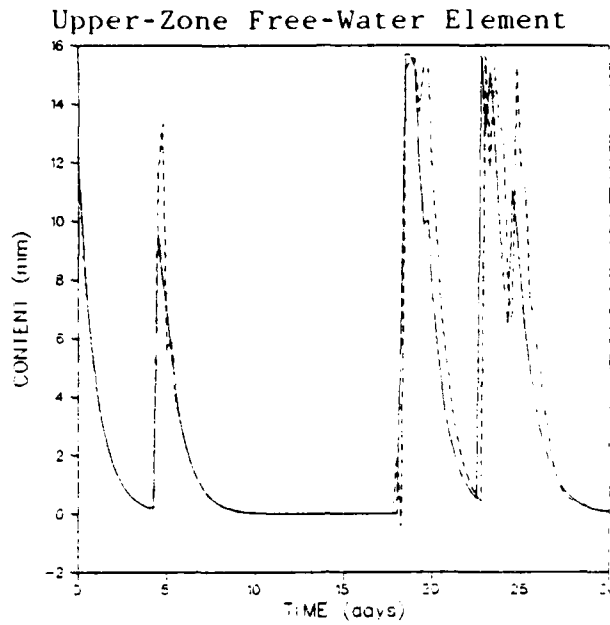


Figure 2.6-6 Upper-Zone Free-Water Content for Precipitation Record BCl: True Values (Solid Line) and Predicted Values With Measurement Covariance R_1 (Dashed Line)

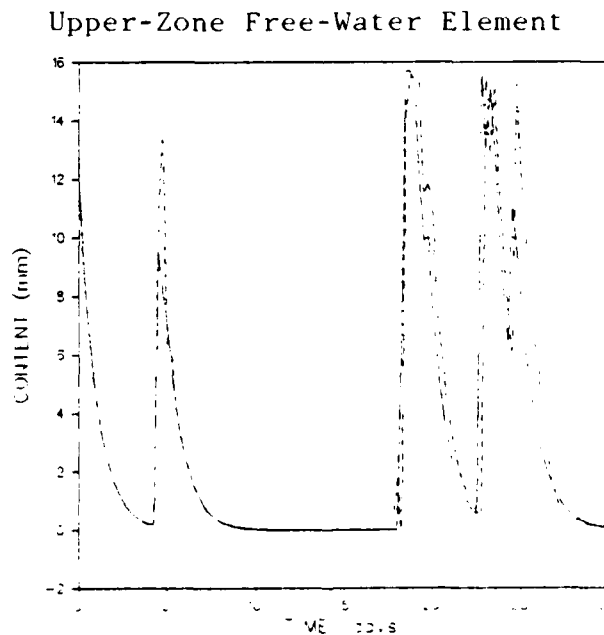


Figure 2.6-7 Upper-Zone Free-Water Content for Precipitation Record BCl: True Values (Solid Line) and Predicted Values With Measurement Covariance R_2 (Dashed Line)

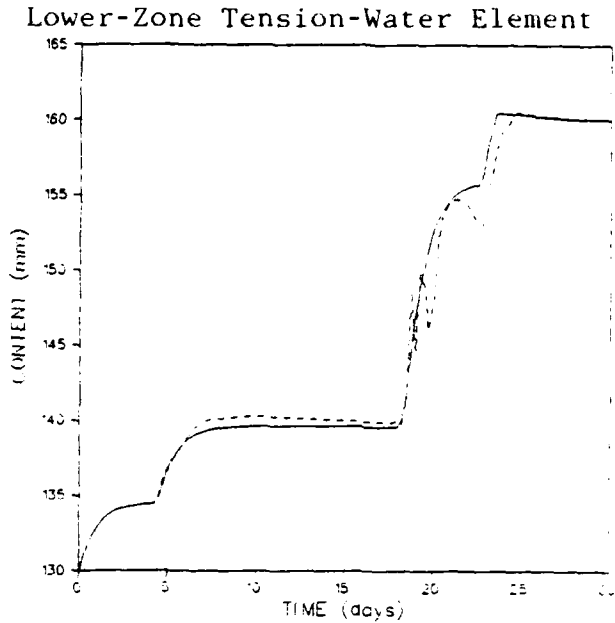


Figure 2.6-8 Lower-Zone Tension-Water Content for Precipitation Record BCl: True Values (Solid Line) and Predicted Values With Measurement Covariance R_1 (Dashed Line)

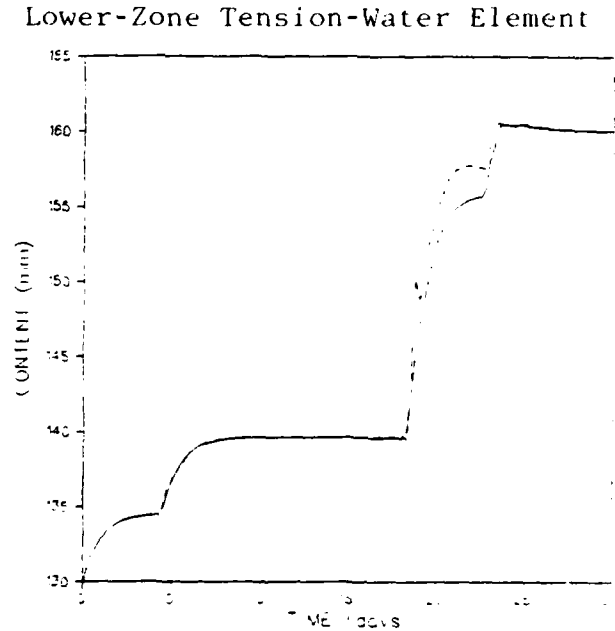


Figure 2.6-9 Lower-Zone Tension-Water Content for Precipitation Record BCl: True Values (Solid Line) and Predicted Values With Measurement Covariance R_2 (Dashed Line)

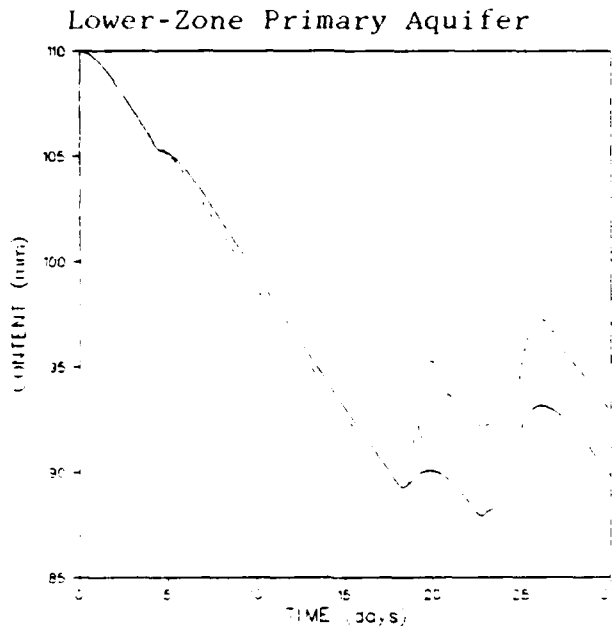


Figure 2.6-10 Lower-Zone Primary Aquifer Content for Precipitation Record BCl: True Values (Solid Line) and Predicted Values With Measurement Covariance R_1 (Dashed Line)

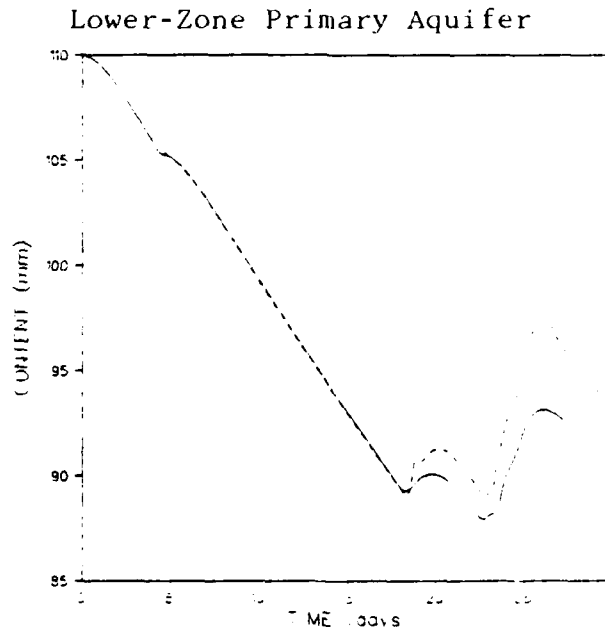


Figure 2.6-11 Lower-Zone Primary Aquifer Content for Precipitation Record BCl: True Values (Solid Line) and Predicted Values With Measurement Covariance R_2 (Dashed Line)

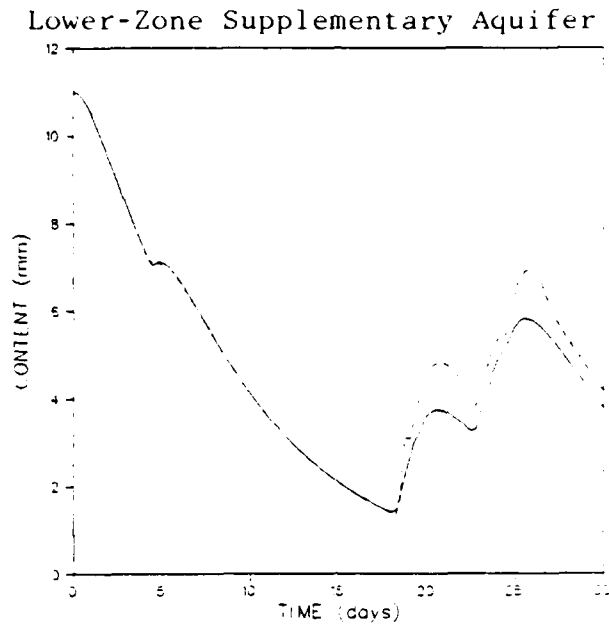


Figure 2.6-12 Lower-Zone Supplementary Aquifer Content for Precipitation Record BCl: True Values (Solid Line) and Predicted Values with Measurement Covariance R_1 (Dashed Line)

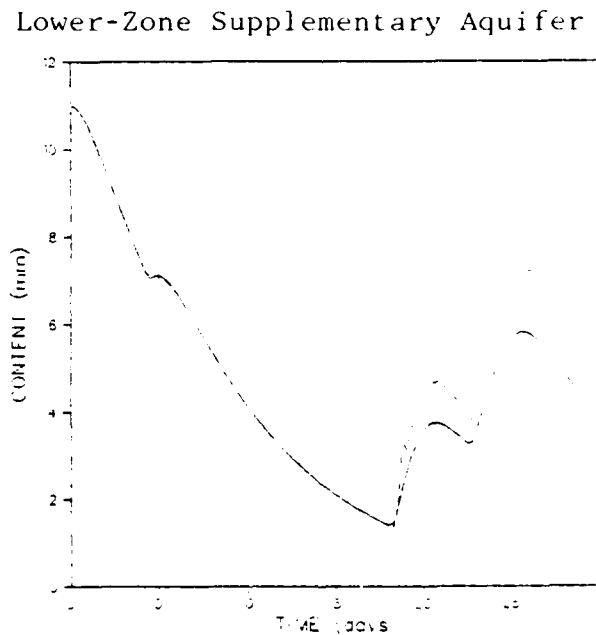


Figure 2.6-13 Lower-Zone Supplementary Aquifer Content for Precipitation Record BCl: True Values (Solid Line) and Predicted Values with Measurement Covariance R_2 (Dashed Line)

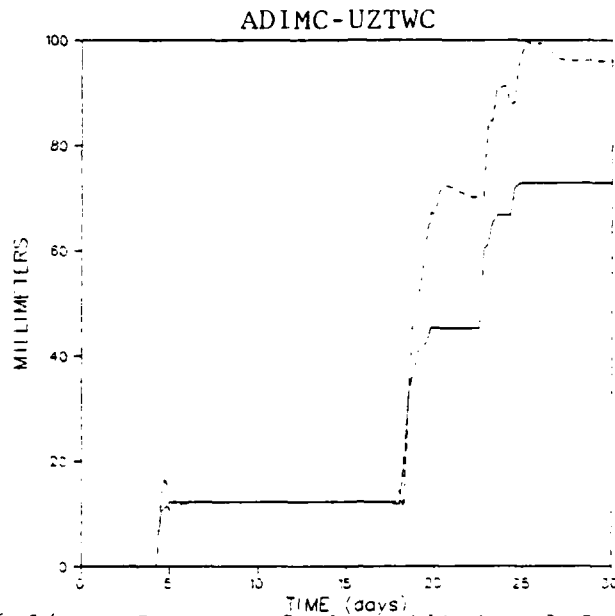


Figure 2.6-14 Excess of the Additional Impervious Area Content Over the Upper-Zone Tension-Water Content for Precipitation Record BCl: True Values (Solid Line) and Predicted Values with Measurement Covariance R_1 (Dashed Line)

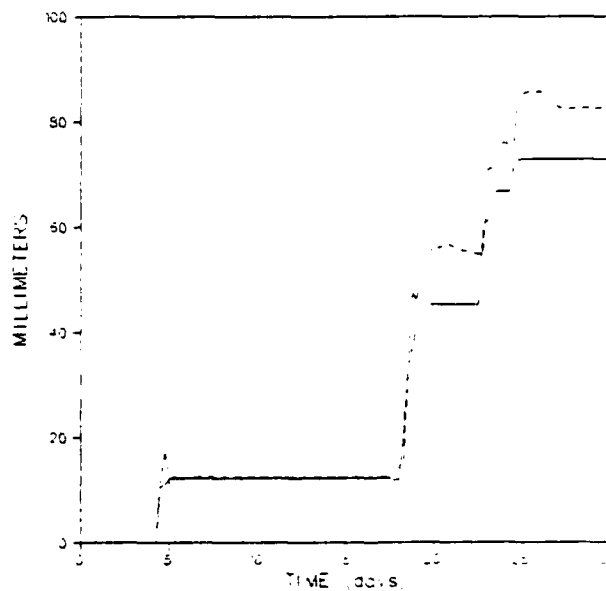


Figure 2.6-15 Excess of the Additional Impervious Area Content Over the Upper-Zone Tension-Water Content for Precipitation Record BCl: True Values (Solid Line) and Predicted Values with Measurement Covariance R_2 (Dashed Line)

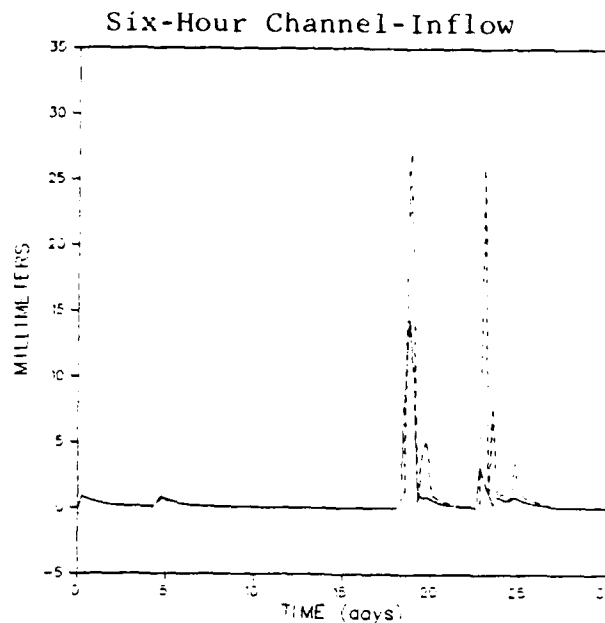


Figure 2.6-16 Six-Hour Accumulated Channel-Inflow for Precipitation Record BCI: True Values (Solid Line) and Predicted Values With Measurement Covariance R_1 (Dashed Line)

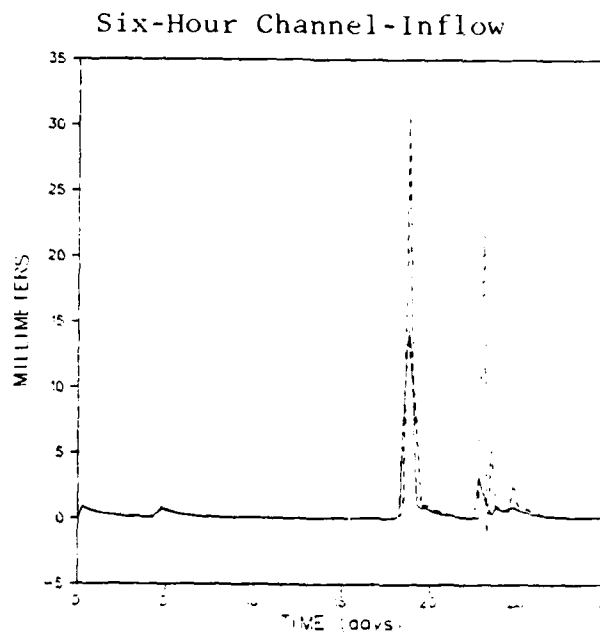


Figure 2.6-17 Six-Hour Accumulated Channel-Inflow for Precipitation Record BCI: True Values (Solid Line) and Predicted Values With Measurement Covariance R_2 (Dashed Line)

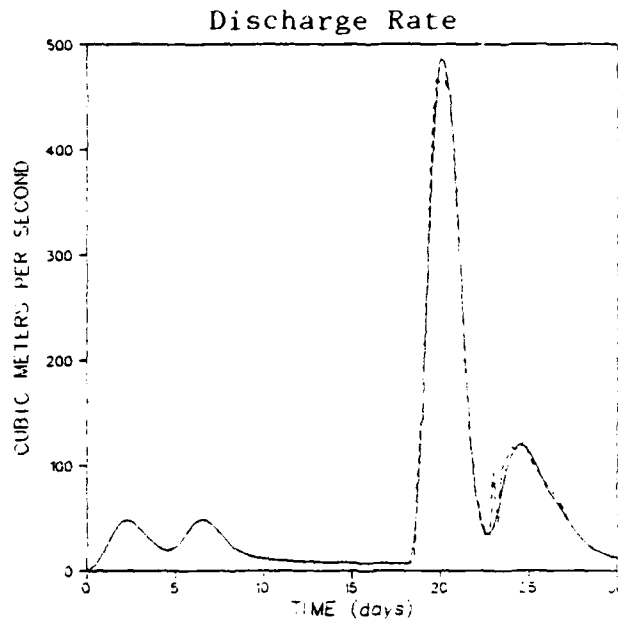


Figure 2.6-18 Instantaneous Discharge for Precipitation Record BCl: True Values (Solid Line) and Predicted Values with Measurement Covariance R_1 (Dashed Line)

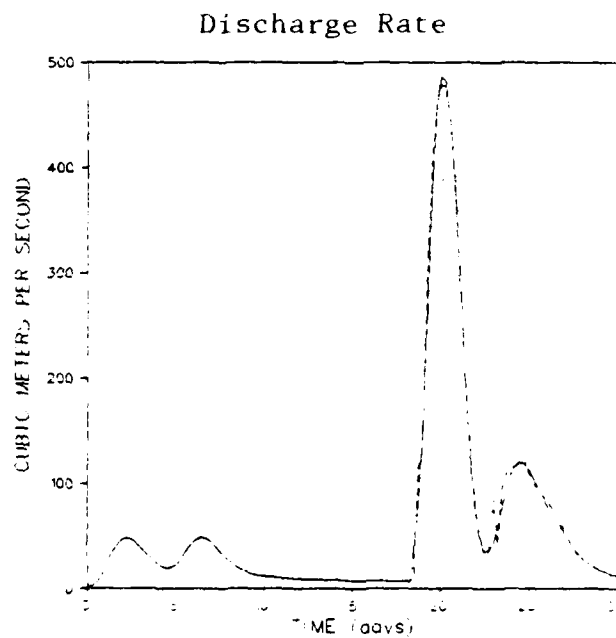


Figure 2 6-19 Instantaneous Discharge for Precipitation Record BCl: True Values (Solid Line) and Predicted Values with Measurement Covariance R_2 (Dashed Line)

The root-mean-square (rms) errors associated with R_1 are $\sigma_1 = 0.073$ mm for the precipitation measurement and $\sigma_2 = 0.29$ m³/sec for the discharge rate measurements. These values correspond to errors of round-off to the closest 1/100 of an inch for precipitation and 1 m³/sec for discharge. Odd numbered figures correspond to the covariance matrix

$$R_2 = \begin{pmatrix} 0.13 & 0 \\ 0 & 2.1 \end{pmatrix} \quad (2.6-2)$$

for which the rms errors are five times larger than those of R_1 .

The predicted values of instantaneous channel discharge obtained with the use of the covariance matrices R_1 and R_2 are presented in Figs. 2.6-18 and 2.6-19, respectively. The predicted discharge agrees better with the true values when the larger covariances are used. The rms difference between predicted and true discharge is 7.8 m³/sec for R_1 and 7.2 m³/sec for R_2 . The same type of observation applies to all states of the SSM model (Figs. 2.6-4 through 2.6-17) except for the lower-zone supplementary free-water content (Figs. 2.6-12 and 2.6-13) where the fi. obtained with the use of R_1 is slightly better than that obtained with R_2 .

The fact that larger measurement error covariances produce better results can be explained as follows: With a small measurement error covariance the measurements are presented to the filter as being extremely precise. As a consequence small differences between the predicted and measured values are heavily weighted by the filter (i.e., the Kalman gains are very large). The filter responds quickly to differences between estimated and observed values and tends to have a fast oscillatory response. This behavior is particu-

larly well exemplified in the estimates of the upper and lower zone's tension-water content (Figs. 2.6-4 and 2.6-8). Note that these oscillations happen to occur when the upper-zone tension-water element is full and in some instances (see Fig. 2.6-6) when surface runoff is being produced. When the measurement error covariance is increased, the filter places more trust in the estimates it is computing and small differences between predicted and measured values are given less emphasis. The response of the filter is somewhat slower but its overall performance is improved.

The initial state covariance matrix, $P(0)$, used in obtaining the results given in Figs. 2.6-4 through 2.6-19 was taken to be a diagonal matrix, P' , whose elements along the diagonal were $p'_{11} = 1.44 \text{ mm}^2$, $p'_{22} = 0.0225 \text{ mm}^2$, $p'_{33} = 2.56 \text{ mm}^2$, $p'_{44} = 1.96 \text{ mm}^2$, $p'_{55} = 0.0196 \text{ mm}^2$, $p'_{66} = 2.56 \text{ mm}^2$ and $p'_{ii} = 0$ for $i > 6$. These values correspond to an initial state uncertainty of 1% of the capacity of each of the elements of the SSM model.*

In order to examine the behavior of the filter for different assumptions on the initial state uncertainty, a comparison was made of the results obtained for the Bird Creek model with the use of the initial state covariance P' and those obtained with a larger covariance matrix, P'' , with diagonal elements $p''_{11} = 144 \text{ mm}^2$, $p''_{22} = 2.25 \text{ mm}^2$, $p''_{33} = 256 \text{ mm}^2$, $p''_{44} = 196 \text{ mm}^2$, $p''_{55} = 1.96 \text{ mm}^2$, $p''_{66} = 256 \text{ mm}^2$ and $p''_{ii} = 0$ for $i > 6$, corresponding to an rms uncertainty of 10% of the capacity of

*The maximum value of x_6 , the excess of the additional impervious area content over the upper-zone tension water content is x_3^c , the capacity of the lower-zone tension water element.

the states of the SSM model. Six-hour measurements of precipitation and instantaneous discharge were used by the filter. The measurement error covariance matrix was R_2 .

To prevent the state-covariance from changing significantly from its initial values before abrupt changes in the system occur, the precipitation record BC2, shown in Fig. 2.6-20, was used in the comparison. The results are presented in Figs. 2.6-21 through 2.6-36. Odd numbered figures correspond to results obtained with the initial state covariance P' , even numbered figures to those obtained with P'' . As before, true values and one-step-ahead filter predictions are indicated by solid and dashed lines, respectively.

Six-Hour Accumulated Precipitation

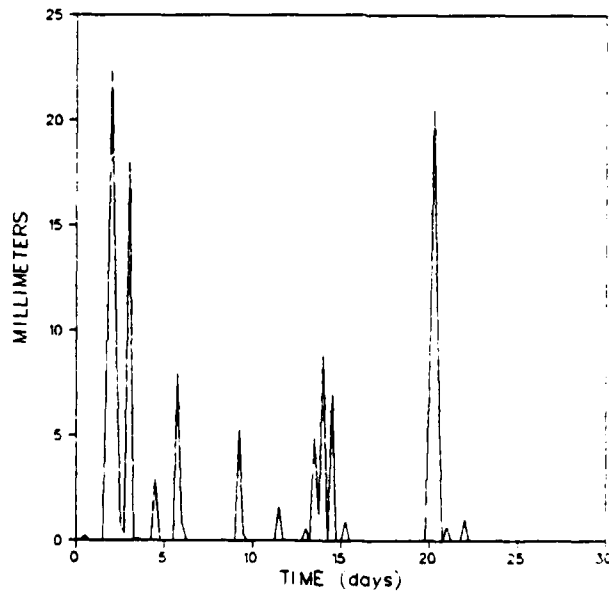


Figure 2.6-20 Precipitation Record BC2

Upper-Zone Tension-Water Element

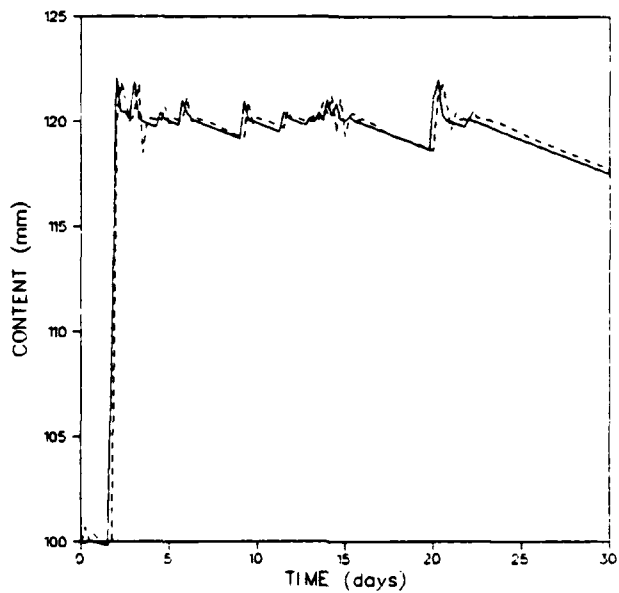


Figure 2.6-21 Upper-Zone Tension-Water Content for Precipitation Record BC2: True Values (Solid Line) and Predicted Values With $P(0) = P'$ (Dashed Line)

Upper-Zone Tension-Water Element

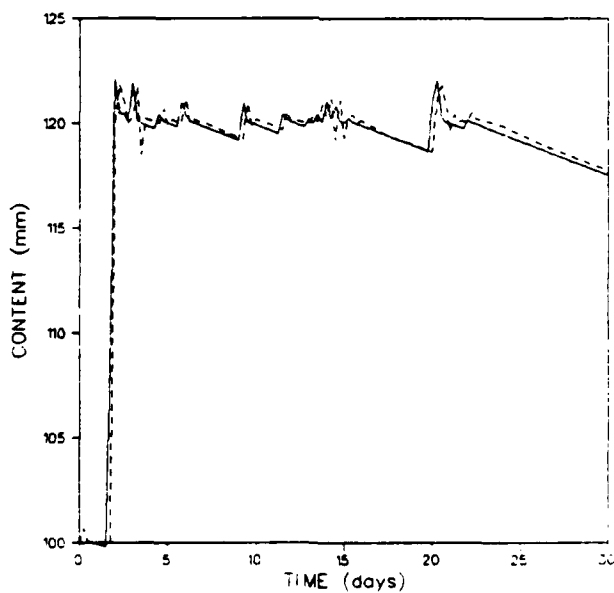


Figure 2.6-22 Upper-Zone Tension-Water Content for Precipitation Record BC2: True Values (Solid Line) and Predicted Values With $P(0) = P''$ (Dashed Line)

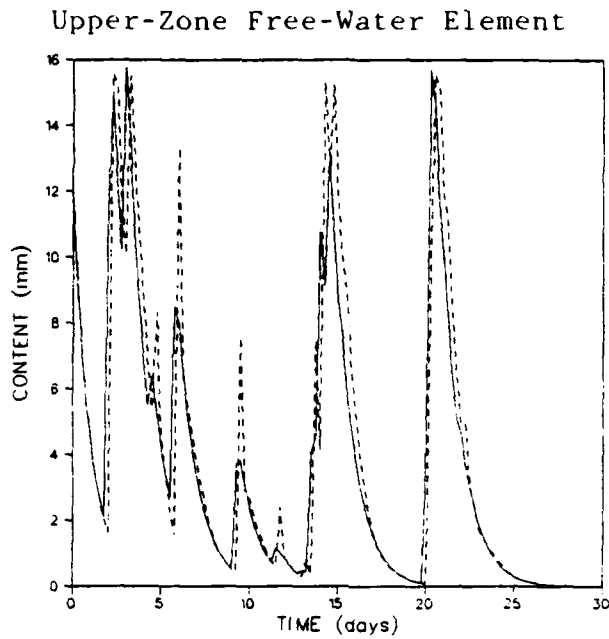


Figure 2.6-23 Upper-Zone Free-Water Content for Precipitation Record BC2: True Values (Solid Line) and Predicted Values With $P(0) = P'$ (Dashed Line)

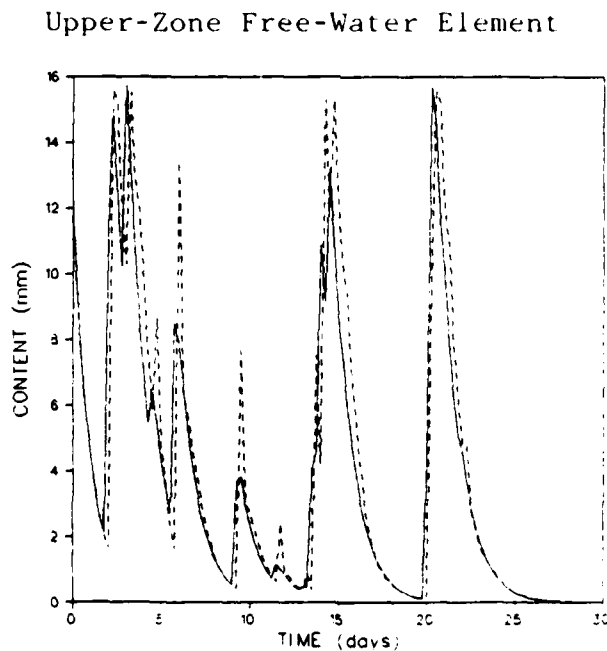


Figure 2.6-24 Upper-Zone Free-Water Content for Precipitation Record BC2: True Values (Solid Line) and Predicted Values With $P(0) = P''$ (Dashed Line)

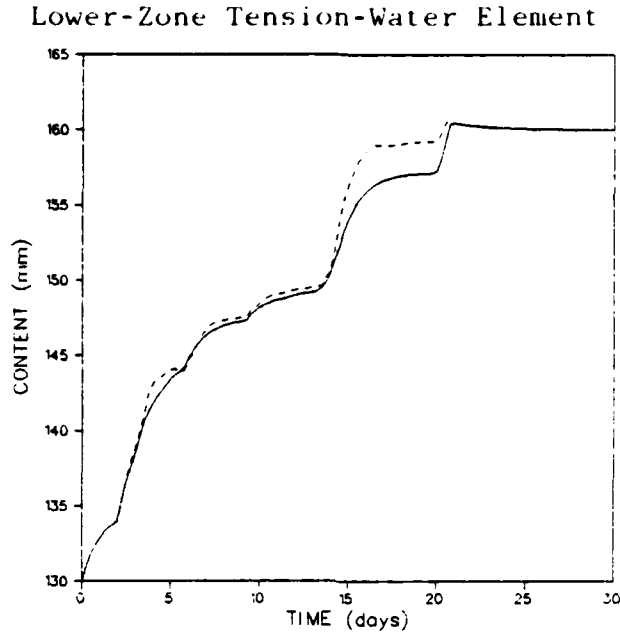


Figure 2.6-25 Lower-Zone Tension-Water Content for Precipitation Record BC2: True Values (Solid Line) and Predicted Values with $P(0) = P'$ (Dashed Line)

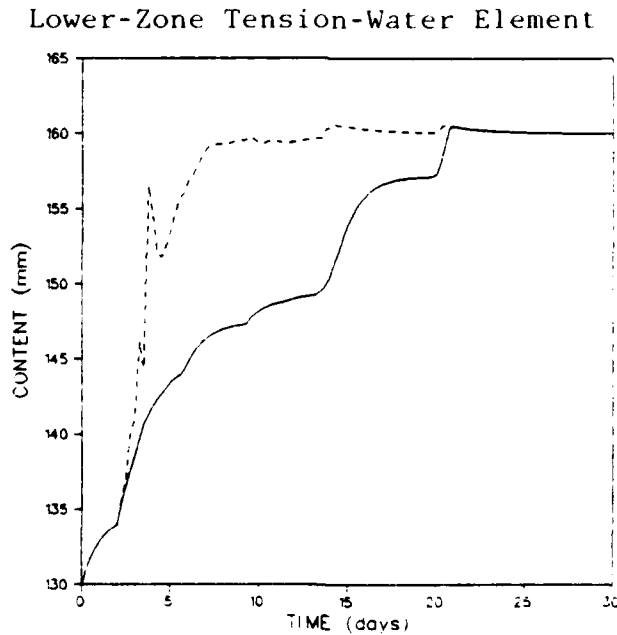


Figure 2.6-26 Lower-Zone Tension-Water Content for Precipitation Record BC2: True Values (Solid Line) and Predicted Values with $P(0) = P''$ (Dashed Line)

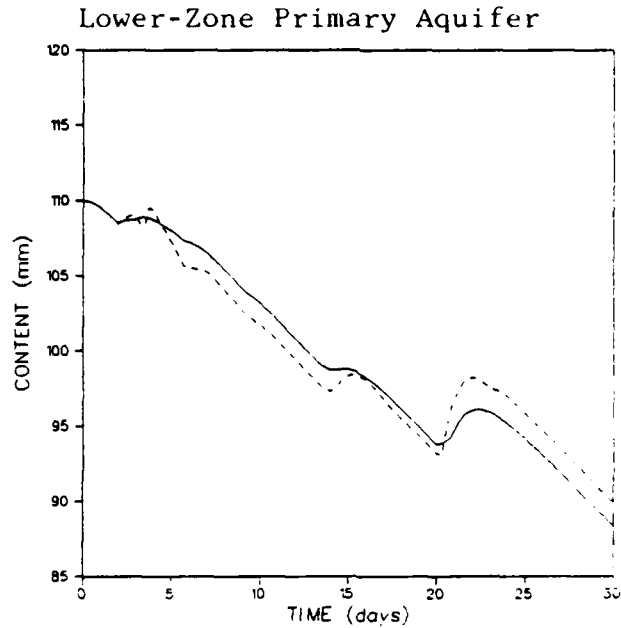


Figure 2.6-27 Lower-Zone Primary Free-Water Content for Precipitation Record BC2: True Values (Solid Line) and Predicted Values With $P(0) = P'$ (Dashed Line)

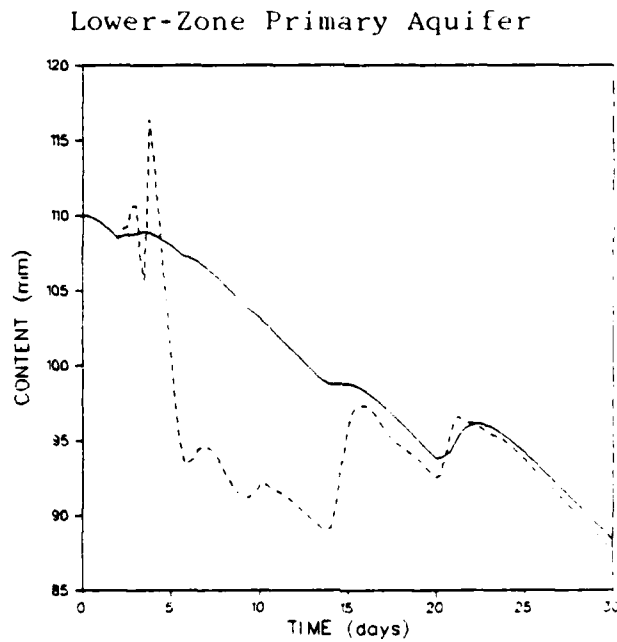


Figure 2.6-28 Lower-Zone Primary Free-Water Content for Precipitation Record BC2: True Values (Solid Line) and Predicted Values with $P(0) = P''$ (Dashed Line)

Lower-Zone Supplementary Aquifer

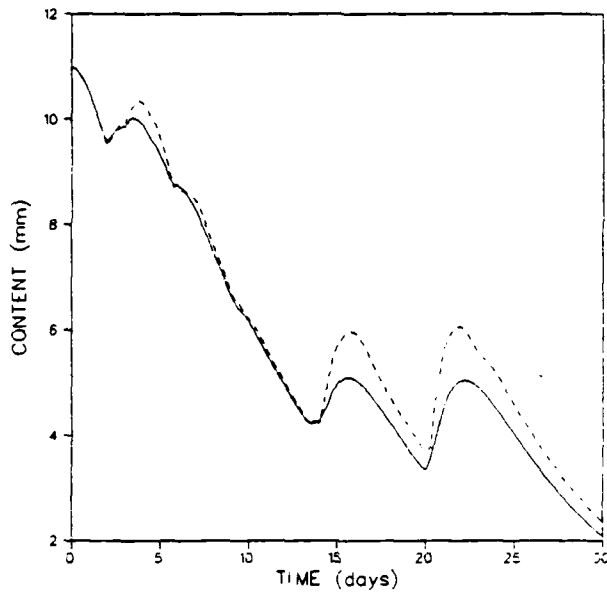


Figure 2.6-29 Lower-Zone Supplementary Free-Water Content for Precipitation Record BC2: True Values (Solid Line) and Predicted Values With $P(0) = P'$ (Dashed Line)

Lower-Zone Supplementary Aquifer

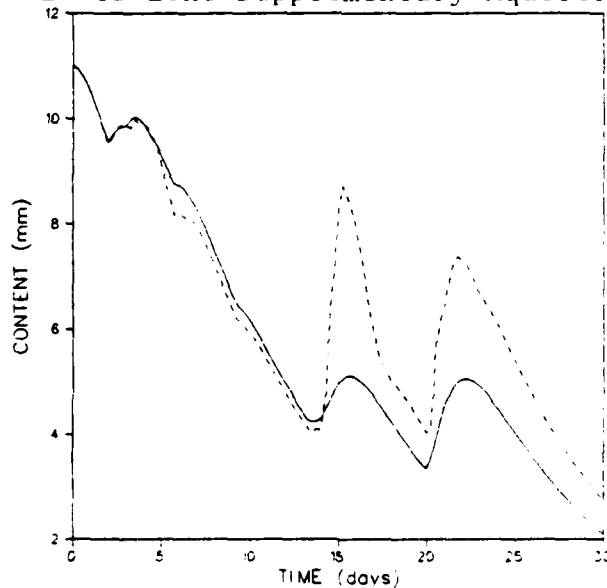


Figure 2.6-30 Lower-Zone Supplementary Free-Water Content for Precipitation Record BC2: True Values (Solid Line) and Predicted Values With $P(0) = P''$ (Dashed Line)

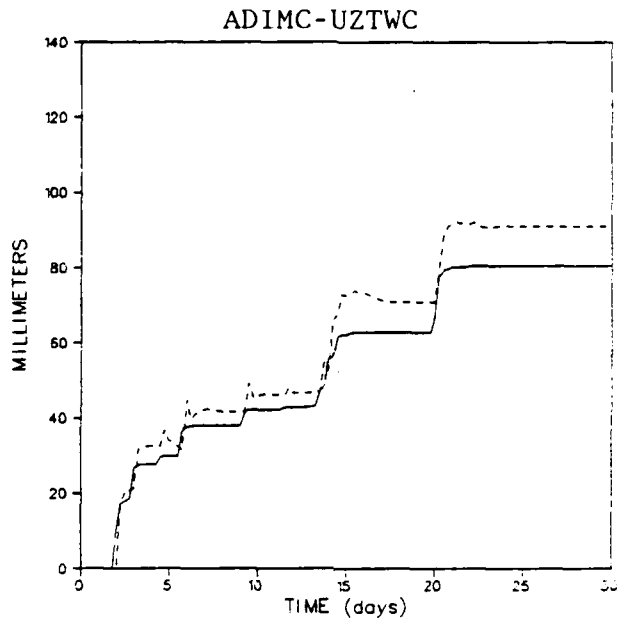


Figure 2.6-31 Excess of the Additional Impervious Area Content Over the Upper-Zone Tension-Water Content for Precipitation Record BC2: True Values (Solid Line) and Predicted Values with $P(0) = P'$ (Dashed Line)

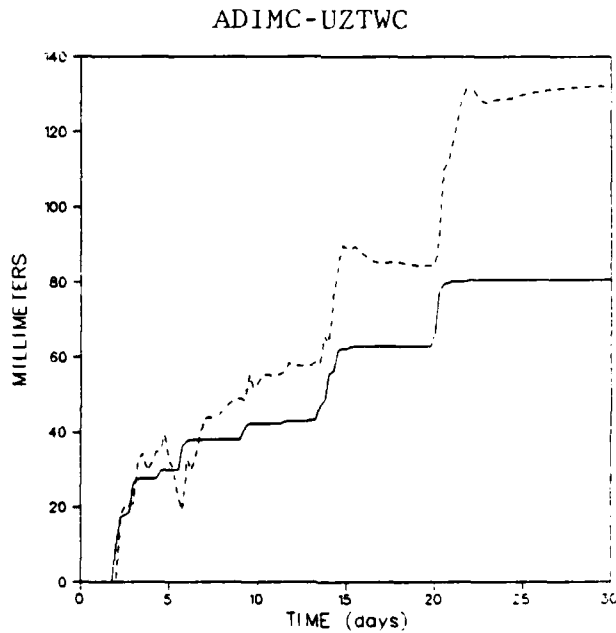


Figure 2.6-32 Excess of the Additional Impervious Area Content Over the Upper-Zone Tension-Water Content for Precipitation Record BC2: True Values (Solid Line) and Predicted Values with $P(0) = P''$ (Dashed Line)

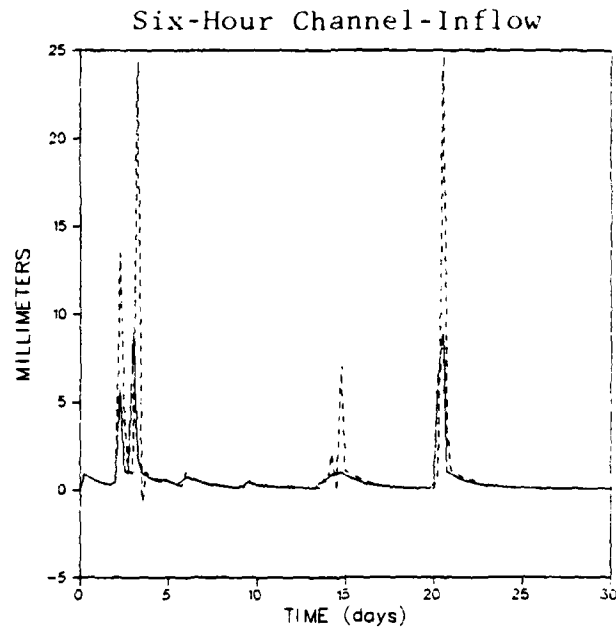


Figure 2.6-33 Six-Hour Accumulated Channel-Inflow for Precipitation Record BC2: True Values (Solid Line) and Predicted Values With $P(0) = P'$ (Dashed Line)

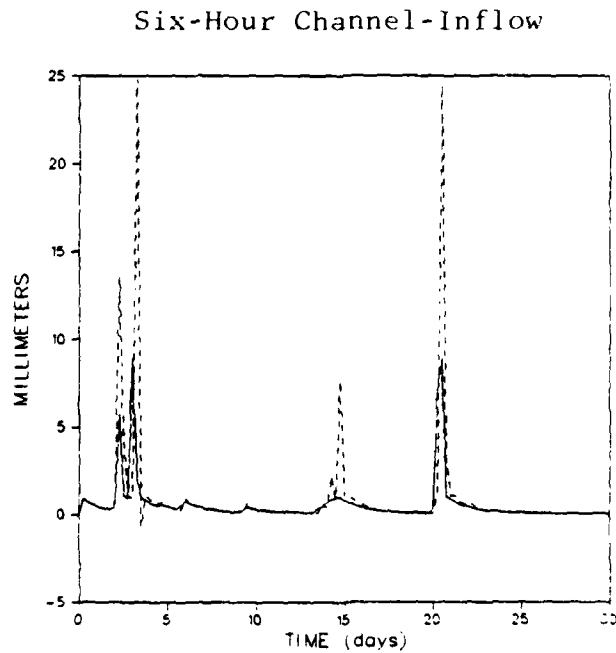


Figure 2.6-34 Six-Hour Accumulated Channel-Inflow for Precipitation Record BC2: True Values (Solid Line) and Predicted Values With $P(0) = P''$ (Dashed Line)

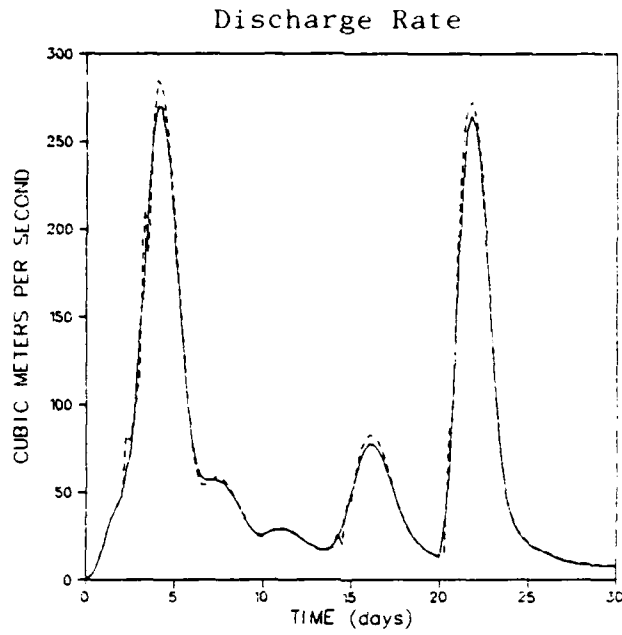


Figure 2.6-35 Instantaneous Discharge for Precipitation Record BC2: True Values (Solid Line) and Predicted Values With $P(0) = P'$ (Dashed Line)

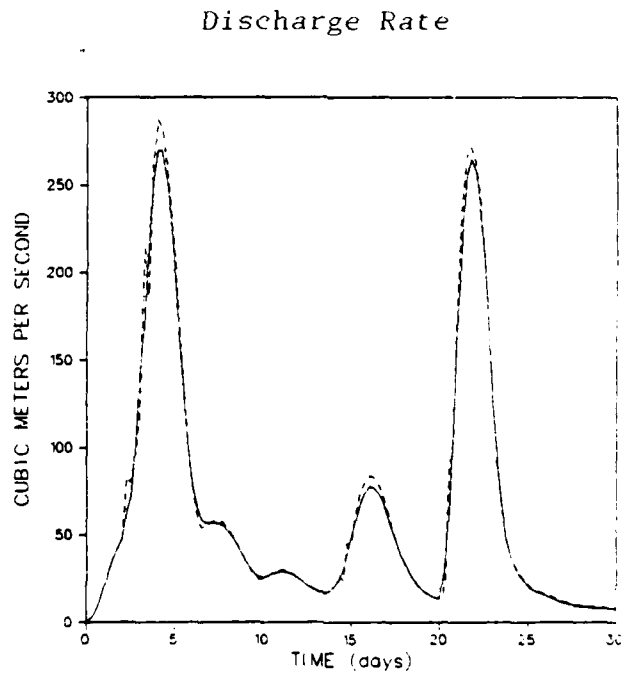


Figure 2.6-36 Instantaneous Discharge for Precipitation Record BC2: True Values (Solid Line) and Predicted Values With $P(0) = P''$ (Dashed Line)

2-63

Surface runoff occurred on three different occasions: on days two, three and twenty (see Figs. 2.6-23 and 2.6-24). Instantaneous discharge plots are given in Figs. 2.6-35 and 2.6-36. For both initial state covariance matrices, the rms differences between the predicted and true discharges are very close: $7.2 \text{ m}^3/\text{sec}$ for the case in which P' was used and $7.3 \text{ m}^3/\text{sec}$ for the case in which P'' was used. The one-step-ahead prediction of the values of the upper-zone states obtained with the use of P' and P'' (Figs. 2.6-21 through 2.6-24) are practically identical and agree very well with the true values. However, for the rest of the states of the SSM model (Figs. 2.6-25 through 2.6-32), the agreement between predicted and true values is much better for the estimates obtained with the use of P' , the smaller covariance matrix. In fact, the same input sequences were used in a filter in which the initial rms values for the uncertainty in the values of the states of the SSM model was set equal to 20% of the maxima of the state values. This filter became unstable during the fifth day of operation.

Therefore, it is recommended that in practice, on-line operation of the filter be started when there is little uncertainty as to the correct values of the states (e.g., during the dry season) or that previously collected precipitation and discharge data be used to carry the filter into steady-state. Another alternative is to try to identify the initial state. This possibility is discussed in Section 4.

The White River basin model was used to test the response of the filter for a set of parameters other than those of the Bird Creek basin. The initial state values in the simulation and filtering algorithms were arbitrarily chosen as $x_1(0) = 40 \text{ mm}$, $x_2(0) = 20 \text{ mm}$, $x_3(0) = 200 \text{ mm}$, $x_4(0) = 40 \text{ mm}$, $x_5(0) = 100 \text{ mm}$ and $x_i(0) = 0$ for $i > 5$. For the filter, the rms uncertainty in the initial states was taken to be 1% of

the element's capacity for the first six states and zero for the remaining states.

Measurements produced by the simulation were precipitation at six-hour intervals and mean discharge at 24-hour intervals. Thus, $k=6$, $\ell=1$ and $m=4$. The precipitation record produced by the simulation is depicted in Fig. 2.6-37. The measurement error covariance matrix used by the filter, R_3 , was that implied by the covariance matrix R_2 for mean daily discharge, i.e.,

$$R_3 = \begin{pmatrix} 0.13 & 0 \\ 0 & 0.52 \end{pmatrix} \quad (2.6-3)$$

Six-Hour Accumulated Precipitation

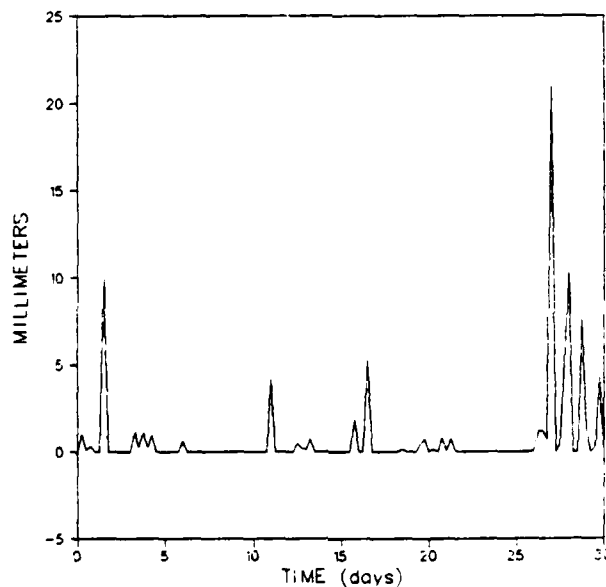


Figure 2.6-37 Precipitation Record for White River Basin

The results obtained are presented in Figs. 2.6-37 through 2.6-45. The excellent fit between the one-step-ahead (six hours) predicted mean daily discharge and the true discharge shown in Fig. 2.6-45 is typical of the results obtained for both the Bird Creek and White River basins when there is no surface runoff. The rms difference between the predicted and true mean daily discharge is only $1.4 \text{ m}^3/\text{sec}$.

It was not possible to obtain simulation results for the White River basin in which surface runoff appeared. Note that even with the substantial amount of rainfall produced during the last four days of simulation,* the drainage and percolation rates from the upper-zone free-water element (Fig. 2.6-39) preclude the value of the state from reaching its maximum and, thus prevent the appearance of surface runoff.

The same random sequence that was used in the simulation to produce the precipitation record of Fig. 2.6-37 and the mean daily discharge indicated by the solid line in Fig. 2.6-45 was used in a simulation in which the precipitation record of Fig. 2.6-37 was reproduced but values of instantaneous discharge instead of mean daily discharge were generated ($k=6, l=1, m=1$). These results served as measurements for a Kalman filter in which the initial covariance matrix was the same as in the previous case and the measurement error covariance matrix was R_2 . The results for the instantaneous discharge rate prediction are given in Fig. 2.6-46. The rms difference between predicted and true discharge is $3.8 \text{ m}^3/\text{sec}$.

*The expected monthly precipitation is 42 mm. Total precipitation for the record of Fig. 2.6-37 is 86 mm. For the last four days, the amount of precipitation is 53.7 mm.

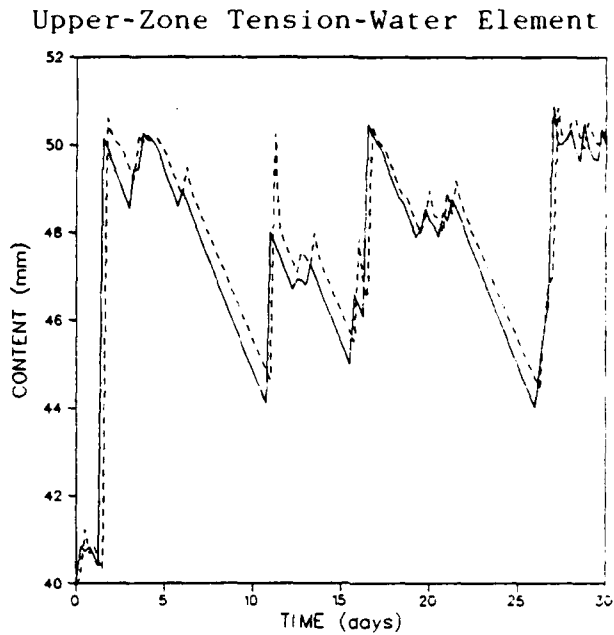


Figure 2.6-38 White River Basin. Upper-Zone Tension-Water Content: True Values (Solid Line) and Predicted Values (Dashed Line)

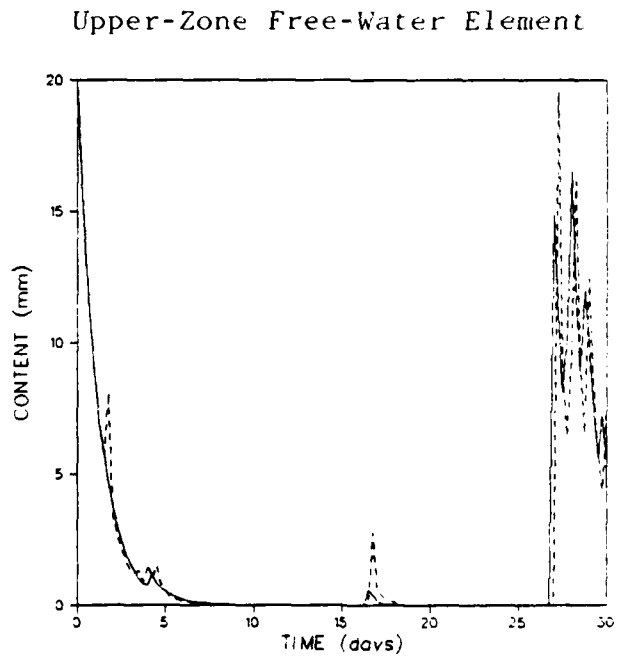


Figure 2.6-39 White River Basin. Upper-Zone Free-Water Content: True Values (Solid Line) and Predicted Values (Dashed Line)

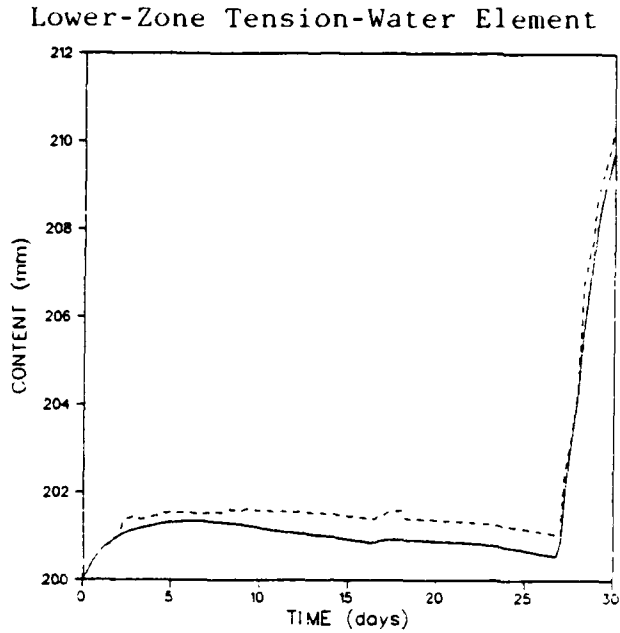


Figure 2.6-40 White River Basin. Lower-Zone Tension-Water Content: True Values (Solid Line) and Predicted Values (Dashed Line)

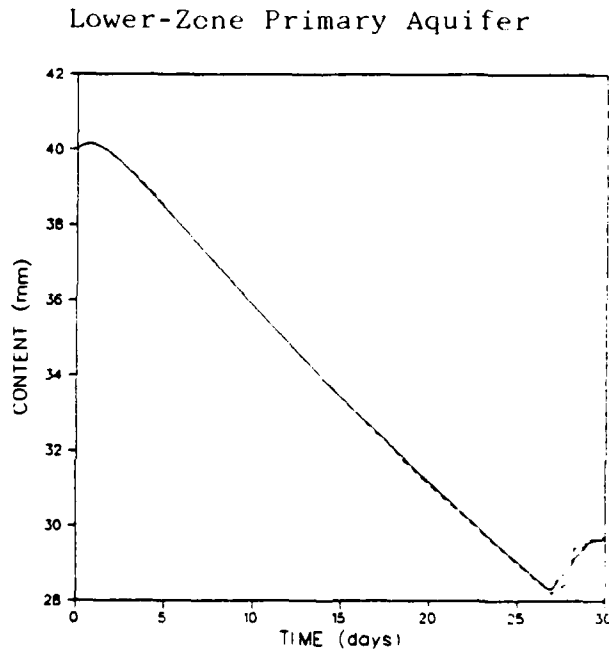


Figure 2.6-41 White River Basin. Lower-Zone Primary Free-Water Content: True Values (Solid Line) and Predicted Values (Dashed Line)

Lower-Zone Supplementary Aquifer

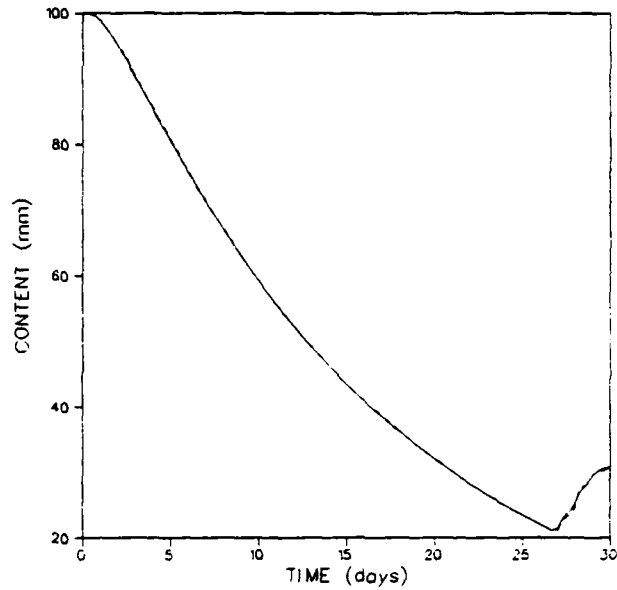


Figure 2.6-42 White River Basin. Lower-Zone Supplementary Free-Water Content: True Values (Solid Line) and Predicted Values (Dashed Line)

ADIMC-UZTWC

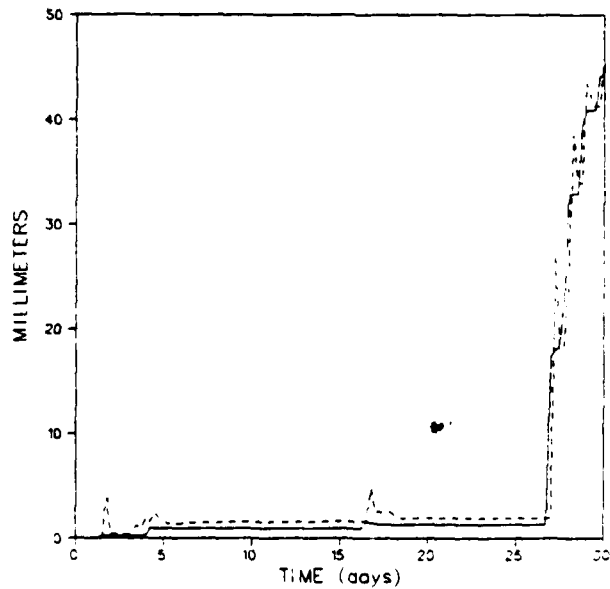


Figure 2.6-43 White River Basin. Excess of the Additional Impervious Area Content Over the Upper-Zone Tension-Water Content: True Values (Solid Line) and Predicted Values (Dashed Line)

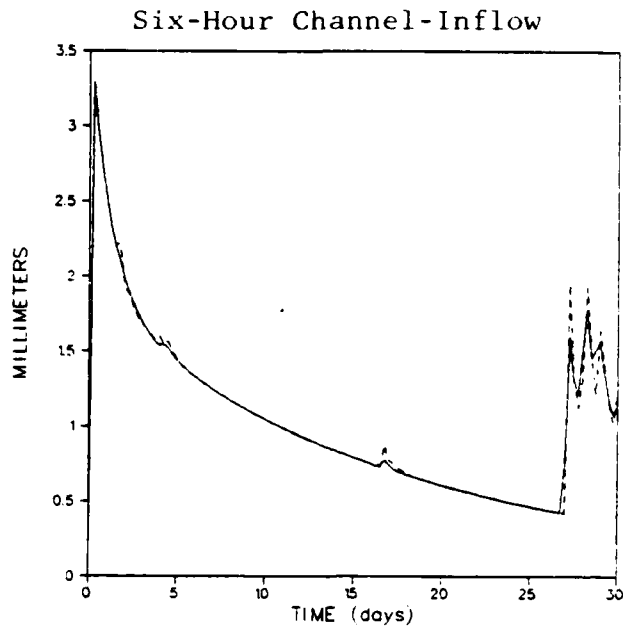


Figure 2.6-44 White River Basin. Six-Hour Accumulated Channel-Inflow: True Values (Solid Line) and Predicted Values (Dashed Line)

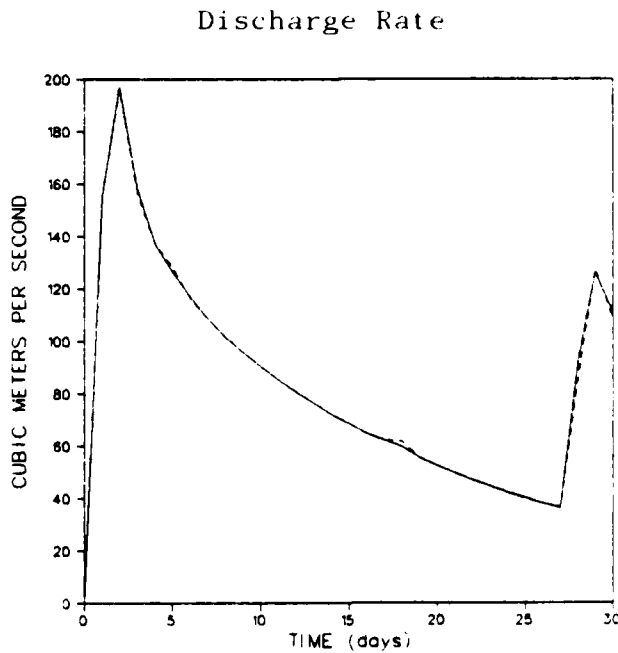


Figure 2.6-45 White River Basin. Mean Daily Discharge: True Values (Solid Line) and Predicted Values (Dashed Line)

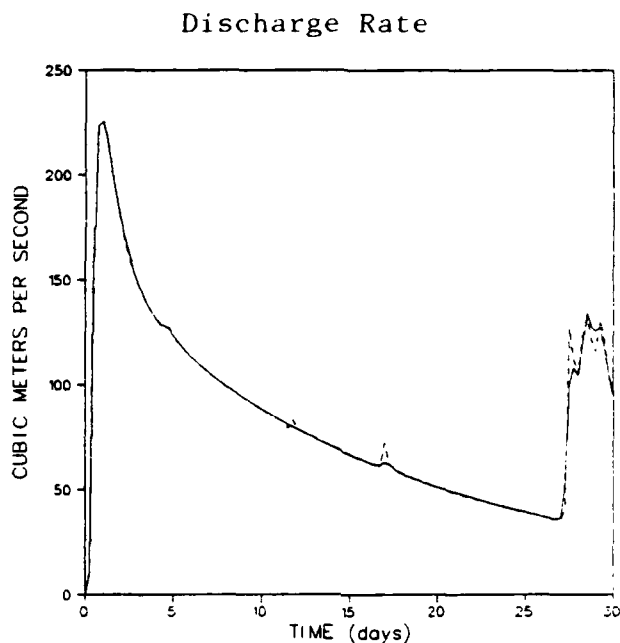


Figure 2.6-46 White River Basin. Instantaneous Discharge: True Values (Solid Line) and Predicted Values (Dashed Line)

The results obtained show that notwithstanding the strong nonlinearities of the soil moisture model, the extended Kalman filtering technique described in Section 2.5 performs extremely well on the combined basin model. The occurrence of the peaks of the predicted discharge and their magnitude agree very well with the simulation results.

3. STATE-SPACE MODEL DEVELOPMENT FOR
 UNIT HYDROGRAPHS

The objective of the work performed under this task was to develop a computer program which will create state-space models approximating the impulse response of a unit hydrograph. This computer program is intended to be included in the NWSRFS forecast component. A users manual documents the computer program and its operation in detail (Ref. 1). The computer program has the following capabilities.

- Creation of a discrete-time state-space model (with selectable output time step) based on the input of a unit hydrograph
- Production of an output file of river discharge predictions calculated from the state-space model and an input file of channel inflow values
- Output of graphical summaries and tabulations of the state-space model impulse response, and the squared magnitude spectrum and phase spectrum of the transfer function.

The canonical variate method is used in the approximation of unit hydrographs by reduced-order models of state-space form. This section describes the mathematical method by which the state-space models are created and presents some results based on unit hydrographs supplied by NOAA/NWS to TASC for use in this study. Section 3.1 formulates the problem of unit hydrograph approximation as a reduced-order filtering problem. Section 3.2 presents the concept of canonical variate decomposition of the past and future of a random process. The optimality of several canonical variate procedures are discussed

in Section 3.3. The decomposition of past and future is used in Section 3.4 to compute explicitly the optimal reduced-order state-space model. Section 3.5 presents results of the application of this method to unit hydrographs supplied by the NWS.

3.1 FORMULATION OF THE PROBLEM

Consider the problem in which a unit hydrograph $h(\tau)$ is given that specifies the response at lag τ to a unit input at time zero. It is desired to find a state-space model, preferably of low order, which is a good approximation in some sense to the given unit hydrograph. This problem cannot be separated from the characteristics of the input process since the modes of $h(\tau)$ that are excited and, hence, the output depend strongly upon the input process. Nominally, it will be assumed that the input process is white noise which excites all frequencies proportionately. If the typical input signal power spectrum is known and different from white noise, this fact can be easily included in the method described below and would lead to an alternative approximating state-space model. It will be shown in Section 3.5 that the white noise assumption leads to excellent approximations of the unit hydrograph with low order state-space models.

A schematic description of the problem is shown in Fig. 3.1-1. The problem of determining a state-space model which does a "good" job of predicting the output $v(t)$ from the input $u(t)$ can be viewed as a reduced-order filtering problem. Consider $u(t)$ and $v(t)$ as two related random processes. (In Section 3.4.3 we will consider the case of a vector output process $\underline{v}(t)$.) Given the past of $u(t)$ for $t=0, -1, \dots$, it is desired to predict the future evolution of $v(t)$ for $t=1, 2, \dots$. A recursive or state-space filter of some specified state order

R-45964

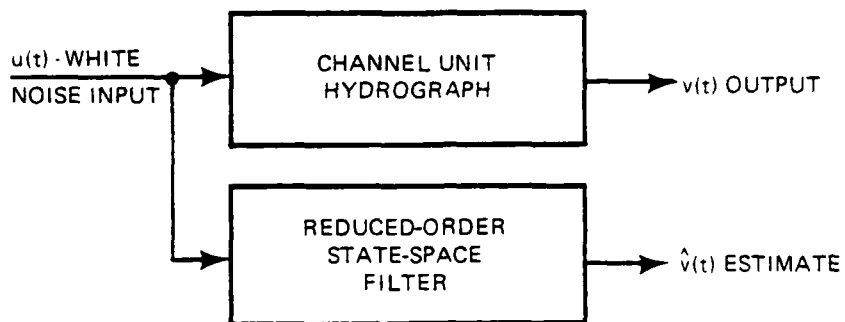


Figure 3.1-1 Approximation of Unit Hydrograph by a Reduced Order Filter

will be derived from the unit hydrograph. The approach and criterion of approximation is described in the next two sections, and the filter derived in the following section.

3.2 CANONICAL VARIATE DECOMPOSITION OF PAST AND FUTURE

The central concept in the approach involves use of the canonical variate decomposition of the past of one random process and the future of another process (Refs. 9, 10, and 11). This corresponds to a particular coordinatization of the predictor space (Ref. 12) in a way that leads very naturally to the selection of reduced-order models and filters which are optimal in several senses discussed in Section 3.3.

Suppose $u(t)$ and $v(t)$, for t an integer, are time series which are jointly stationary in the wide sense. We are

primarily interested in prediction of the future evolution of $\underline{v}(t)$ based upon the past realization of $u(t)$ and so consider the two vectors of random variables

$$\underline{z}_1(t) = \begin{pmatrix} u(t) \\ u(t-1) \\ \vdots \\ u(t-p+1) \end{pmatrix}, \quad \underline{z}_2(t) = \begin{pmatrix} \underline{v}(t+1) \\ \underline{v}(t+2) \\ \vdots \\ \underline{v}(t+p) \end{pmatrix} \quad (3.2-1)$$

where p is some specified number of shifts. We call $\underline{z}_1(t)$ the past of $u(t)$ and $\underline{z}_2(t)$ the future of $\underline{v}(t)$. The integer p is generally somewhat larger than the maximal "state" order to be considered but, in theory, may be infinite.

In the reduced-order filtering problem, the relationship between the past $\underline{z}_1(t)$ and the future $\underline{z}_2(t)$ is to be approximated by a Markov process model of specified state order k . In particular, the k^{th} -order state expressible as k linear combinations of the past $\underline{z}_1(t)$ that best predicts the future $\underline{z}_2(t)$ is to be determined. For the immediate discussion "best" means best percent error prediction which corresponds to maximal reduction in error in prediction of $\underline{z}_2(t)$ on a percent error basis as given by the canonical correlation criterion discussed in Section 3.3. The best k linear combinations of $\underline{z}_1(t)$ for predicting $\underline{z}_2(t)$ are those having maximal correlation with $\underline{z}_2(t)$. Finding these best linear combinations of $\underline{z}_1(t)$ having maximal correlation with $\underline{z}_2(t)$ is precisely the classical canonical correlations and variates problem of mathematical statistics (Refs. 13, 14). The more general canonical prediction criterion is discussed in Section 3.3.2 as a simple modification of the classical canonical correlations and variate problem. The solution to the canonical variate problem is obtained by putting the covariance structure of $\underline{z}_1(t)$ and $\underline{z}_2(t)$ in a canonical

A new generalization, the canonical prediction criterion, is also discussed below which is optimal in the sense of

- Minimizing the expected weighted squared prediction error.

The canonical prediction criterion applied to unit hydrographs gives much lower order state-space models which adequately approximate the unit hydrographs. Comparisons of state-space models fitted using both the canonical correlation and prediction criteria are given in Section 3.5.1.

3.3.1 Canonical Correlation Criterion

The canonical variate problem was originally formulated (Ref. 13, also see Ref. 14) as a sequential selection procedure. As discussed in Section 3.2, the procedure is concerned with the optimal selection of k linear combinations of a vector \underline{z}_1 of random variables for optimal prediction of a related vector \underline{z}_2 of random variables. First a pair of linear combinations $a_1 = \underline{j}_1^T \underline{z}_1$ and $b_1 = \underline{l}_1^T \underline{z}_2$ of the respective vectors of random variables \underline{z}_1 and \underline{z}_2 are determined which have maximal correlation. Next, a second pair $a_2 = \underline{j}_2^T \underline{z}_1$ and $b_2 = \underline{l}_2^T \underline{z}_2$ are found which are uncorrelated with a_1 and b_1 and which have maximal correlation. The procedure continues up to the specified number k of linear combinations of \underline{z}_1 which are permitted. Thus the canonical variate procedure finds the k mutually uncorrelated components of \underline{z}_1 which are maximally correlated with \underline{z}_2 . Hotelling (Ref. 13) defines an intuitive scalar measure of correlation between the two vectors of random variables \underline{z}_1 and \underline{z}_2 , called the vector correlation coefficient, which is simply expressed in terms of the non-zero canonical correlations r_1, \dots, r_n as

$$Q^2 = r_1 r_2 \dots r_n \quad (3.3-1)$$

It can be shown that the choice of k linear combinations of \underline{z}_1 which have maximal vector correlation coefficient are the first k canonical variates.

The canonical correlation method maximizes the mutual information. Shannon and Weaver (Ref. 16) define the information in one random vector \underline{z}_1 about another random vector \underline{z}_2 , now commonly called mutual information, by

$$J(\underline{z}_1; \underline{z}_2) = \int p_{12}(\underline{z}_1, \underline{z}_2) \log \frac{p_{12}(\underline{z}_1, \underline{z}_2)}{p_1(\underline{z}_1) p_2(\underline{z}_2)} d\underline{z}_1 d\underline{z}_2 \quad (3.3-2)$$

where the base of the logarithm is arbitrary and determines the particular units of information, and where p_{12} is the joint and p_1 and p_2 the marginal probability densities. Gelfand and Yaglom (Ref. 17) showed that the mutual information is simply expressed in terms of the canonical correlations r_1, \dots, r_n between the two vectors by

$$J(\underline{z}_1; \underline{z}_2) = -\frac{1}{2} \sum_{j=1}^n \log (1 - r_j^2) = -\frac{1}{2} \log w \quad (3.3-3)$$

where Hotelling (Ref. 13) defines the vector alienation coefficient

$$w = (1 - r_1^2) \dots (1 - r_n^2) \quad (3.3-4)$$

as a measure of independence of \underline{z}_1 and \underline{z}_2 . Gelfand and Yaglom (Ref. 17) extend the definition of mutual information to vectors

of infinitely many random variables, e.g., random processes in both continuous time and discrete time. This development also provides the basis for extending canonical variates to random processes (Ref. 18).

Now, if a restricted number k of linear combinations (a_1, \dots, a_k) of one random process $\underline{u}(t)$ are used to predict another random process $\underline{v}(t)$, then the choice maximizing the mutual information is the first k canonical variates and the mutual information is expressed by the first k canonical correlations

$$\max_{a_1, \dots, a_k} J(a_1, \dots, a_k; \underline{v}(t)) = -\frac{1}{2} \log \prod_{j=1}^k (1 - r_j^2) \quad (3.3-5)$$

Thus the canonical correlation method provides an optimal procedure in terms of mutual information for choosing a finite state representation of one random process for prediction of another.

3.3.2 Canonical Prediction Criterion

A more general criterion of prediction error is the expected weighted square prediction error

$$h(\underline{z}_2 - \hat{\underline{z}}_2) = E(\underline{z}_2 - \hat{\underline{z}}_2)^T \theta^{-1} (\underline{z}_2 - \hat{\underline{z}}_2) \quad (3.3-6)$$

where θ is an arbitrary positive definite symmetric weighting matrix, $\hat{\underline{z}}_2$ is the minimum variance estimate of \underline{z}_2 based upon the k selected linear combinations of \underline{z}_1 , and E is expectation. The optimal choice of k linear combinations of \underline{z}_1 that minimizes h corresponds to the first k canonical variates for a canonical correlation analysis with the "correlation" structure

$$E \begin{pmatrix} \underline{z}_1 \\ \underline{z}_2 \end{pmatrix} (\underline{z}_1^T \quad \underline{z}_2^T) = \begin{pmatrix} \Sigma_{11} & \Sigma_{12} \\ \Sigma_{21} & \theta \end{pmatrix} \quad (3.3-7)$$

although this is not, in general, a covariance matrix. That is, the true covariance Σ_{22} of \underline{z}_2 is replaced by the weighting matrix θ . The minimum prediction error is simply expressed by

$$\min h(\underline{z}_2 - \hat{\underline{z}}_2) = \text{tr } \theta^{-1} \Sigma_{22} - (r_1^2 + \dots + r_k^2) \quad (3.3-8)$$

in terms of the canonical predictors r_i which play the same role as the canonical correlations.

Thus it can be seen that when θ is set equal to Σ_{22} , the canonical correlation problem can be viewed as weighting the squared error by the inverse covariance so that the percent error or error relative to the variance of each variable, is the criterion considered. The criterion given by Eq. 3.3-7 is more general than that usually considered in the canonical variate method and permits arbitrary quadratic weighting of the prediction errors.

Such weighting is particularly useful in reduced-order state-space modeling of unit hydrographs and permits weighting the more important variables to be estimated. In particular, it is found that the criterion of the expected sum squared prediction error

$$h(\underline{z}_2 - \hat{\underline{z}}_2) = E(\underline{z}_2 - \hat{\underline{z}}_2)^T (\underline{z}_2 - \hat{\underline{z}}_2) \quad (3.3-9)$$

of the predicted future $\hat{\underline{z}}_2$ gives markedly improved state-space model approximations to some unit hydrographs. This corresponds to setting θ equal to 1, the identity matrix.

3.4 OPTIMAL REDUCED-ORDER MODELING

The canonical variates and correlations analysis is used in this section to derive optimal reduced-order filters. In the reduced-order filter problem, a process $u(t)$ and a related process $\underline{v}(t)$ are given, and predictions of $\underline{v}(t)$ based upon past observations $u(t), u(t-1), \dots$ using a reduced-order filter are required. As in the canonical variate analysis in Section 3.2, let $\underline{z}_1(t)$ be the past of $u(t)$ and $\underline{z}_2(t)$ be the future of $\underline{v}(t)$ (e.g., Eq. 3.2-1).

3.4.1 State Vector Determination

For a given order k for a reduced-order filter, finding a best k -element state is equivalent to finding the k linear combinations of the past $\underline{z}_1^T = (u^T(0), u^T(-1), \dots)$ which have the best ability to predict the future $\underline{z}_2^T = (\underline{v}^T(1), \underline{v}^T(2), \dots)$. If the best predictive ability means to minimize percent error in predicting all components of \underline{z}_2 , then this problem is precisely the canonical variates and correlations problem of Section 3.3.1. Or more generally we can use the canonical prediction criterion of Section 3.3.2. To solve this problem, nonsingular transformations of the past \underline{z}_1 and future \underline{z}_2 are determined

$$\underline{a} = J\underline{z}_1, \quad \underline{b} = L\underline{z}_2 \quad (3.4-1)$$

such that in this new basis the past \underline{a} and future \underline{b} have a canonical structure as in (3.2-3).

Once the canonical variate problem is solved, an optimal reduced-order filter of order k can be determined for each $k < \ell$ with the minimal-order realization given for $k = \ell$. If k linear combinations of the past \underline{z}_1 are to be used to predict the future \underline{z}_2 , then the optimal choice is the first k canonical

variates. These k linear combinations specify the optimal state vector of the k^{th} -order filter. Specifically, the state vector is

$$\underline{x}(t) = J_k \underline{z}_1(t) \quad \text{where} \quad J_k = (I_k, 0)J \quad (3.4-2)$$

with I_k the $k \times k$ identity matrix.

3.4.2 State-Space Realization

The remainder of the problem is to obtain a state-space realization of the optimal reduced-order filter. In particular, expressions for the calculation of the state-space matrices in terms of the canonical variate analysis are needed. The desired state-space form of the filter is

$$\underline{x}(t) = \Phi \underline{x}(t-1) + Gu(t) \quad (3.4-3)$$

$$\hat{y}(t) = H\underline{x}(t-1) \quad (3.4-4)$$

with the output $\hat{y}(t)$ the optimal reduced-order filter estimate of $y(t)$. The output $y(t)$ is related to the state $\underline{x}(t-1)$ at time $t-1$ to insure a lag between the input and output, i.e., so that an input does not produce an instantaneous output. This is a conventional discrete time system description - see Section 3.4.4 for the modification involved when the input $u(t)$ is a continuous accumulation of channel inflow over the time interval $(t-1, t)$. By calculating the covariance of $\underline{x}(t)$ with $\underline{x}(t-1)$ and $u(t)$ using Eq. 3.4-3, the matrix Φ and G must satisfy

$$\Sigma(\underline{x}_t, \underline{x}_{t-1}) = \Phi \Sigma(\underline{x}_{t-1}, \underline{x}_{t-1}) + G \Sigma(u_t, \underline{x}_{t-1}) \quad (3.4-5)$$

$$\Sigma(\underline{x}_t, u_t) = \Phi \Sigma(\underline{x}_{t-1}, u_t) + G \Sigma(u_t, u_t) \quad (3.4-6)$$

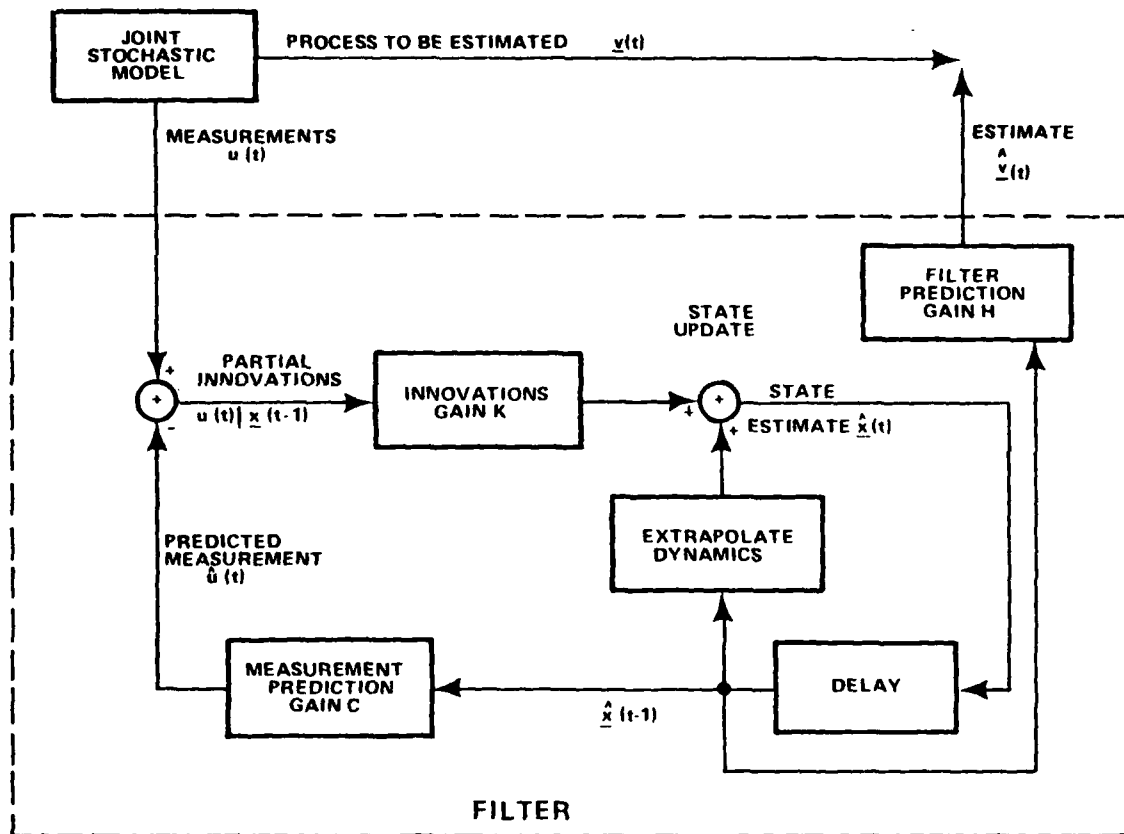


Figure 3.4-1 Partial Innovations Representation of Optimal Reduced Order Filter

where $\Sigma(,)$ denotes the covariance matrix between two vectors and the shorthand $\underline{x}_t \triangleq \underline{x}(t)$ is used.

These equations are easily solved for Φ and G explicitly in terms of the various covariance matrices. The filter (3.4-3) and (3.4-4) can be put into feedback form

$$\underline{x}(t) = A \underline{x}(t-1) + K(u(t) - C \underline{x}(t-1)) \tag{3.4-7}$$

where the matrices A , K , and C are

$$A = \Delta(\underline{x}_t, \underline{x}_{t-1}) \Sigma^{-1}(\underline{x}_{t-1}, \underline{x}_{t-1}) \tag{3.4-8}$$

$$K = \left[\Sigma(\underline{x}_t, u_t) - \Sigma(\underline{x}_t, \underline{x}_{t-1}) \Sigma^{-1}(\underline{x}_{t-1}, \underline{x}_{t-1}) \Sigma(\underline{x}_{t-1}, u_t) \right] \\ \left[\Sigma(u_t, u_t) - \Sigma(u_t, \underline{x}_{t-1}) \Sigma^{-1}(\underline{x}_{t-1}, \underline{x}_{t-1}) \Sigma(\underline{x}_{t-1}, u_t) \right]^{-1} \quad (3.4-9)$$

$$C = \Sigma(u_t, \underline{x}_{t-1}) \Sigma^{-1}(\underline{x}_{t-1}, \underline{x}_{t-1}) \quad (3.4-10)$$

The state-space form (3.4-3) through (3.4-4) has matrices Φ and G given by

$$\Phi = A - KC, \quad G = K \quad (3.4-11)$$

These matrices have a simple interpretation as regression coefficients. The matrix A is the regression of $\underline{x}(t)$ on $\underline{x}(t-1)$, i.e., the best prediction of $\underline{x}(t)$ given $\underline{x}(t-1)$. The term $C \underline{x}(t-1)$ is the best prediction of $u(t)$ based upon $\underline{x}(t-1)$. The feedback gain matrix K is the regression of the conditional random variables $\underline{x}(t)$ given $\underline{x}(t-1)$ on the conditional random variable $u(t)$ given $\underline{x}(t-1)$. This gives the best prediction of $\underline{x}(t)$ based upon $u(t)$, having already accounted for the dependence upon $\underline{x}(t-1)$. The quantity $u(t) - c \underline{x}(t-1)$ can be called the partial innovations of the process $u(t)$ with respect to the past of the process $\underline{x}(t-1)$ (i.e., the new information in $u(t)$ uncorrelated with the past reduced-order states $\underline{x}(t-1), \underline{x}(t-2), \dots$). The remaining quantity to be specified is the prediction gain matrix

$$H = \Sigma(\underline{v}_t, \underline{x}_{t-1}) \Sigma^{-1}(\underline{x}_{t-1}, \underline{x}_{t-1}) \quad (3.4-12)$$

for predicting $\underline{v}(t)$ based upon $\underline{x}(t-1)$. The partial innovations realization of the optimal reduced-order filter is illustrated in Fig. 3.4-1 and has the same structure as the Kalman filter in terms of optimal extrapolation, prediction of the measurement, calculation of the partial innovation and update (Ref. 19). The matrices can be explicitly computed using Eq. 3.4-2,

the covariance structure between $z_1(t)$ and $z_2(t)$, and the canonical form, Eq. 3.2-3.

3.4.3 Multirate Unit Hydrographs

There are a number of situations in which the channel inflow is the result of accumulations of water over a time interval greater than the time between discharge measurements. For example accumulated channel inflow may be calculated every 12 hours corresponding to the precipitation measurements and channel outflow is measured every 6 hours. To accommodate this situation, a multirate state space model is needed which has inputs every 12 hours and outputs every 6 hours. By properly setting up the unit hydrograph as a single input multi-output unit hydrograph, the above algorithms apply exactly as they are.

We make the following conventions. Let $u(t)$ be the input channel inflow, $t=1,2,\dots$, with the input sample rate normalized to 1 time unit. Let $\underline{v}(t)$, t an integer, be the vector of output channel outflow occurring at times $[s-1] < s \leq [s]$ where $[s]$ denotes the least integer greater than or equal to s . Figure 3.4-2 gives an illustration of the input, the output grouping and labeling, the unit hydrograph and the pulse input used in its definition.

If Δt is the output sample rate then

$$\underline{v}(t) = \begin{pmatrix} \text{output } (t-1 + \Delta t) \\ \vdots \\ \text{output } (t-1 + r\Delta t) \end{pmatrix} \quad (3.4-13)$$

where $r = 1/\Delta t$. The vector unit response function $g(\tau)$, $\tau=1,\dots,q$, is defined in terms of the unit hydrograph $h(\tau)$ by

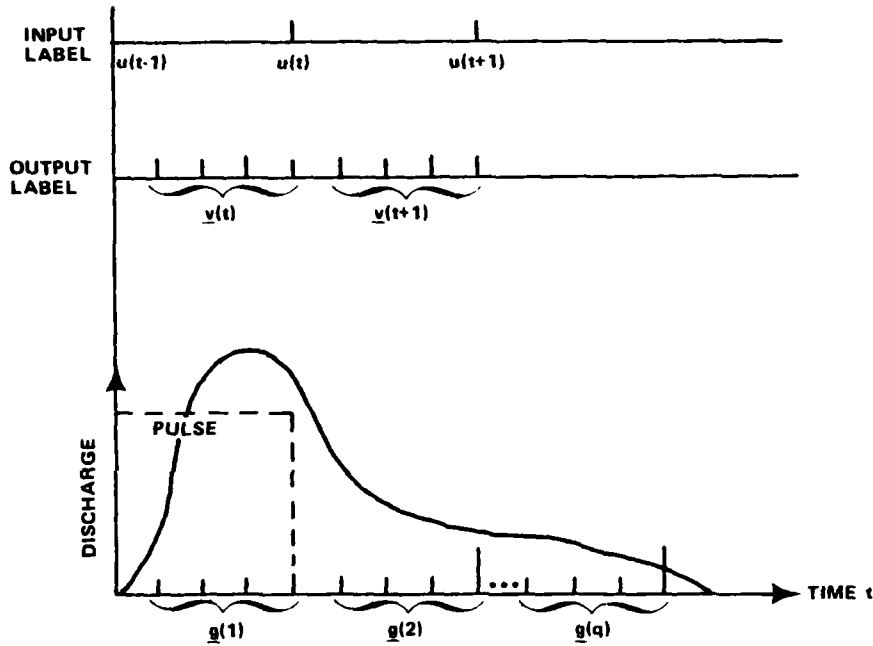


Figure 3.4-2 Multirate Unit Hydrograph

$$g(\tau) = \begin{pmatrix} h(\tau-1 + \Delta t) \\ \vdots \\ h(\tau-1 + r\Delta t) \end{pmatrix} \quad (3.4-14)$$

Once the conventions of $\underline{v}(t)$ as a vector output and $\underline{g}(\tau)$ as a vector unit hydrograph are made, the canonical variate analysis and reduced order state space models are derived as in Section 3.4.2. Note that the state space model operates at the input sample rate so that the state vector only changes when there is a new input.

The transfer function is a useful tool in studying a multirate discrete time system. It can be used to describe the response of the system to a sampled sine wave at the input. In Section 3.5.2, an example will show that situations arise

where the response to a sampled sine wave input at a given frequency may include a substantial sampled sine wave component at much higher frequency than the input. While this is a difficulty in the present forecasting system due to multirate unit hydrographs, it is completely avoided when using the continuous catchment model as in Section 2.

Consider the multirate system where $u(t)$, $t = \dots, -2r, r, 0, r, \dots$, $u_k = u(kr)$ is the input and $v(t)$, $t = -2, -1, 0, 1, 2, \dots$ is the output with r an integer. Let k and ℓ be integers so that the output at time $t = (k-1)r + \ell$, $0 < \ell \leq r$, is related to the input by the finite unit hydrograph function $g_\ell(\tau)$ as

$$v(kr + \ell - r) = \sum_{\tau=1}^q g_\ell(\tau) u(kr - \tau r) \quad (3.4-15)$$

To find the transfer function, we compute the Fourier transform $V(\omega)$ of $v(t)$ for $-\pi < \omega < \pi$

$$\begin{aligned} V(\omega) &= \sum_{t=-\infty}^{\infty} v(t) e^{-i\omega t} = \sum_{\ell=1}^r \sum_{k=-\infty}^{\infty} v(kr + \ell - r) e^{-i\omega(kr + \ell - r)} \\ &= \sum_{\ell=1}^r e^{-i\omega(\ell - r)} \sum_{k=-\infty}^{\infty} \sum_{\tau=1}^q g_\ell(\tau) u_{k-\tau} e^{-i\omega r k} \\ &= \sum_{\ell=1}^r e^{i\omega(r - \ell)} G_\ell(\omega r) \frac{1}{r} U(\omega r) \end{aligned} \quad (3.4-16)$$

where $G_\ell(\lambda)$ and $U(\lambda)$ are the Fourier transforms of $g_\ell(k)$ and u_k respectively.

The transform $U(\lambda)$, $-\pi \leq \lambda \leq \pi$, of the input process $u_k = u(kr)$ is periodic with period 2π and in (3.4-16) repeats up to frequency $\lambda = \pm\pi r$. This is the Fourier extension or Nyquist interpolation of the input to a higher sample rate. The transfer function

$$G(\omega) = \sum_{\ell=1}^r e^{i\omega(r-\ell)} G_{\ell}(\omega r) \quad (3.4-17)$$

is then applied to this interpolated input function to obtain the output function. If the input is a sine wave $u_k = \sin(\lambda k + \phi)$ for $0 \leq \lambda \leq \pi$, then the output time function is

$$v(t) = \sum_{\omega \in \Omega} |G(\omega)| \frac{1}{r} \sin(\omega t + \arg G(\omega) + \phi) \quad (3.4-18)$$

where Ω is the periodic repetition of λ in terms of the output sample rate

$$\Omega = \left\{ \omega : \omega = \frac{\lambda}{r} \pm \frac{2\pi m}{r}, |\omega| < \pi, m \text{ integer} \right\} \quad (3.4-19)$$

3.4.4 Continuous Accumulation of Channel Inflow

There is a minor inconsistency between the usual way of specifying a discrete time and a continuous time system in terms of the unit pulse response and that of implementing a continuous/discrete time filter. This requires a minor modification of the reduced order filter given by Eqs. 3.4-3 and 3.4-4.

Figure 3.4-3(a) shows a constant pulse input and the resulting continuous unit pulse response in (b). A discrete response is shown in (d) which is conceptually considered as

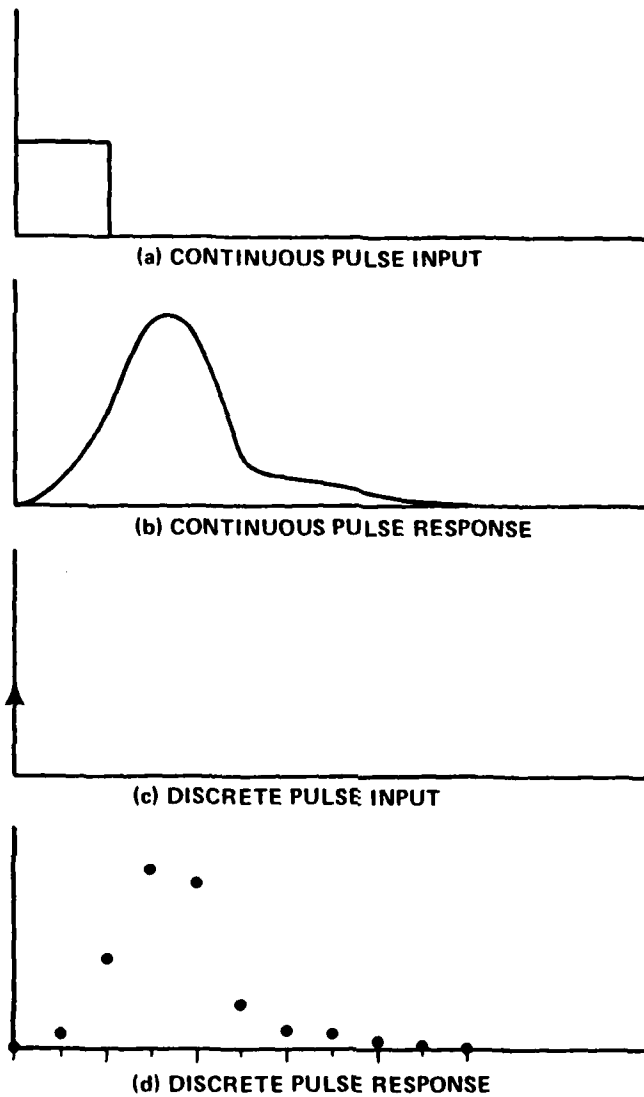


Figure 3.4-3 Relationship Between Continuous and Discrete Time Unit Pulse Response

the response to an input (c) at time $t = 0$, i.e., the pulse has been accumulated and applied at the time corresponding to the pulse beginning. The discrete time system is constrained so that there is no instantaneous output and hence no effect occurs until the end of the pulse.

The inconsistency occurs when a usual continuous/discrete time filter is implemented as in Chapter 2. It is natural in such recursive schemes to associate the end time of the pulse with the accumulated channel inflow rather than the start time of the pulse. If this convention is adopted then the state space representation (Eqs. 3.4-3 and 3.4-4) is modified to

$$\underline{x}(t) = \Phi \underline{x}(t-1) + Gu(t) \quad (3.4-20)$$

$$\hat{y}(t) = H\underline{x}(t) \quad (3.4-21)$$

where the quantity $H\underline{x}(t-1)$ of Eq. 3.4-4 has been shifted one time step. This applies to both the cases of single output and multirate output unit hydrographs. Note the convention that time is normalized so that the time between inputs is unity.

Associating the input time with the end time of the pulse also introduces a phase shift in the transfer function (3.4-17) of $e^{i\omega r}$. Consequently the transfer function is modified from (3.4-17) to

$$G(\omega) = \sum_{\ell=1}^r e^{-i\omega\ell} G_{\ell}(\omega r) \quad (3.4-22)$$

3.5 RESULTS

The reduced-order state-space modeling described above has been applied to unit hydrographs for a number of basins supplied by NWS. The character of the reduced-order models is illustrated in Section 3.5.1 and described in more detail in Refs. 2 and 4. The problem of spurious high frequency behavior inherent in some multirate unit hydrographs is discussed in Section 3.5.2.

3.5.1 Reduced-Order State-Space Models

The differences in reduced-order models obtained from the canonical correlation and canonical prediction criteria depend very strongly upon the spectral shape of the hydrograph transfer function. A striking comparison in fit using the two criteria was obtained for the Bird Creek basin. The six-hour unit hydrographs based upon the input hydrographs and the canonical correlation procedure are shown in Figs. 3.5-1 and 3.5-2 for 4- and 8-state models respectively. The respectively squared magnitude transfer functions are shown in Figs. 3.5-3 and 3.5-4. Fits obtained using the canonical prediction procedure are illustrated by the unit hydrographs in Figs. 3.5-5 and 3.5-6 and by the squared magnitude transfer functions in Figs. 3.5-7 and 3.5-8. Note that even the 8-state unit hydrograph from the canonical correlation procedure has a significant nonzero tail whereas the 4-state unit hydrograph from the canonical prediction procedure produces an excellent fit. Figures 3.5-3 and 3.5-4 clearly illustrate the tendency of the canonical correlation procedure to fit all frequencies with nearly equal percent error, whereas from Figs. 3.5-7 and 3.5-8 it is seen that in the canonical prediction procedure frequency bands of highest energy are emphasized. Thus for a hydrograph with a large spectral peak and complicated spectral shape, i.e., requiring a high order rational function for a good approximation, the canonical prediction criterion can be expected to excel.

3.5.2 Multirate Unit Hydrographs

The reduced-order modeling of multirate unit hydrographs produces results very similar to those described in Section 3.5.1 for unit hydrographs with the same input and output rates. The major differences encountered for multirate

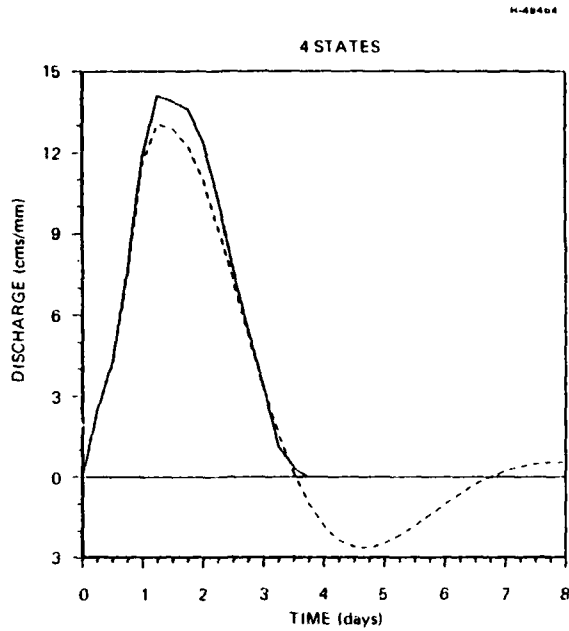


Figure 3.5-1 6-Hour Unit Hydrographs for Bird Creek, Original Hydrograph (Solid Line) and Fourth-Order State-Space Approximation Using the Canonical Correlation Procedure (Dashed Line)

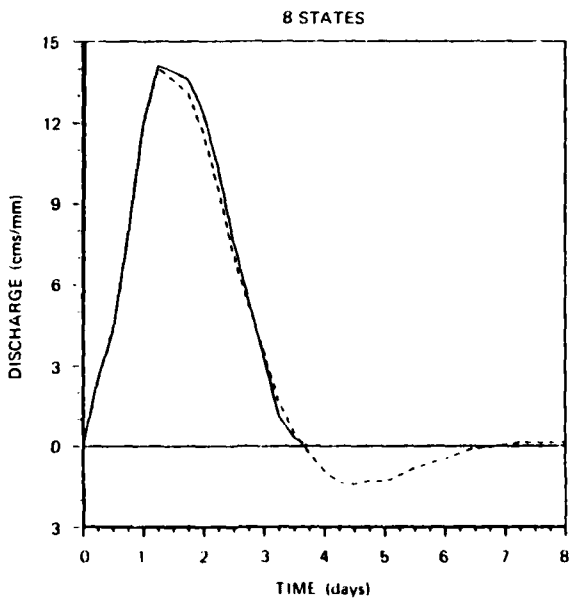


Figure 3.5-2 6-Hour Unit Hydrographs for Bird Creek, Original Hydrograph (Solid Line) and Eight-Order State-Space Approximation Using the Canonical Correlation Procedure (Dashed Line)

R-48465

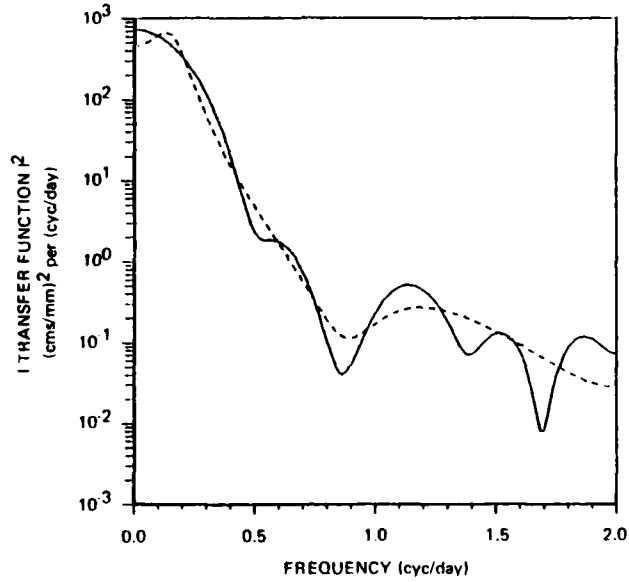


Figure 3.5-3 Squared Magnitude Transfer Function of 6-Hour Unit Hydrographs for Bird Creek, Original Hydrograph (Solid Line) and Four-Order State-Space Approximation Using the Canonical Correlation Procedure (Dashed Line)

R-48465

8 STATES

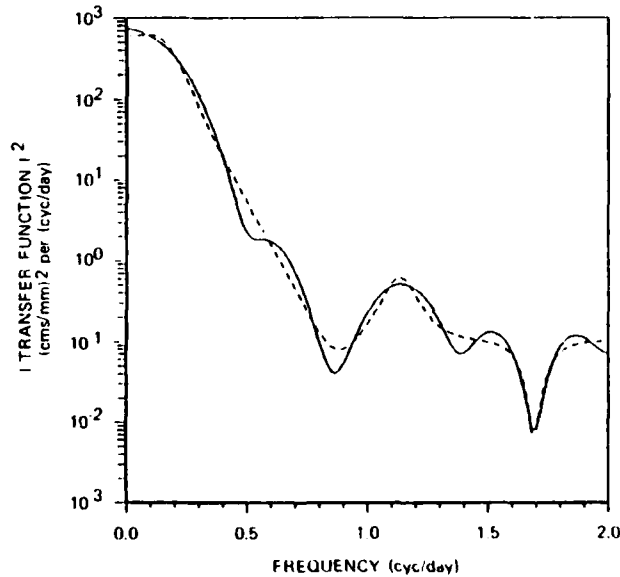


Figure 3.5-4 Squared Magnitude Transfer Function of 6-Hour Unit Hydrographs for Bird Creek, Original Hydrograph (Solid Line) and Eight-Order State-Space Approximation Using the Canonical Correlation Procedure (Dashed Line)

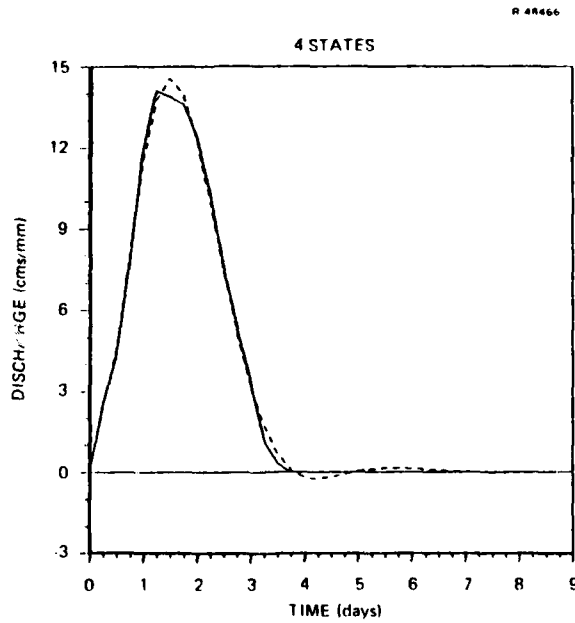


Figure 3.5-5 6-Hour Unit Hydrographs for Bird Creek, Original Hydrograph (Solid Line) and Fourth-Order State-Space Approximation Using the Canonical Prediction Procedure (Dashed Line)

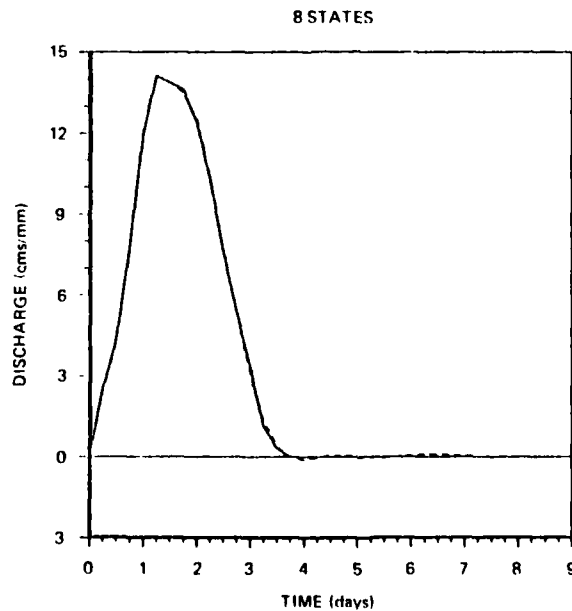


Figure 3.5-6 6-Hour Unit Hydrographs for Bird Creek, Original Hydrograph (Solid Line) and Eight-Order State-Space Approximation Using the Canonical Prediction Procedure (Dashed Line)

H-48467

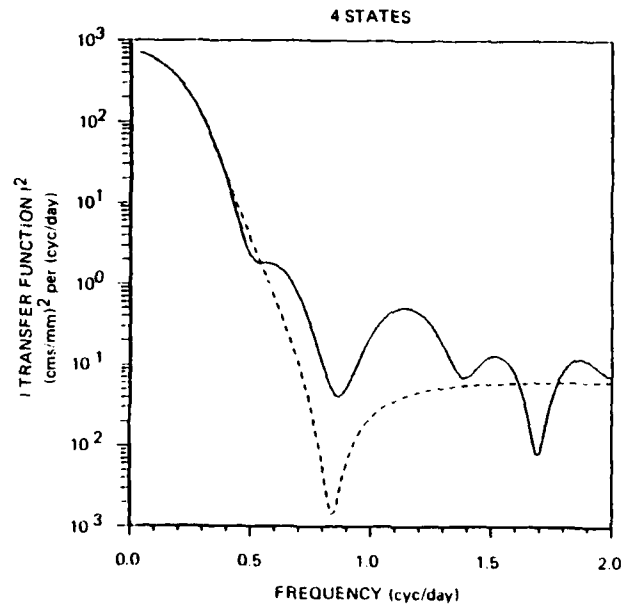


Figure 3.5-7 Squared Magnitude Transfer Function of 6-Hour Unit Hydrographs for Bird Creek, Original Hydrograph (Solid Line) and Fourth-Order State-Space Approximation Using the Canonical Prediction Procedure (Dashed Line)

H-48470

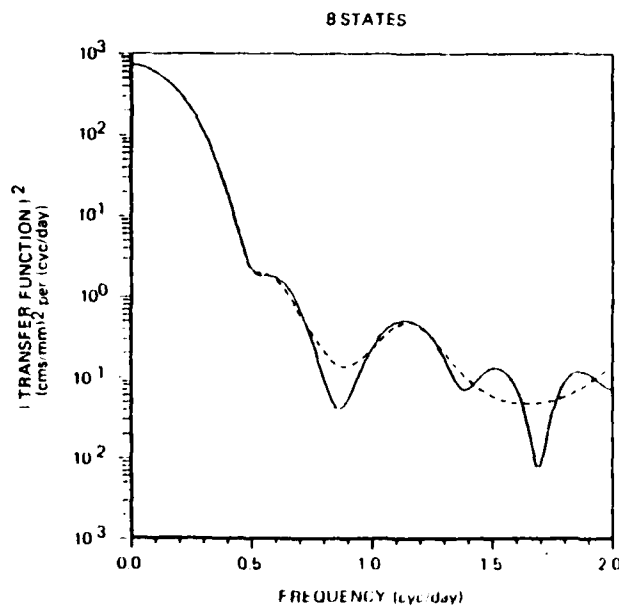


Figure 3.5-8 Squared Magnitude Transfer Function of 6-Hour Unit Hydrographs for Bird Creek, Original Hydrograph (Solid Line) and Eight-Order State-Space Approximation Using the Canonical Prediction Procedure (Dashed Line)

unit hydrographs is inherent in their multirate nature and involves the production of components at the output which are of substantially higher frequency than the input.

For example, consider the unit hydrograph with input every 6 hrs and output every 3 hrs shown in Fig. 3.5-9 with transfer function shown in Fig. 3.5-10. As expressed in Eq. 3.4-18, an excitation by a sampled sine wave at frequency f cyc/day for $0 < f < 2$ produces at the output the sum of two sine waves

$$A_1 \sin(2\pi f + \phi_1) + A_2 \sin(2\pi(4-f) + \phi_2)$$

where A_1^2 and A_2^2 come from Fig. 3.5-10 at frequencies f_1 and $4-f_1$ cyc/day respectively. If a 0.5 cyc/day diurnal component is exciting the unit hydrograph, then the output is the sum of a 0.5 cyc/day and a 3.5 cyc/day with amplitude about one-eighth the 0.5 cyc/day component. The input and output are illustrated in Figs. 3.5-11 and 3.5-12 where the boxes denote the sampling times.

The problem of spurious high frequency components in the output of some multirate unit hydrographs occurs in the present NOAA/NWS forecast system because the catchment model operates at the same rate as the precipitation measurement. This difficulty is completely avoided by implementing the continuous catchment model as discussed in Section 2 so that a channel inflow is produced at the same rate as the channel discharge.

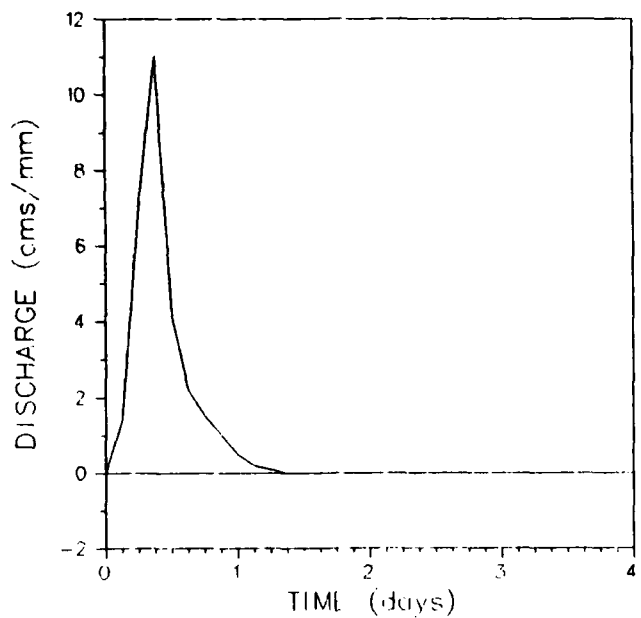


Figure 3.5-9 Multirate Unit Hydrograph With 6-Hour Inputs and 3-Hour Outputs

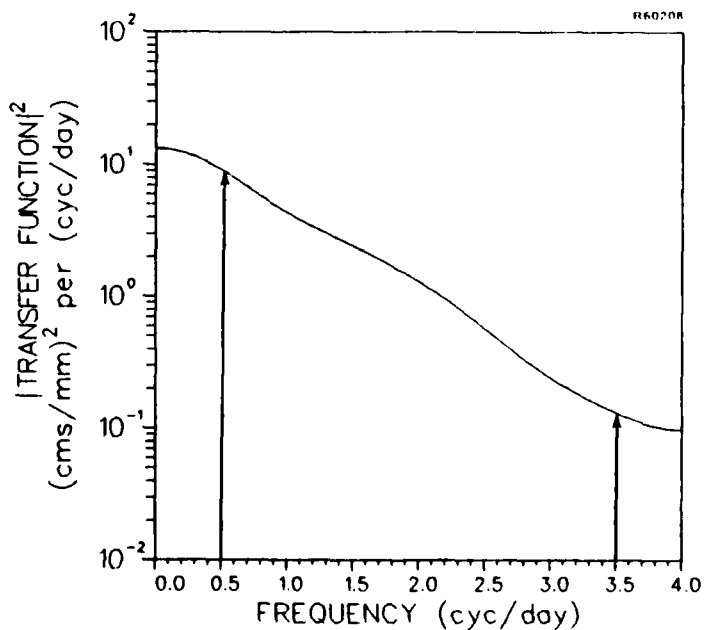


Figure 3.5-10 Squared Magnitude Transfer Function of Multirate Unit Hydrograph Showing Output Components in Response to a 0.5 cyc/day Input

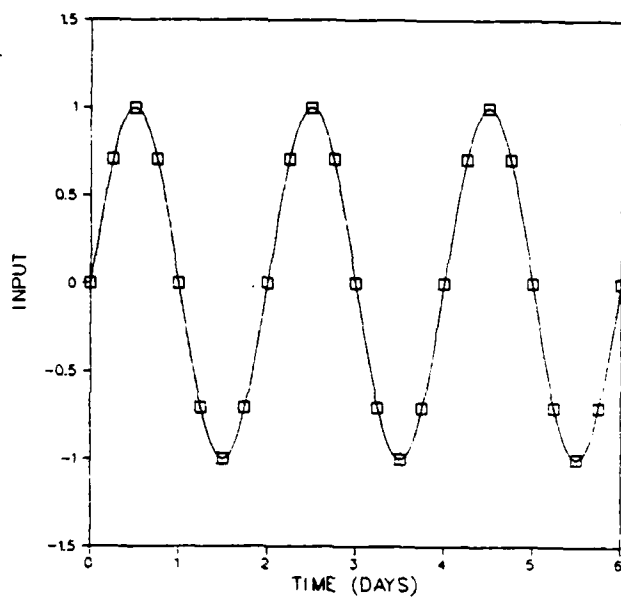


Figure 3.5-11 Input Sine Wave and Sampled Values

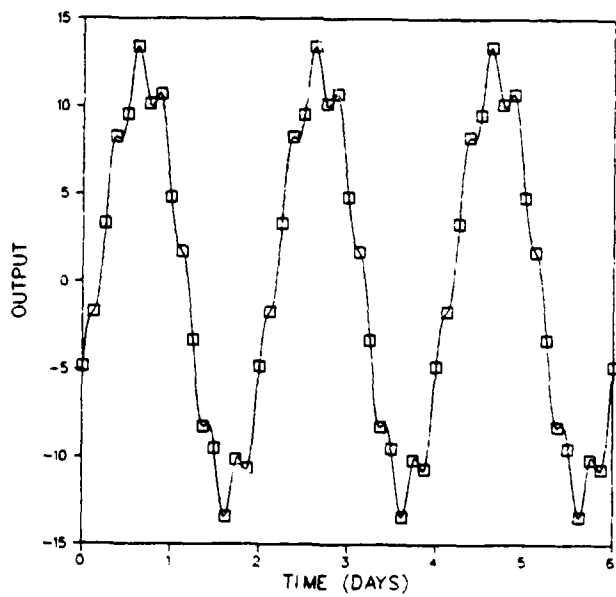


Figure 3.5-12 Output Function With 0.5 cyc/day and 3.5 cyc/day Components

4. PARAMETER IDENTIFICATION FOR CATCHMENT MODELING

The NWS has developed a general conceptual hydrologic model for catchment modeling including a soil moisture accounting program. In Section 2, a continuous time dynamical model of catchment dynamics was derived and discussed in detail. To "tune" this model for specific catchment systems, it is necessary to identify parameters within the structure of the NWS model (Ref. 8). In the calibration of the NWS catchment model, problems of convergence have been encountered. These difficulties are typical of problems arising in similar applications of parameter estimation in many dynamic systems. The objective of this task is to perform an initial analysis of the potential application of maximum likelihood methods to the catchment model parameter estimation problem.

While other methods are useful in particular situations such as recursive online processing or preliminary analysis, the most powerful and robust technique developed to date is the maximum likelihood (ML) method. Important advantages of the maximum likelihood method not generally available in other procedures include:

- Parameter estimates are unbiased and of minimum variance for large samples
- Tests of hypotheses about model structure or order based upon ML estimates are optimum for large samples
- Distributions of the estimation error and test statistics are readily computed

- Computation of the ML estimates is an optimization problem with many different ways available to take advantage of sparse model structures.

The major computational problem is to obtain maximum likelihood estimates of the model parameters using numerical optimization. The early development of system identification techniques was plagued by ill-conditioned optimization problems caused by "nonidentifiable" parameters. Models often include parameters which have little or no effect upon the measurements. Although the statistical problem of estimating such parameters is still well defined and meaningful, severe numerical problems can arise in the optimization procedure. As discussed below, these problems can be largely avoided by inspecting the Fisher information matrix which defines the parameters or combinations of parameters that are not identifiable. The optimization is then constrained to those parameters which are identifiable.

In Section 4.1.1, a general description of the dynamical model of a river basin for the purpose of parameter identification is given. A more detailed description is given in Section 2 and previous progress reports (Refs. 2, 4, 5). Section 4.1.2 is devoted to evaluation of the likelihood function using a Kalman filter and to related computations used in optimization. A detailed description of the Kalman filter for the hydrologic model was given in Chapter 2 of this report. The parameter sensitivities of the state estimate and its error covariance which are required in the optimization are detailed in Section 4.1.3. In Section 4.2, optimization considerations are discussed including a new identifiability theory which avoids ill-conditioning due to nonidentifiability of parameters. Details of a quadratic optimization algorithm and statistical convergence criterion are described. Finally reparameterizations which will accelerate convergence are considered. In

Section 4.3, results from determining parameter identifiability and demonstrating the algorithms on simulated precipitation and channel discharge data are presented.

4.1 LIKELIHOOD FUNCTION FOR DYNAMICAL MODELS

To apply the maximum likelihood method to estimate the parameters of a dynamical hydrological model from observation data requires a procedure for evaluation of the likelihood function for such models. First, the form of the parametric dynamical model is described, and then computational procedures for evaluation of the likelihood function and related quantities needed in the optimization procedure are discussed.

4.1.1 Dynamical Parametric Models

The dynamical model of a basin described in Chapter 2 can be regarded as parametric in the parameters θ as listed in Table 2.2-1. This model is described by the dynamic relationships

$$\dot{\underline{x}}(t) = \underline{f}(\underline{x}, \underline{u}, \underline{w}, \underline{\theta}, t) \quad (4.1-1)$$

with initial condition $\underline{x}(t_0) = \underline{x}_0$ at time t_0 where $\underline{x}(t)$ is the state vector, $\underline{u}(t)$ is a known deterministic input, $\underline{w}(t)$ is white noise with covariance matrix $Q(t)$ and t is time. The initial condition \underline{x}_0 can be considered as a fixed but unknown constant and included in the vector of parameters to be estimated. The measurement model is of the form

$$\underline{z}(t_i) = \underline{h}(\underline{x}, \underline{u}, \underline{v}, \underline{\theta}, t) \quad (4.1-2)$$

where $\underline{v}(t)$ is white measurement noise with covariance matrix $R(t)$. The noise covariance matrices $Q(t, \underline{\theta})$ and $R(t, \underline{\theta})$ can also be considered as functions of unknown parameters to be estimated.

These equations and the correlation structure of the system noise terms imply a correlation structure among the observations $\underline{z}^T = (\underline{z}_1^T, \dots, \underline{z}_N^T)$. To determine maximum likelihood estimates of the parameters $\underline{\theta}$ given the observations \underline{z} requires a procedure for evaluating and maximizing the likelihood function.

4.1.2 Likelihood Function Calculations

The optimization method outlined in section 4.2 requires, for a specified value of the parameters $\underline{\theta}$, calculation of the

- Log likelihood function $\ln p(\underline{z}, \underline{\theta})$
- Gradients $\partial \ln p(\underline{z}, \underline{\theta}) / \partial \theta_i$, $i=1, \dots, k$
- Fisher information matrix with elements $-E[\partial^2 \ln p(\underline{z}, \underline{\theta}) / \partial \theta_i \partial \theta_j]$, $i, j, =1, \dots, k$

where $p(\underline{z}, \underline{\theta})$ is the probability density of the measurements \underline{z} .

These computations are performed by the modular and general PARAIDETM (parameter identification) computer software for maximum likelihood parameter identification. The calculations are structured as follows and described in more detail in following sections:

- Linearize the differential and measurement equations (4.1-1) and 4.1-2) using

PARAIDE is a trademark of The Analytic Sciences Corporation.

symbolic differentiation to obtain the state space matrices F , G , H specifying the linear state space equations about each filtered state estimate $\hat{x}_{i/i}$.

- Implement a Kalman filter using the linearized state equation model to propagate the state estimate and its error covariance matrix $P_{i/i}$.
- Calculate the innovations sequence from the Kalman filter and the resulting error covariance matrices. Evaluate the log likelihood function.
- Calculate the sensitivity functions $\partial F/\partial \theta$, $\partial G/\partial \theta$, $\partial H/\partial \theta$, $\partial Q/\partial \theta$, $\partial R/\partial \theta$ by further symbolic differentiation of the differential and measurement equations (4.1-1) and (4.1-2).
- Implement a Kalman-type algorithm to propagate $\hat{x}_{i/i}/\partial \theta_j$ and $\partial P_{i/i}/\partial \theta_j$ for each θ_j and to evaluate the j^{th} gradient component of the log likelihood function $\partial \ln p(\underline{z}, \underline{\theta})/\partial \theta_j$.
- Evaluate the Fisher information matrix using the gradient calculations.

A method is described for evaluating the joint likelihood function $p(\underline{z}, \underline{\theta})$ of the observations $\underline{z}^T = (z_1^T, \dots, z_N^T)$ for the model described in Eqs. 4.1-1 and 4.1-2 with a particular assumed value $\underline{\theta}$ for the parameters. The approach is to take advantage of the independence properties of the innovations of a Kalman filter.

Consider a value of $\underline{\theta}$ for which evaluation of the likelihood function is desired. If the observations \underline{z} were produced by the model Eqs. 4.1-1 and 4.1-2 with true parameters equal to $\underline{\theta}_0$, then the Kalman filter based upon this model would produce an innovations sequence $\underline{v}_1, \dots, \underline{v}_N$ with

$$\underline{v}_i = \underline{z}_i - H_i \hat{\underline{x}}_{i/i-1} \quad (4.1-3)$$

such that \underline{v}_i is independent of \underline{v}_j for $i \neq j$ with the covariance of \underline{v}_i

$$B_i = H_i P_{i/i-1} H_i^T + R_i \quad (4.1-4)$$

For a linear model the innovations have a Gaussian distribution, and for mild nonlinearities the model is approximately Gaussian. In any case, the quadratic term in Eq. 4.1-5 gives a weighted squared measure of the innovations \underline{v}_i . Assuming a Gaussian distribution for the innovations leads to the expression for the logarithm of the probability density

$$\ln p(\underline{z}, \underline{\theta}_0) = - \frac{1}{2} \sum_{i=1}^N (\ln B_i + \underline{v}_i^T B_i^{-1} \underline{v}_i) + \text{constant} \quad (4.1-5)$$

where the constant depends only on N and not \underline{z} or $\underline{\theta}_0$. This expression was arrived at by taking $\underline{\theta}$ to be the true value $\underline{\theta}_0$ of the process generating the actual observations \underline{z} . However, this is not significant since a formula for evaluating the probability density $p(\underline{z}, \underline{\theta}_0)$ as a function of both \underline{z} and $\underline{\theta}_0$ must yield the correct result for any possible \underline{z} whether or not it in fact came from a model with $\underline{\theta}_0$ the true parameter value.

To maximize the likelihood function, gradients of the log likelihood function are needed. This is obtained by differentiating the log likelihood function with respect to each component θ_j of $\underline{\theta}$

$$\frac{\partial \ln p(\underline{z}, \underline{\theta})}{\partial \theta_j} = - \frac{1}{2} \sum_{i=1}^N \left[\text{tr}(B_i^{-1} \frac{\partial B_i}{\partial \theta_j}) - \underline{v}_i^T B_i^{-1} \frac{\partial B_i}{\partial \theta_j} B_i^{-1} \underline{v}_i + 2 \underline{v}_i^T B_i^{-1} \frac{\partial \underline{v}_i}{\partial \theta_j} \right] \quad (4.1-6)$$

The sensitivities $\partial B_i / \partial \theta_j$ and $\partial \underline{v}_i / \partial \theta_j$ are expressed for a given θ_j in terms of the sensitivities $\partial P_{i/i} / \partial \theta_j$ and $\partial \hat{x}_{i/i} / \partial \theta_j$ of the state estimation error covariance and state estimate by differentiating Eq. 4.1-3 and 4.1-4. This gives

$$\frac{\partial \underline{v}_i}{\partial \theta_j} = - \frac{\partial H_i}{\partial \theta_j} \hat{x}_{i/i-1} - H_i \frac{\partial \hat{x}_{i/i-1}}{\partial \theta_j} \quad (4.1-7)$$

$$\frac{\partial B_i}{\partial \theta_j} = \frac{\partial H_i}{\partial \theta_j} P_{i/i-1} H_i^T + H_i \frac{\partial P_{i/i-1}}{\partial \theta_j} H_i^T + H_i P_{i/i-1} \frac{\partial H_i^T}{\partial \theta_j} + \frac{\partial R_i}{\partial \theta_j} \quad (4.1-8)$$

The sensitivities of the state estimate and its covariance matrix needed in the above equations are obtained in Section 4.1.3 by straightforward but lengthy differentiation of all the Kalman filter equations with respect to θ_j . This results in a set of equations similar in form to the Kalman filter (and in order of computation) except that instead of propagating the state estimate $\hat{x}_{i/i}$ and its covariance matrix $P_{i/i}$, the sensitivities $\partial \hat{x}_{i/i} / \partial \theta_j$ and $\partial P_{i/i} / \partial \theta_j$ are propagated.

Finally, an approximation to the Fisher information matrix is obtained from the gradient calculations. The (i,j) element of the Fisher information is approximated as (Ref. 20)

$$\begin{aligned}
 F_{ij} &= \left(E \frac{\partial \ln p(\underline{z}, \underline{\theta})}{\partial \theta_i} \frac{\partial \ln p(\underline{z}, \underline{\theta})}{\partial \theta_j} \right) \\
 &= \left(\sum_k \frac{\partial v_k^T}{\partial \theta_i} B_k^{-1} \frac{\partial v_k}{\partial \theta_j} + \frac{1}{2} \operatorname{tr} \left(B_k^{-1} \frac{\partial B_k}{\partial \theta_i} B_k^{-1} \frac{\partial B_k}{\partial \theta_j} \right) \right. \\
 &\quad \left. + \frac{1}{4} \operatorname{tr} \left(B_k^{-1} \frac{\partial B_k}{\partial \theta_i} \right) \operatorname{tr} \left(B_k^{-1} \frac{\partial B_k}{\partial \theta_j} \right) \right) \quad (4.1-9)
 \end{aligned}$$

4.1.3 Propagation of State and Covariance Sensitivities

Propagation of sensitivities of the state estimate $\partial \hat{x}_{i/i} / \partial \theta_j$ and its error covariance matrix $\partial P_{i/i} / \partial \theta_j$ with respect to a parameter θ_j are detailed in this section. This involves straightforward differentiation of the Kalman filter equations detailed in Section 2. First the state sensitivities are discussed and then the covariance sensitivities given.

To begin with, we note that the nonlinear differential equations (2.4.1) are parameter dependent so that we write $F_c(\underline{x}_c, \underline{\theta}, t)$ as dependent upon the parameters $\underline{\theta}$. To avoid possible confusion in differentiation, all derivatives of F_c with respect to \underline{x}_c are considered with \underline{x}_c as independent of $\underline{\theta}$ - the chain rule is used to take into account subsequent dependence of \hat{x}_c on $\underline{\theta}$.

The discrete and continuous state estimates \hat{x}_d and \hat{x}_c are propagated according to (2.5-3) and (2.4-5) with the term ξ' deleted. Straightforward differentiation with respect to θ_j , noting that A and B are not functions of θ_j , gives

$$\frac{\partial \hat{x}_c(t_o + \Delta)}{\partial \theta_j} = \frac{\partial \hat{x}_c(t_o)}{\partial \theta_j} + \frac{\partial D}{\partial \theta_j} h + D \frac{\partial h}{\partial \theta_j} \quad (4.1-10)$$

$$\frac{\partial \hat{x}_d[(vk)^0]}{\partial \theta_j} = A \frac{\partial \hat{x}_d[(vk)^-]}{\partial \theta_j} + B \frac{\partial \hat{x}_c[(vk)^-]}{\partial \theta_j} \quad (4.1-11)$$

where

$$\underline{h} = \underline{F}_c(\hat{x}_c(t_0, \underline{\theta}), \underline{\theta}, t_0) \quad (4.1-12)$$

$$\tilde{F}_c = \left. \frac{\partial \underline{F}_c}{\partial \underline{x}_c^T} \right|_{(\hat{x}_c(t_0), \underline{\theta}, t_0)} \quad (4.1-13)$$

and D is the matrix function $(\exp(\tilde{F}_c \Delta) - 1)\tilde{F}_c^{-1}$. Partial derivatives $\partial \underline{h}/\partial \theta_j$ are computed by the chain rule

$$\frac{\partial \underline{h}}{\partial \theta_j} = \left. \frac{\partial \underline{F}_c}{\partial \underline{x}_c^T} \right|_{(\hat{x}_0, \underline{\theta}, t)} \left(\frac{\partial \hat{x}_c}{\partial \theta_j} + \frac{\partial \underline{F}_c}{\partial \theta_j} \right) \quad (4.1-14)$$

Denoting $F = \tilde{F}_c$, the computation of $\Phi(t, t_{i-1})$ and $D(t, t_{i-1})$ can be done along with their partial derivatives as

$$\Phi(\Delta t) = I + \sum_{n=1}^{\infty} \frac{(F\Delta t)^n}{n!} \quad (4.1-15)$$

$$D(\Delta t) = I + \sum_{n=1}^{\infty} \frac{(F\Delta t)^n}{(n+1)!} \Delta t \quad (4.1-16)$$

$$\frac{\partial \Phi(\Delta t)}{\partial \theta_j} = \sum_{n=1}^{\infty} \frac{1}{n!} \frac{\partial (F\Delta t)^n}{\partial \theta_j} \quad (4.1-17)$$

with $\partial (F\Delta t)^n / \partial \theta_j$ computed recursively as

$$\frac{\partial (F\Delta t)^n}{\partial \theta_j} = \Delta t \frac{\partial F}{\partial \theta_j} (F\Delta t)^{n-1} + F\Delta t \frac{\partial (F\Delta t)^{n-1}}{\partial \theta_j} \quad (4.1-19)$$

To accelerate convergence of these series, Φ and D can be computed using these series for a time increment $\Delta t 2^{-n}$ and then $\Phi(\Delta t)$ and $D(\Delta t)$ computed recursively by

$$\Phi(\Delta t 2^{-k}) = [\Phi(\Delta t 2^{-k-1})]^2 \quad (4.1-20)$$

$$\begin{aligned} D(\Delta t 2^{-k}) &= F^{-1}(I - \Phi(\Delta t 2^{-k-1})) (I + \Phi(\Delta t 2^{-k-1})) \\ &= D(\Delta t 2^{-k-1}) (I + \Phi(\Delta t 2^{-k-1})) \end{aligned} \quad (4.1-21)$$

and the partial derivatives $\partial\Phi(\Delta t 2^{-k})/\partial\theta_j$ and $\partial D(\Delta t 2^{-k})/\partial\theta_j$ computed by differentiating these two recursive relations.

Sensitivities of the state estimation error covariance matrix can be conveniently propagated along with the state sensitivities. The partials of the state covariance matrices $\partial P_c/\partial\theta_j$, $\partial P_d/\partial\theta_j$, $\partial P_{cd}/\partial\theta_j$ are obtained by differentiating items 9 and 12 of the Filtering Algorithm in Section 2.5 as

$$\frac{\partial P_c}{\partial\theta_j} \leftarrow \left(\frac{\partial\Phi}{\partial\theta_j}\right) P_c \Phi_c^T + \Phi_c \left(\frac{\partial P_c}{\partial\theta_j}\right) \Phi_c^T + \Phi_c P_c \left(\frac{\partial P_c}{\partial\theta_j}\right)^T + \partial Q \quad (4.1-22)$$

$$\frac{\partial P_{cd}}{\partial\theta_j} \leftarrow \frac{\partial\Phi}{\partial\theta_j} P_{cd} + \Phi_c \frac{\partial P_{cd}}{\partial\theta_j} \quad (4.1-23)$$

for time transition $(v(k+1))^-$ to $(v(k+1))^0$ and

$$\begin{aligned} \frac{\partial P_d}{\partial\theta_j} &\leftarrow \left(\frac{\partial A}{\partial\theta_j}\right) P_d A^T + A \left(\frac{\partial P_d}{\partial\theta_j}\right) A^T + A P_d \left(\frac{\partial A}{\partial\theta_j}\right)^T + \frac{\partial}{\partial\theta_j} (B P_{cd} A^T) \\ &+ \frac{\partial}{\partial\theta_j} (B P_{cd} A^T)^T + \frac{\partial}{\partial\theta_j} (B P_c B^T) \end{aligned} \quad (4.1-24)$$

$$\frac{\partial P_{cd}}{\partial \theta_j} \leftarrow \left(\frac{\partial P_{cd}}{\partial \theta_j} \right) A^T + P_{cd} \left(\frac{\partial A}{\partial \theta_j} \right)^T + \left(\frac{\partial P_c}{\partial \theta_j} \right) B^T + P_c \left(\frac{\partial B}{\partial \theta_j} \right)^T \quad (4.1-25)$$

for time transition $(v(k+1))^-$ to $(v(k+1))^0$.

The remaining relations concern the Kalman update. The Kalman gain sensitivity is

$$\frac{\partial K}{\partial \theta_j} = \left[\frac{\partial P}{\partial \theta_j} H^T + P \frac{\partial H^T}{\partial \theta_j} - (HPH^T + R)^{-1} \frac{\partial H}{\partial \theta_j} PH^T + H \frac{\partial P}{\partial \theta_j} H^T + HP \left(\frac{\partial H}{\partial \theta_j} \right)^T + \frac{\partial R}{\partial \theta_j} \right] (HPH^T + R)^{-1} \quad (4.1-26)$$

Sensitivities of the updated state estimate and its error covariance matrix are given by differentiating items 17 and 18 of the Filtering Algorithm in Section 2.5:

$$\frac{\partial \hat{x}}{\partial \theta_j} \leftarrow \frac{\partial \hat{x}}{\partial \theta_j} + \frac{\partial K}{\partial \theta_j} v + K \frac{\partial v}{\partial \theta_j} \quad (4.1-27)$$

$$\frac{\partial P}{\partial \theta_j} \leftarrow \frac{\partial P}{\partial \theta_j} - \frac{\partial K}{\partial \theta_j} HP - K \frac{\partial H}{\partial \theta_j} P - KH \frac{\partial P}{\partial \theta_j} \quad (4.1-28)$$

4.2 OPTIMIZATION

One of the greatest challenges in parameter identification has been the solution of numerically ill-conditioned or even ill-posed maximization problems. This is a problem receiving considerable attention in least-squares methods and much less attention in the maximum likelihood case. The design of general purpose algorithms which work reliably and efficiently is necessary for the general application of maximum likelihood theory. This is particularly relevant for the

identification of catchment parameters where the differential equations are time varying and involve saturation effects with structural changes in the equations at overflow of various reservoirs. Because of these complications, a general and reliable procedure is required.

Described below is an approach based upon a new small sample theory of identifiability which is usable even when some functions of the parameters are nonidentifiable, i.e., when perturbations of some combinations of the parameters θ produce no change in the likelihood function. In this approach, the nonidentifiable parameters are first determined by inspecting the Fisher information matrix. Then a Levenburg-Marquardt optimization procedure is used in the subspace of parameter space that is orthogonal to the nonidentifiable parameters to compute an identifiable set of parameters.

4.2.1 Identifiability Theory

The introduction of parametric statistical inference concepts and methods by R.A. Fisher (Ref. 21) was one of his major contributions to statistics. Unfortunately, a major difficulty in identifiability problems has been an overemphasis by many researchers on inference about a parameter vector θ rather than inference about the class $F = \{p(z, \theta)\}$ of probability densities indexed by the parameter θ . Most definitions of identifiability concern properties of the resulting parameter estimates rather than intrinsic properties of the class F indexed by the parameter θ . Indeed, some definitions require a hypothetical infinite sample and define identifiability in terms of asymptotic convergence of the estimates to the true parameter values.

This overemphasis on the parameter values rather than the class of probability densities indexed by the parameters

has developed despite the early and fundamental contribution of Ref. 22. This paper explicitly defines identifiability of the class F if unique parameter values produce unique probability densities. This formulation of the problem of specifying probability models for statistical inference includes the identifiability problem - i.e., whether or not the specified models are "observationally" unique. Later developments in the literature seem to have largely overlooked this basic concept except for a few econometric papers (see Ref. 23 and cited references).

In the approach selected for this study, the properties of the parameterized class $\{p(\underline{z}, \underline{\theta}), \underline{\theta} \in \Theta\}$ are the central issue. The above definition of identifiability (Ref. 22) as formulated for the parametric case by Ref. 23 is adopted:

Two parameter points $\underline{\theta}_1$ and $\underline{\theta}_2$ are said to be observationally equivalent if $p(\underline{z}, \underline{\theta}_1) = p(\underline{z}, \underline{\theta}_2)$ with probability 1. A parameter point $\underline{\theta}_1$ is said to be globally identifiable if there is no other $\underline{\theta} \in \Theta$ which is observationally equivalent. A parameter point $\underline{\theta}_1$ is said to be locally identifiable if there exists an open neighborhood of $\underline{\theta}_1$ containing no other $\underline{\theta}$ in Θ which is observationally equivalent.

This approach exploits the equivalence between local identifiability and full rank of the Fisher information matrix as in Ref. 23. To extend this connection much more generally, a powerful new result on existence of identifiable reparameterizations is used (Ref. 24).

Reparameterization Theorem - If the Fisher information matrix $F_{\underline{\theta}}$ of a parameterization $\underline{\theta}$ of the likelihood function has constant rank h in a neighborhood of a point $\underline{\theta}_0$ of parameter space, then there exists a reparameterization $\underline{\psi}(\underline{\theta})$ such

that (ψ_1, \dots, ψ_h) is locally identifiable and the likelihood function is not a function of $(\psi_{h+1}, \dots, \psi_k)$. Furthermore the gradient vectors

$$(\partial\psi_j/\partial\theta_1, \dots, \partial\psi_j/\partial\theta_k)^T \text{ for } j = h+1, \dots, k$$

span the null space of $F_{\underline{\theta}}$.

By using reparameterizations resulting in a nonsingular Fisher information matrix, a complete characterization of local identifiability by the Fisher information is possible in the singular case. Previous results have carefully avoided reparameterizations where existence is not trivially guaranteed by constraints, etc. Such a reparameterization seems to be necessary to obtain these general results.

Another aspect of the identifiability approach is to exploit the special structure involving the Fisher information matrix to devise efficient and numerically well conditioned methods for maximizing the likelihood function. Using the general results on reparameterizations, it is possible to generalize and to make precise a procedure for using generalized inverses in the method of scoring when the Fisher information matrix is singular (Ref. 25). Specifically how the reparameterization result is useful in studying the special structure of the maximum likelihood optimization problem is discussed in detail in the following section.

4.2.2 Maximization of likelihood Functions

Lack of uniqueness, i.e., nonidentifiability, manifests itself as ill-conditioning in computation of least squares or maximum likelihood estimates. Even when the parameters are identifiable, ill-conditioning often arises because of the

considerable difference in sensitivity of the likelihood or squared error functions to changes in different parameters. Some past work used the special structure of least squares problems to devise efficient optimization methods which recognize any nonuniqueness or illconditioning and solve for the parameters within the equivalence due to the nonuniqueness (Refs. 26, 27). Very little progress along these lines has been made in the maximum likelihood problem although a very general method has been proposed (Ref. 25). The maximum likelihood method provides practical parameter estimation and test of hypothesis procedures for many complex random processes, and also provides the needed approximate distribution theory which is not generally available with alternative procedures. Most maximum likelihood methods require that the class of models be reparameterized uniquely so all parameters are identifiable. There are no conditions given for when such a reparameterization is possible. To answer questions of existence and to actually reparameterize involves solving a system of nonlinear partial differential equations.

The method proposed in Ref. 25 presumes that there exists a reparameterization for which the Fisher information matrix is nonsingular and evidently equates such nonsingularity to identifiability although any rigorous discussion or even definition of identifiability in the nonlinear case is lacking. It is argued that the method of scoring (using the Fisher information matrix in place of the Hessian in a Newton type algorithm) can be implemented entirely in the original nonidentifiable parameterization using the pseudoinverse of the Fisher information matrix to restrict the maximization to a locally identifiable subspace of parameter space. This would avoid any need to reparameterize in terms of an identifiable set of parameters. Presently the only alternative method to preclude identifiability difficulties is to actually carry out such a reparameterization

which is often exceedingly difficult if at all feasible computationally. Because of the complexity of the catchment model discussed above, determining such a reparameterization almost certainly would not be feasible.

One of the objectives of the present approach is to use the special structure of the maximum likelihood estimation problem to devise efficient, numerically accurate and stable maximization methods. In particular the method of Ref. 25 can be shown to work very generally utilizing the new result described in Section 4.2.1 which guarantees the local existence of an identifiable reparameterization whenever the Fisher information matrix has constant rank locally. This also generalizes the equivalence of identifiability and full rank of the Fisher information matrix (Ref. 23) to the reduced rank case (the null space is the local equivalence class).

The method of scoring is not only attractive in removing identifiability problems, but it has several other attractive computational features. In a number of problems the Fisher information can be computed from the gradient computations with little additional work. Thus Hessian information is obtained from the gradients without additional computation. It has been found in practice that this Hessian approximation gives excellent approximation to the eigenvectors which dominate the numerical behavior of approximate Hessian methods. This suggests further special structure of the problem since Hessian approximations in illconditioned cases usually result in poor algorithm performance unless there is some special structure.

4.2.3 Quadratic Algorithm for Identifiable Parameters

The above theory provides a basis for an efficient and well behaved algorithm even though there may be nonidenti-

fiable parameters present. The first step is to perform an eigenvalue-eigenvector decomposition of the Fisher information matrix F in the form

$$F = U \Lambda U^T \quad (4.2-1)$$

where the columns of U are orthogonal vectors so $U^T U = I$ and where Λ is diagonal with elements arranged in descending order $\lambda_1 \geq \dots \geq \lambda_n \geq 0$. The algorithm should automatically check that F is positive definite to detect numerical difficulties that might have occurred in computing F . To determine identifiability, a threshold ϵ , say 10^{-12} for double precision with 15 decimal places, is set and any eigenvalues $\lambda_i \leq \epsilon \lambda_1$ are modified as

$$\lambda_i \text{ mod} = \begin{cases} \lambda_i & \text{if } \lambda_i > \epsilon \lambda_1 \\ 0 & \text{if } \lambda_i \leq \epsilon \lambda_1 \end{cases} \quad (4.2-2)$$

The eigenvectors corresponding to the modified eigenvalues set to zero specify the locally nonidentifiable linear combinations $\underline{u}_i^T \underline{\theta}$ of the parameters. The optimization is constrained to the subspace of linear combinations of parameters that are orthogonal to these nonidentifiable combinations, i.e., constrained to the subspace of parameter space spanned by the eigenvectors $\underline{u}_1, \dots, \underline{u}_k$ corresponding to the unmodified eigenvalues.

A quadratic algorithm is one which uses local quadratic information about the log likelihood function, i.e., the gradient (first partial derivatives) and the Hessian (second partial derivatives). The identifiability theory guarantees that the null space of the Hessian will exactly coincide with that of the Fisher information matrix so that perturbations of linear combinations in the null space of the Fisher information matrix will have no effect upon the likelihood function. Since

the log likelihood function is in general only locally quadratic, some procedure is needed to constrain the step $\Delta\theta$ in parameter space to a region in which this quadratic approximation is a reasonable one. An excellent procedure is the so-called Levenburg-Marquardt procedure (Ref. 28) which is discussed in a statistical setting in Ref. 29 as an optimal step that maximizes the quadratic approximation subject to a fixed step length. If, in addition, the optimization is constrained to be orthogonal to the nonidentifiable parameters, then the algorithm has the form

$$\Delta\theta = -(F_{\text{mod}} + \lambda I_{\text{mod}})^{\dagger} \nabla \ln p \quad (4.2-3)$$

where

$\nabla \ln p$ = vector of gradients $\partial \ln p(\underline{z}, \theta) / \partial \theta_i$

$$F_{\text{mod}} = U \Lambda_{\text{mod}} U^T$$

$$I_{\text{mod}} = U \Omega U^T$$

Ω is diagonal with $w_{ii} = \begin{cases} 1 & \text{if } \lambda_{i\text{mod}} > 0 \\ 0 & \text{if } \lambda_{i\text{mod}} = 0 \end{cases}$

λ is a step length parameter

\dagger is the pseudoinverse operation

The calculation is implemented using only vector products as

$$\Delta\theta = - \sum_{i=1}^k \frac{u_i^T (\nabla \ln p)}{\lambda_i + \lambda} u_i \quad (4.2-4)$$

where $\nabla \ln p$ is the gradient vector $\partial \ln p / \partial \theta$.

Trial steps are made with an initial value of λ from initialization of the program or from the last iteration. For

the trial step $\underline{\theta}_{i+1} = \underline{\theta}_i + \Delta\underline{\theta}$, the log likelihood function is evaluated and the quadratic prediction criterion

$$\rho = 1 - \frac{\text{predicted log likelihood}}{\text{actual log likelihood}} \quad (4.2-5)$$

is calculated where the predicted log likelihood $\ln \hat{p}$ is based upon the quadratic approximation

$$\ln \hat{p}(\underline{\theta}_{i+1}) = \ln p(\underline{\theta}_i) + \Delta\underline{\theta}^T \underline{\nabla} \ln p + \Delta\underline{\theta}^T F_{\text{mod}} \Delta\underline{\theta} \quad (4.2-6)$$

The step length parameter λ is adjusted by powers of 2 until

$$.25 < \rho < .75 \quad (4.2-7)$$

or until $\lambda < \lambda_k/8$ in which case λ is set equal to zero and a modified Newton step results.

The above optimization procedure is implemented in the PARAIDETM computer software. This procedure has been used on a number of very complex nonlinear parameter identification problems in the past with very good numerical behavior and convergence.

4.2.4 Acceleration of Convergence by Reparameterization

The rate of convergence of the quadratic algorithm depends upon the goodness of the quadratic approximation to the log likelihood function. This quadratic approximation can be improved by choice of an appropriate parameterization of the likelihood function which stabilizes the Fisher information matrix, that is, which results in a nearly constant matrix with changes in the parameters (Ref. 30). Such a stabilizing parameterization also improves the approximate distribution

theory on the parameter estimates and results in very nearly normal distributions of the estimates even for quite small samples (Ref. 31). This is true in spite of the very nonlinear nature of the catchment model so that with an appropriate reparameterization the problem is nearly quadratic.

Stabilizing reparameterizations are obtained from a given parameterization $\underline{\theta}$ and its Fisher information matrix F_{θ} by finding a reparameterization $\underline{\phi}(\underline{\theta})$ of $\underline{\theta}$ with a gradient $\Delta_{\theta}\phi$ such that

$$F_{\phi} = (\nabla_{\theta}\phi)^{-1T} F_{\theta} (\nabla_{\theta}\phi)^{-1} \quad (4.2-8)$$

is nearly constant independent of the point $\underline{\phi}$ of parameter space, where $\nabla_{\theta}\phi$ is the matrix of partial derivatives with (i,j) element $\partial\phi_i/\partial\theta_j$. This is in general difficult to do, but in many cases there are simple reparameterizations which will yield considerable improvement. Two examples are the variance parameter σ^2 and the correlation coefficient ρ which are improved by the reparameterizations

$$\phi(\sigma^2) = \ln \sigma^2 \quad (4.2-9)$$

$$\phi(\rho) = \frac{1}{2} \ln \frac{1+\rho}{1-\rho} = \text{arc tanh } (\rho) \quad (4.2-10)$$

In general for a single parameter θ the stabilizing reparameterization is given by integrating Eq. 4.2-8 as

$$\phi(\theta) = \int_{\theta_0}^{\theta} (F_{\theta})^{1/2} d\theta \quad (4.2-11)$$

4.2.5 Statistical Convergence Criterion

A convergence criterion is used to decide when the maximum of the likelihood function has been found with suf-

ficient precision. The objective is to make the error $\underline{\theta}_k - \hat{\underline{\theta}}$ between the computed value $\underline{\theta}_k$ at iteration k and the true maximum $\hat{\underline{\theta}}$ small relative to the expected error in $\hat{\underline{\theta}}$ due to sampling variability. Thus the convergence measure

$$(\underline{\theta}_k - \hat{\underline{\theta}})^T [\text{cov}(\hat{\underline{\theta}})]^{-1} (\underline{\theta}_k - \hat{\underline{\theta}}) \leq (\underline{\theta}_k - \hat{\underline{\theta}})^T F(\hat{\underline{\theta}}) (\underline{\theta}_k - \hat{\underline{\theta}}) = \delta \quad (4.2-12)$$

is used, where the inequality follows from the Cramér-Rao lower bound (Ref. 32). Since the function is usually nearly quadratic close to the solution, we have

$$\underline{\theta}_k - \hat{\underline{\theta}} \cong \underline{\theta}_k - \underline{\theta}_{k+1} = - F_k^\dagger \underline{\nabla}_k (\ln p) \quad (4.2-13)$$

and using the notation $\underline{\nabla}_k = \underline{\nabla}_k (\ln p)$ yields

$$\delta \cong \underline{\nabla}_k^T F_k^\dagger \underline{\nabla}_k \quad (4.2-14)$$

Also the error in computing the value of the function $\ln p(\hat{\underline{\theta}})$ is

$$\begin{aligned} \ln p(\hat{\underline{\theta}}) - \ln p(\underline{\theta}_k) &= \underline{\nabla}_k^T (\hat{\underline{\theta}} - \underline{\theta}_k) + (\hat{\underline{\theta}} - \underline{\theta}_k)^T H(\hat{\underline{\theta}} - \underline{\theta}_k) \\ &\cong \underline{\nabla}_k^T (\underline{\theta}_{k+1} - \underline{\theta}_k) + (\underline{\theta}_{k+1} - \underline{\theta}_k)^T H(\underline{\theta}_{k+1} - \underline{\theta}_k) \\ &= \underline{\nabla}_k^T (\underline{\theta}_{k+1} - \underline{\theta}_k) + (\underline{\theta}_{k+1} - \underline{\theta}_k)^T H(\underline{\theta}_{k+1} - \underline{\theta}_k) \\ &= \underline{\nabla}_k^T F_k^\dagger \underline{\nabla}_k + \underline{\nabla}_k^T F_k^\dagger H F_k^\dagger \underline{\nabla}_k \end{aligned} \quad (4.2-15)$$

where H denotes the Hessian matrix. Thus on the average, the maximum value $\ln p(\hat{\underline{\theta}})$ is underestimated by

$$E|\ln p(\hat{\underline{\theta}}) - \ln p(\underline{\theta}_k)| = 2 \underline{\nabla}_k^T F_k^\dagger \underline{\nabla}_k = 2\delta \quad (4.2-16)$$

The quantity $-2\ln p(\hat{\theta})$ is basic in tests of hypotheses. It can be shown that the addition of each unnecessary parameter to the model will decrease the value of the test statistic $-2\ln p(\hat{\theta})$ by a chi-square random variable χ_1^2 on one degree of freedom (Ref. 16). Since $\text{Var}(\chi_1^2) = 2$, the error in computing $-2 \ln p(\hat{\theta})$ as $-2 \ln p(\hat{\theta}_k)$ is 4δ . Thus for $\delta = 10^2$, the error in computing $2 \ln p(\hat{\theta})$ is small compared with the expected sampling variation.

4.3 RESULTS

The maximum likelihood parameter estimation methods are demonstrated on precipitation and discharge measurements simulated using a NWS supplied catchment model. The parameter identifiability question is discussed, and then the local behavior of the algorithms and nature of the parameter estimates described.

4.3.1 Parameter Identifiability

The identifiability of catchment model parameters is illustrated in this section for two contrasting cases of heavy and moderate rainfall. The rainfall and channel discharge data was simulated for Bird Creek basin over a one-month period. The hydrologic structures excited by these rainfall records are compared in Table 4.3-1. The rainfall records are illustrated in Figs. 2.2-4 and 2.6-3 for the moderate and heavy rainfall cases respectively. The various catchment model state histories for the heavy rainfall case are illustrated in Figs. 2.6-4 through 2.6-19.

TABLE 4.3-1
COMPARISON OF MODERATE AND HEAVY RAINFALL CASES

CATCHMENT ELEMENT \ CASE	MODERATE RAINFALL	HEAVY RAINFALL
Maximum upper-zone tension water content	1 time	6 times
Surface runoff	none	3 times
Maximum lower-zone tension water content	1 time	none
Upper-zone free-water content	very little	nonzero half of time

The identifiability of parameters for the heavy rainfall case is shown in Table 4.3-2. The first two columns show the catchment model parameters and their true values used in the simulation of channel discharge data. The approximate standard deviations and correlations of the parameter estimation errors were calculated from the inverse Fisher information matrix. When all fifteen parameters are simultaneously estimated, only x_1^0 and x_2^0 have standard deviations around 1 percent, while the parameters x_3^0 , d_u , d_l' , d_l'' , μ , and a_1 are less than about 10 percent, and the remaining parameters have errors of the order of the parameter values themselves. If however all parameters but one were known or presumed known, then the standard deviation due to sampling variability in estimating only that one parameter is reduced as shown in column 4. In some cases the reduction is nearly two orders of magnitude and generally involves high correlations with other parameters when estimating all fifteen parameters. These high correlations indicate near deterministic dependence between the parameters involved and implies that corresponding changes in these parameters have almost no effect upon the predicted observations.

TABLE 4.3-2
IDENTIFIABILITY OF CATCHMENT PARAMETERS
FOR HEAVY RAINFALL CASE

PARAMETER	TRUE VALUE	STANDARD DEVIATION		HIGH CORRELATIONS, 15 PARAMETERS ESTIMATED
		15 PARAMETERS ESTIMATED	1 PARAMETER ESTIMATED	
x_1^0	120 mm	1.08	0.984	
x_2^0	15 mm	.188	0.019	
x_3^0	160 mm	9.8	1.20	0.87 (x_3^0, x_4^0)
x_4^0	140 mm	57	0.88	
x_5^0	14 mm	9.1	0.19	0.88 (x_4^0, y)
d_u	1.486 E-2 1/hr	3.9 E-4	5.1 E-5	-0.90 (x_5^0, d_{ℓ}'')
d_{ℓ}'	5.452 E-4 1/hr	5.8 E-5	5.0 E-6	
d_{ℓ}''	5.612 E-3 1/hr	1.1 E-3	7.0 E-5	0.92 (x_4^0, α)
y	48	42	1.4	0.993 (y, α)
α	2.1	1.2	0.022	
p_f	0.02	0.009	0.0078	
μ	3.55	0.33	0.043	
a_1	0.17	0.015	0.0046	
a_2	0.001	0.00094	0.00049	
s	0.0	0.88	0.30	

In the case of estimating only one parameter with all others known, the error is less than about 1 percent in all parameters except p_f , a_1 , and a_2 . The more difficult to determine parameters are associated with the percolation function (2.2-18) in both cases of estimating one parameter alone or all fifteen simultaneously.

The identifiability of parameters for the moderate rainfall case is shown in Table 4.3-3. It is qualitatively similar to that of the heavy rainfall case except that the estimation error standard deviations are larger, by orders of magnitude in some instances, and the high correlations are more numerous and some very high (greater than 0.99). When all fifteen parameters are estimated, only x_1^0 can be determined to about 1 percent, x_2^0 to about 25 percent, and the rest are not identifiable. Much of this difficulty is due to the inability to differentiate between the effects of perturbations in different parameters upon the discharge measurement. This is apparent since individual estimation of a parameter with the others known results in an error of less than several percent except for the parameters p_f and a_2 . Note as before that the most dramatic reduction in estimation error between the cases of estimating only one parameter and estimating all fifteen simultaneously occurs when very high correlations are involved.

The conclusions apparent from the identifiability results for the moderate and heavy rainfall cases above are that:

- Sufficient rainfall to excite all basin dynamics is required if parameters are to be estimated simultaneously
- Some of the parameters associated with the percolation function are not identifiable even if all other parameters were known exactly.

The identifiability of parameters for a given basin will thus depend very strongly upon the available records of storms or high snowmelt. Just increasing the length of the data used will not significantly improve the identifiability. What is needed is more data involving the excitation of the basic dynamics in different ways.

TABLE 4.3-3
IDENTIFIABILITY OF CATCHMENT PARAMETERS
FOR MODERATE RAINFALL CASE

PARAMETER	TRUE VALUE	STANDARD DEVIATION		HIGH CORRELATIONS, 15 PARAMETERS ESTIMATED
		15 PARAMETERS ESTIMATED	1 PARAMETER ESTIMATED	
x_1^0	120 mm	1.4	1.0	
x_2^0	15 mm	3.5	0.56	0.86 (x_2^0, x_4^0)
x_3^0	160 mm	3600.	2.6	0.84 (x_3^0, d_u)
x_4^0	140 mm	3200.	2.1	-0.87 (x_3^0, x_4^0)
x_5^0	14 mm	120.	0.72	-0.89 (x_3^0, d'_l)
d_u	1.486 E-2 1/hr	14.8 E-2	0.077 E-2	0.83 (x_4^0, d'_l)
d'_l	5.452 E-4 1/hr	7.6 E-4	0.06 E-4	-0.85 (x_3^0, μ)
d''_l	5.612 E-3 1/hr	5.7 E-3	0.21 E-3	0.84 (x_3^0, a_1)
γ	48	2200.	3.1	-0.86 (α, a_1)
α	2.1	56.	0.042	0.95 (γ, α)
p_f	0.02	0.42	0.063	-0.998 (d_u, μ)
μ	3.55	50.	0.039	0.88 (d'_l, μ)
a_1	0.17	7.9	0.007	-0.998 (μ, a_1)
a_2	0.001	0.0025	0.0009	0.9999 (a_1, d_u)
s	0.0	8.7	0.22	-0.98 (x_5^0, s)

4.3.2 Demonstration of Algorithm

The local behavior of the parameter identification algorithm near the maximum of the likelihood function is described. The global behavior from various initial parameter

estimates will require more extensive investigation but is expected to reproduce the generally robust and efficient behavior of quadratic hill climbing methods (Ref. 33).

The case considered is the heavy rainfall case discussed in Section 4.3.1 and the precipitation record is shown in Fig. 2.6-3. To reduce the computer time required, only the first 10 days were used and the three parameters x_1^0 , x_2^0 , and d_u were simultaneously estimated. The computer CPU time on an IBM 370/3031 using a PL/1 optimizing compiler was about 3 min per iteration on the parameter values and was approximately the number of parameters estimated (3 in this case) times the CPU time for a Kalman filter run. There is great potential for considerably reducing the required CPU time by exploiting the special problem structure especially in the initial stages where the parameter estimates are far away from the maximum likelihood estimates. When the maximum is approached, the log likelihood is approximately quadratic and convergence accelerates very rapidly as discussed below. Thus few iterations are needed near the solution.

Table 4.3-4 gives the result of four iterations of the algorithm starting from the true parameter values. These starting values are about 1%, 15%, and 10% respectively from the maximum likelihood for x_1^0 , x_2^0 , and d_u . The standard deviations show little change for x_1^0 but moderate change for x_2^0 and d_u . This suggests that the errors in estimating x_2^0 and d_u have a probability distribution slightly different from normal. A reparameterization may help this problem.

The changes in the likelihood function value are due almost entirely to changes in the quadratic term which is the sum of normalized innovations. If the parameter estimates were normally distributed, then twice the difference of the log likelihood functions evaluated respectively at the true

TABLE 4.3-4
ITERATIONS OF PARAMETER ESTIMATION ALGORITHM

ITERATION		0	1	2	3	4
ESTIMATE	x_1^0	1.20000E+02	1.21162E+02	1.21309E+02	1.21325E+02	1.21328E+02
	x_2^0	1.50000E+01	1.67943E+01	1.71659E+01	1.72048E+01	1.72079E+01
	d_u	1.48600E-02	1.63311E-02	1.66543E-02	1.66872E-02	1.66898E-02
STANDARD DEVIATION	x_1^0	1.12097E+00	1.11972E+00	1.12012E+00	1.12006E+00	1.12000E+00
	x_2^0	6.92976E-01	8.34626E-01	8.68233E-01	8.71832E-01	8.72117E-01
	d_u	5.80146E-04	7.18584E-04	7.49106E-04	7.52249E-04	7.52483E-04
CORRELATION COEFFICIENTS	x_1^0, x_2^0	7.32222E-02	9.62467E-02	1.00572E-01	1.00696E-01	1.00518E-01
	x_1^0, d_u	3.43664E-01	3.70227E-01	3.73503E-01	3.73648E-01	3.73552E-01
	x_2^0, d_u	1.06537E-01	2.57950E-01	2.83361E-01	2.85937E-01	2.86119E-01
GRADIENT	x_1^0	-7.99974E-02	3.64569E-02	1.50046E-03	-7.35625E-04	-4.80486E-04
	x_2^0	-3.38014E+00	-4.22690E-01	-4.04837E-02	-3.26361E-03	-2.44945E-04
	d_u	-3.88762E+03	-5.20219E+02	-4.62047E+01	-3.12653E+00	-6.04826E-02
	NORM	3.88762E+03	5.20219E+02	4.62047E+01	3.12654E+00	6.04850E-02
QUADRATIC TERM	1.56554E+02	1.43843E+02	1.43378E+02	1.43362E+02	1.43361E+02	
LOG DET TERM	-4.94978E+01	-4.88951E+01	-4.87714E+01	-4.87589E+01	-4.87580E+01	
LOG LIKELIHOOD	-5.35280E+01	-4.74742E+01	-4.73031E+01	-4.73014E+01	-4.73014E+01	
CONVERGENCE CRITERION	1.18769E+01	3.19833E-01	3.07043E-03	2.00536E-05	3.84277E-07	

values and maximum likelihood estimated values of the parameters would be a chi-square random variable on 3 degrees of freedom (Ref. 32). This difference is 12.45 which is statistically significant at the 0.01 level, i.e., a departure this large would occur less than 1 percent of the time under the normality assumption. This indicates significant non-normality and/or a nonzero mean due to nonlinearities in the catchment and rainfall models. Also, the quantity $(\hat{\theta} - \theta)^T F(\hat{\theta} - \theta)$ would be a chi-square random variable on 3 degrees of freedom if the parameter estimates were distributed normally with zero mean. This quantity is 18.17 and 9.68 respectively for the Fisher information matrix evaluated at the true parameter θ and at the maximum likelihood estimates $\hat{\theta}$. This further indicates some departure from the theoretical distribution of the estimates. These quantities would be expected to be smaller than about 7.8 ninety-five percent of the time. Such a departure is easily caused by a standard deviation being wrong by a factor of 2. The above discussion indicates that the computed sampling distribution as indicated by the Fisher information and standard deviations are accurate within a factor of 2.

Further nonlinear effects are apparent in the discharge and precipitation innovations. The precipitation innovations in Fig. 4.3-1 show large departures around 4 days. These large departures are due to the nonlinear, nongaussian precipitation model whose probability density has heavy tails so that deviations of 5 standard deviations are not too unlikely. This accounts for the two large peaks in Fig. 4.3-4 which displays the innovations normalized by their inverse covariance matrix. Due to nonlinearities in the precipitation and catchment models, a deterministic filtering error appears in the discharge innovations as shown in Fig. 4.3-2 at the true and estimated parameter values. This deterministic function is somewhat obscured by the innovations noise as shown in Fig. 4.3-3, however in other

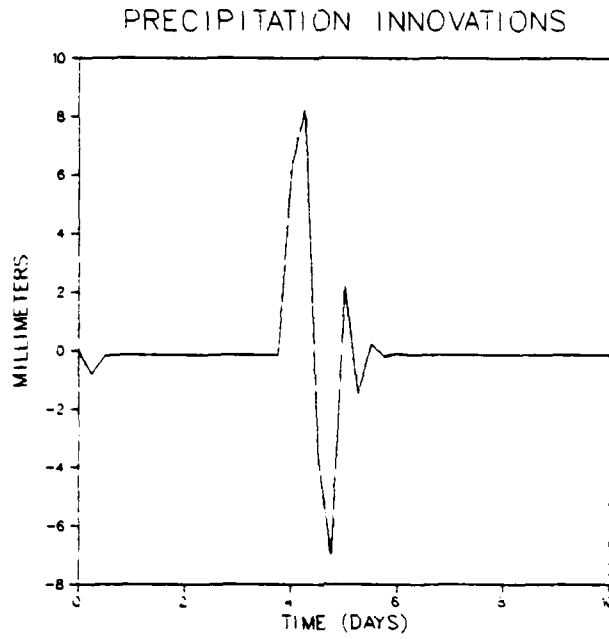


Figure 4.3-1 Precipitation Innovations

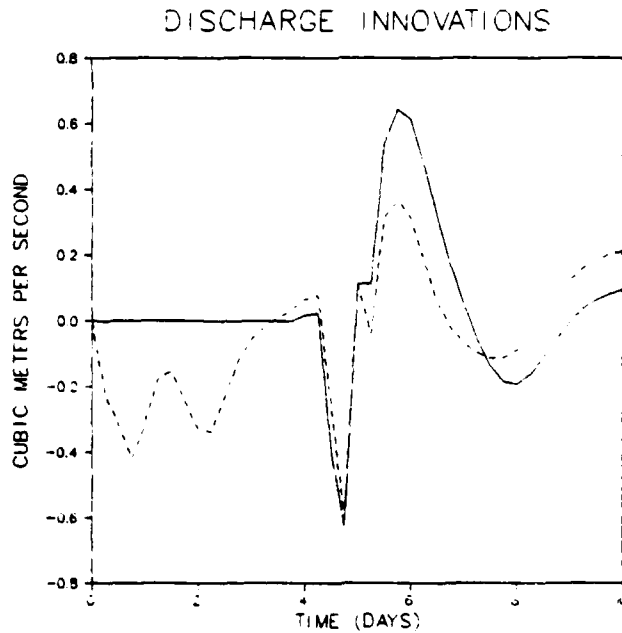


Figure 4.3-2 Deterministic Component of Channel Discharge Innovations for True (Solid Line) and Estimated (Dashed Line) Parameter Values

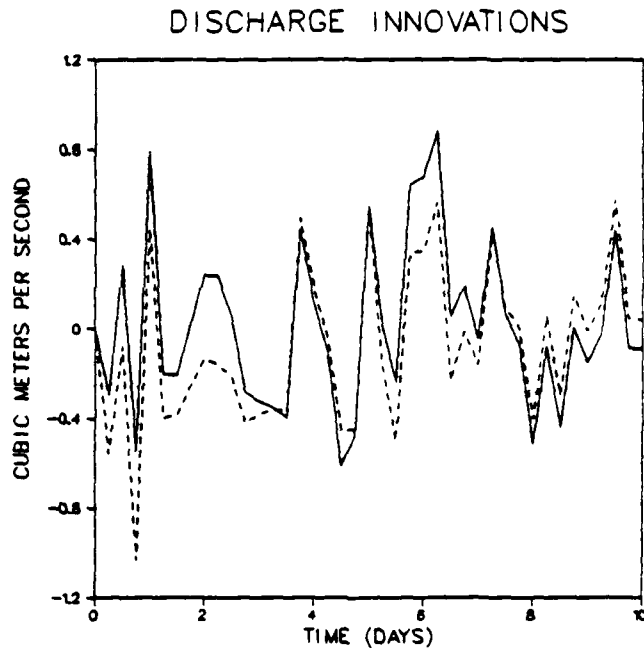


Figure 4.3-3 Discharge Innovations for True (Solid Line) and Estimated (Dashed Line) Parameter Values

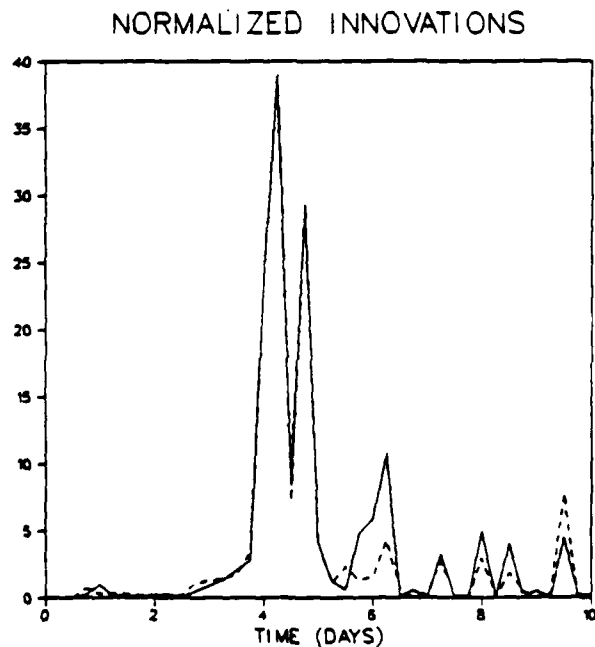


Figure 4.3-4 Normalized Innovations for True (Solid Line) and Estimated (Dashed Line) Parameter Values

cases it can be expected that, relative to the noise, very large deterministic components can occur in the discharge innovations due to nonlinearities. Except for the peaks due to these nonlinearities, the normalized innovations look quite reasonable.

The convergence behavior of the algorithm is indicated by the convergence criterion and confirmed by the gradients and gradient norm (root mean square of gradients). The convergence criterion exhibits a characteristic linear convergence where the convergence criterion δ is reduced by approximately the same factor 10^{-2} on each iteration. Convergence is achieved for practical purposes on the second iteration ($\delta < 10^{-2}$), but the algorithm was continued to demonstrate the character of the convergence and precision of the computations.

The demonstration of the maximum likelihood algorithm shows the potential for its use in NWS river forecast system. The algorithm behaved efficiently and robustly in the presence of nonlinear dynamics and nongaussian noise. Reasonable values for the parameter estimates were obtained which were close to the error predicted by the approximate sampling distribution theory. More extensive testing of the algorithm is required to determine how general these conclusions are.

5. SUMMARY AND CONCLUSIONS

Applications of modern estimation and filtering theory to the requirements of the National Weather Service (NWS) were investigated to assess their potential for improving river flow forecasting and catchment model calibration.

The work was organized into three principal tasks:

- Issues in filter design
- State-space model development for unit hydrographs
- Parameter identification for catchment modeling.

5.1 ISSUES IN FILTER DESIGN

The applications of Kalman filtering techniques to hydrologic forecasting required the development of catchment state-space models. These were obtained by

- Developing continuous-time nonlinear state-space equations for the Sacramento Soil Moisture model
- Modifying the distribution of the percolation to the lower zone to avoid slight inconsistencies in the Sacramento model
- Modeling channel routing with reduced-order state-space models for unit hydrographs

- Using state augmentation techniques to combine the soil moisture and channel routing systems to generate a complete catchment model.

An extended Kalman filter for the estimation of the state of the catchment system and the prediction of the discharge to the channel was designed and its performance tested with simulated data. Excellent agreement between true and forecasted flows was obtained even under surface runoff conditions. The results indicate that the extended Kalman filtering technique constitutes a very well behaved procedure for the practical forecasting of the discharge from a basin.

5.2 STATE-SPACE MODEL DEVELOPMENT FOR UNIT HYDROGRAPHS

The canonical variate method of deriving reduced-order state-space models of unit hydrographs gives

- Optimal reduced-order models in terms of weighted squared prediction error
- An automatic procedure suitable for computer implementation
- A computationally efficient and numerically stable algorithm.

The modeling of NOAA/NWS supplied unit hydrographs indicates that

- The sum square error criterion is superior to the correlation criterion in producing good low order approximations to the unit hydrograph
- Considerable reduction in state order was typical - from order ten or twenty to order three or five

- Multirate unit hydrographs were no more difficult to approximate than those with the same input-output rate.

This reduced order state space modeling effort was highly successful in achieving the objectives of the study. One inherent difficulty in multirate unit hydrographs was discovered - certain particular unit hydrographs introduce spurious high frequencies in the output as a result of a low frequency sampled sine wave input. The need for multirate unit hydrographs is completely avoided by using the continuous catchment model derived in this report and integrating to obtain a discrete time model operating at the same rate as the channel routing model.

5.3 PARAMETER IDENTIFICATION FOR CATCHMENT MODELING

The application of maximum likelihood methods to the catchment model parameter identification problem provides an initial evaluation of its potential use by NOAA/NWS. The maximum likelihood methods described in this study provide

- A determination of parameter identifiability
- A robust optimization algorithm which is immune to parameter nonidentifiability
- Estimates of the identifiable parameters and their estimation error covariances
- An automatic procedure suitable for computer implementation.

These methods were used on simulated precipitation and channel discharge data generated using a NOAA/NWS supplied catchment model for the Bird Creek basin. Identification of the catchment model parameters indicates that

- Parameter identifiability is determined by the extent to which the data excites the relevant hydrologic structures
- The optimization algorithm converges very rapidly near the solution.

The maximum likelihood method has been demonstrated as a powerful, automatic procedure with potential for wide spread use in the fitting of NOAA/NWS catchment models.

5.4 RECOMMENDATIONS

There are several important areas for future investigation suggested by this study in the identification of catchment model parameters

- Initialization and improved computational efficiency in recursive refinement of parameter estimates
- Tests of hypotheses between alternative hydrological model structures
- Use of robust methods on data for handling outliers
- Application of both the Kalman filtering and parameter identification to a number of data sets for a variety of basins.

Such future study would demonstrate the generality with which these methods apply to the NOAA/NWS operational hydrologic forecasting.

APPENDIX A

The constraint on the ratio of free to tension water for the upper zone is analyzed in this appendix. It is shown below that this constraint is superfluous for all basins examined.

When the constraint is removed, the state-equations for the upper zone can be derived as follows (Ref. 2). Consider first the tension-water element. Two quantities can affect the rate of increase of the contents of the tension-water element: the instantaneous moisture input and the evapotranspiration demand. The evapotranspiration rate from the upper-zone tension-water element is $u_2(x_1/x_1^0)$. The moisture input rate, up to the point when tension-water requirements are met, is u_1 . At the time when $x_1 = x_1^0$, two possibilities arise:

- The moisture input rate is larger than or equal to the evapotranspiration demand
- The moisture input rate is smaller than the evapotranspiration demand.

In the first case, part of the input moisture replaces the amount of water which is being lost through the evapotranspiration process. The tension-water content remains at its maximum value and the free-water element receives the excess moisture input (see discussion below). In the second case, the net rate of increase of the tension-water content is negative and x_1 starts to diminish. Summarizing,

$$\dot{x}_1 = \left(u_1 - u_2 \frac{x_1}{x_1^0} \right) [h_e(x_1 - x_1^0) + h_f(x_1 - x_1^0) h_f(u_2 - u_1)] \quad (A-1)$$

where h_e and h_f are given by Eqs. 2.2-23 and 2.2-24.

The moisture input rate available for the upper zone free water element is $(u_1 - u_2) h_f(x_1 - x_1^0) h_e(u_2 - u_1)$. At any given time the upper-zone free-water element loses water through interflow at a rate of $d_u x_2$ and supplies the lower zone through percolation at a rate p given by Eq. 2.2-13. If the net inflow rate to the upper-zone free-water element is positive for a prolonged period of time, x_2 will attain its maximum value and surface runoff will start to occur. The rate at which surface runoff occurs is the excess of the moisture input, $(u_1 - u_2) h_f(x_1 - x_1^0) h_e(u_2 - u_1)$, over the sum of interflow and percolation rates, $d_u x_2 + p$. When this quantity is negative, the upper-zone free-water content starts to diminish. Thus,

$$\begin{aligned} \dot{x}_2 = & [(u_1 - u_2) h_f(x_1 - x_1^0) h_e(u_2 - u_1) - d_u x_2 - p] \\ & \times \{h_e(x_2 - x_2^0) + h_f(x_2 - x_2^0)\} \\ & \times h_f[d_u x_2^0 + p - (u_1 - u_2) h_f(x_1 - x_1^0) h_e(u_2 - u_1)] \end{aligned} \quad (A-2)$$

Recall the constraint on the ratio of free to tension water: the normalized free-water content should not exceed the normalized tension-water content, i.e.,

$$x_2/x_2^0 \leq x_1/x_1^0 \quad (A-3)$$

If at some time, t ,

$$x_2(t)/x_2^0 = x_1(t)/x_1^0 \quad (\text{A-4})$$

then

$$\dot{x}_2(t^+)/x_2^0 \leq \dot{x}_1(t^+)/x_1^0 \quad (\text{A-5})$$

Next, it will be shown that when Eq. A-4 holds, Inequality A-5 is automatically satisfied with the SSM model parameters for 17 different basins. Thus if the state of the system is initialized at a point at which constraint A-3 is satisfied, the constraint will be satisfied from then on.

Suppose Eq. A-4 holds at time t and set

$$\psi = \frac{x_1(t)}{x_1^0} = \frac{x_2(t)}{x_2^0} \quad (\text{A-5})$$

Three different possibilities arise

- $x_1(t) = x_2(t) = 0$, ($\psi = 0$)
- $0 < x_1(t) < x_1^0$ and $0 < x_2(t) < x_2^0$, ($0 < \psi < 1$)
- $x_1(t) = x_1^0$ and $x_2(t) = x_2^0$, ($\psi = 1$).

In the first case, the inflow rates to the tension and free-water elements are

$$\dot{x}_1(t) = u_1 \quad (\text{A-7})$$

and

$$\dot{x}_2(t) = 0 \quad (\text{A-8})$$

Therefore, Inequality A-5 is automatically satisfied.

Consider, next, the second alternative. The state equations for the upper-zone elements become

$$\dot{x}_1(t) = u_1 - u_2 x_1 / x_1^0 \quad (A-9)$$

$$\dot{x}_2(t) = -d_u x_2 - p \quad (A-10)$$

Therefore, the normalized inflow rates are

$$\frac{\dot{x}_1(t)}{x_1^0} = \frac{u_1}{x_1^0} - \psi \frac{u_2}{x_1^0} \quad (A-11)$$

and

$$\frac{\dot{x}_2(t)}{x_2^0} = -d_u \psi - \frac{p}{x_2^0} \quad (A-12)$$

In this case, Inequality A-5 is equivalent to

$$-d_u \psi - \frac{p}{x_2^0} \leq \frac{u_1}{x_1^0} - \psi \frac{u_2}{x_1^0} \quad (A-13)$$

which can be rewritten as

$$-(d_u - \frac{u_2}{x_1^0}) \psi \leq \frac{u_1}{x_1^0} + \frac{p}{x_2^0} \quad (A-14)$$

Since the expression on the right hand side of last inequality is nonnegative, the inequality will certainly hold if

$$d_u \geq u_2 / x_1^0 \quad (A-15)$$

Table A-1 compares the values of the interflow parameter d_u with the maximum evapotranspiration rate, u_2^0 , normalized by the capacity of the upper-zone tension water element,

TABLE A-1
COMPARISON OF EVAPOTRANSPIRATION AND DRAINAGE RATES

BASIN	u_2^0 (mm/hr)	x_1^0 (mm)	u_2^0/x_1^0 (1/hr)	d_u (1/hr)
White River	5.8333E-2	50	1.1667E-3	1.4861E-2
French Broad	5.0000E-2	85	5.8824E-4	1.4861E-2
Bird Creek	2.7850E-2	120	2.3958E-4	1.4861E-2
Leaf River	5.6250E-2	20	2.8125E-3	1.7949E-2
Meramec River	5.3333E-2	93	5.7347E-4	1.7313E-2
Danville, VA	1.9250E-1	249	7.7309E-4	4.6194E-2
Ariton, Ala.	1.9167E-1	75	2.5556E-3	9.2976E-3
Fulton, Miss.	2.2917E-1	70	3.2739E-3	3.3271E-2
Culloden, Ga.	1.9583E-1	132	1.4836E-3	1.7949E-2
Northside, NC	2.6458E-1	78	3.3921E-3	3.5555E-2
Eagle River	1.4583E-1	10	1.4583E-2	1.4861E-2
	1.8333E-1	20	9.1665E-3	1.4861E-2
S. Yamhill River	1.1875E-1	120	9.8958E-4	1.7949E-2
Clear Boggy Creek	4.1667E-2	25	1.6667E-3	3.6103E-3
Illinois River	8.3333E-2	28	2.9762E-3	8.1166E-3
Beaver Creek	5.4167E-2	27	2.0062E-3	1.3457E-2
Baron Fork	8.3333E-2	21	3.9682E-3	1.1107E-2
Shoal Creek	6.2500E-2	20	3.1250E-3	1.5521E-2

x_1^0 , for 17 different basins. In all instances Inequality A-15 is satisfied.

Finally, for the last possibility, $x_1 = x_1^0$ and $x_2 = x_2^0$.
The state equations become

$$\dot{x}_1(t) = (u_1 - u_2) h_f(u_2 - u_1) \quad (A-16)$$

$$\begin{aligned} \dot{x}_2(t) = & [(u_1 - u_2) h_e(u_2 - u_1) - d_u x_2^0 - p] \\ & \times h_f[d_u x_2^0 + p - (u_1 - u_2) h_e(u_2 - u_1)] \end{aligned} \quad (A-17)$$

If $u_1 > u_2$, Eqs. A-16 and A-17 reduce to

$$\dot{x}_1(t) = 0 \quad (A-18)$$

$$\dot{x}_2(t) = (u_1 - u_2 - d_u x_2^0 - p) h_f(d_u x_2^0 + p - u_1 + u_2) \quad (A-19)$$

Thus, $\dot{x}_2(t) \leq 0$ and, consequently, Inequality A-5 must be satisfied. If $u_1 \leq u_2$, the state-equations are identical to Eqs. A-9 and A-10 and the same analysis used for the case $0 < \psi < 1$ shows that the normalized inflow rates into the upper-zone elements satisfy Inequality A-5.

Therefore, for all basins listed in Table A-1, the constraint on the ratio of free to tension-water for the upper-zone is ineffective.

REFERENCES

1. Ayres, C.L., "Reduced Order Unit Hydrograph Program Documentation," The Analytic Sciences Corporation, Report No. TR-1480-2, March 1980.
2. Brammer, R.F., Goldstein, J.D., and Larimore, W.E., "Quarterly Progress Report for the Period Ending 30 June 1979," The Analytic Sciences Corporation, Report No. PR-1480-1, July 1979.
3. Goldstein, J.D., "Lower-Zone and Channel-Inflow State-Equations for the Sacramento Soil Moisture Model," The Analytic Sciences Corporation, Report No. TIM-1480-1, August 1979.
4. Brammer, R.F., Goldstein, J.D., and Larimore, W.E., "Quarterly Progress Report for the Period Ending 30 September 1979," The Analytic Sciences Corporation, Report No. PR-1480-2, October 1979.
5. Brammer, R.F., Goldstein, J.D., and Larimore, W.E., "Quarterly Progress Report for the Period Ending 31 December 1979," The Analytic Sciences Corporation, Report No. PR-1480-3, January 1980.
6. Kitanidis, P.K., and Bras, R.L., "Real Time Forecasting of River Flows," Report No. 235, Department of Civil Engineering, Massachusetts Institute of Technology, Cambridge, June 1978.
7. Gelb, A. (Editor), Applied Optimal Estimation MIT Press, Cambridge, 1974.
8. Peck, E., "Catchment Modeling and Initial Parameter Estimation for the National Weather Service River Forecast System," NOAA Technical Memorandum NWS HYDRO-31, June 1976.
9. Akaike, H., "Canonical Correlation Analysis of Time Series and the Use of An Information Criterion," System Identification: Advances and Case Studies, R.K. Mehra and D.G. Lainiotis, Eds., New York: Academic Press, pp. 27-96, 1976.

REFERENCES (Continued)

10. Akaike, H., "Markovian Representation of Stochastic Processes by Canonical Variables," SIAM J. Contr., Vol. 13, pp. 162-173, 1975.
11. Akaike, H., "Markovian Representation of Stochastic Processes and Its Application to the Analysis of Autoregressive Moving Average Processes," Ann. Inst. Stat. Math., Vol. 26, pp. 363-387, 1974.
12. Akaike, H., "Stochastic Theory of Minimal Realization," IEEE Trans. Automat. Contr., Vol. 19, pp. 667-674, 1974.
13. Hotelling, H., "Relations Between Two Sets of Variates," Biometrika, Vol. 28, pp. 321-377, 1936.
14. Anderson, T.W., An Introduction to Multivariate Statistical Analysis, New York: Wiley, 1958.
15. Golub, G.H., "Matrix Decompositions and Statistical Calculations," Statistical Computation, R.C. Milton and J.A. Nelder, Eds., New York: Academic Press, pp. 365-397, 1969.
16. Shannon, C.E., and Weaver, W., Mathematical Theory of Communication, Urbana, Illinois: University of Illinois Press, 1962.
17. Gelfand, I.M., and Yaglom, A.M., "Calculation of the Amount of Information About a Random Function Contained in Another Such Function," Amer. Math. Soc. Transl., Series (2), Vol. 12, pp. 199-246, 1959 (original Usp. Mat. Nauk., Vol. 12, pp. 3-52, 1956).
18. Yaglom, A.M., "Outline of Some Topics in Linear Extrapolation of Stationary Random Processes," Proc. Fifth Berkeley Symp. Math. Stat. and Prob., Berkeley, California, Californi Press, pp. 259-278, 1970.
19. Kalman, R.E., "A New Approach to Linear Filtering and Prediction," Trans. ASME, J. Basic Eng., Vol. 82, pp. 35-45, 1960.
20. Gupta, N.K., and Mehra, R.K., "Computational Aspects of Maximum Likelihood Estimation and Reduction in Sensitivity Function Calculations," IEEE Trans. Automat. Contr., Vol. 19, pp. 774-783, 1974.

REFERENCES (Continued)

21. Fisher, R.A., "On the Mathematical Foundations of Theoretical Statistics," Phil. Trans. Roy. Soc. London, Ser. A, Vol. 222, pp. 309-386, 1922.
22. Koopmans, T.C., and Reiersol, O., "The Identification of Structural Characteristics," Ann. Math. Stat., Vol. 21, pp. 165-181, 1950.
23. Rothenberg, T.J., "Identification in Parametric Models," Econometrica, Vol. 39, pp. 577-591, 1971.
24. Larimore, W.E., "Identifiability and Maximization of Likelihood," Draft in preparation.
25. Rao, C.R., and Mitra, S.K., Generalized Inverse of Matrices and Its Applications, New York: Wiley and Sons, 1971.
26. Biggs, M.C., "The Estimation of the Hessian in Nonlinear Least Squares Problems With Non-Zero Residuals," Mathematical Programming, Vol. 12, pp. 67-80, 1977.
27. Fletcher, R., "Generalized Inverse Methods for the Best Least Squares Solution of Nonlinear Equations," Computer J., Vol. 10, pp. 392-399, 1967.
28. Marquardt, D.W., "An Algorithm for Least Squares Estimation of Nonlinear Parameters," SIAM, Vol. 2, pp. 431-441, 1963.
29. Goldfeld, S.M., Quandt, R.E., and Trotter, H.F., "Maximization by Quadratic Hill-Climbing," Econometrica, Vol. 34, pp. 541-551, 1966.
30. Edwards, A.W.F., Likelihood, Cambridge: Cambridge Univ. Press, 1972.
31. Sprott, D.A., "Normal Likelihoods and Their Relation to Large Sample Theory of Estimation," Biometrika, Vol. 60, pp. 457-465, 1973.
32. Rao, C.R., Linear Statistical Inference and Its Applications, New York: Wiley and Sons, 1965.
33. Goldfeld, S.M., and Quandt, R.E., Nonlinear Methods in Econometrics, Amsterdam: North-Holland Pub. Co., 1972.